UiT The Arctic University of Norway

Faculty of Health Sciences, Department of Pharmacy

Mass cultivation of the marine diatom *Porosira glacialis*:

Method development and comparison of pigment composition in response to irradiance wavelength

Agnethe Hansen Bæverud

Master's thesis in Pharmacy, May 2022

Acknowledgement

The work presented in this thesis was carried out in the period of August 2021 to May 2022 at the Natural Products and Medicinal Chemistry Research Group, Department of Pharmacy (IFA) at UiT The Arctic University of Norway in collaboration with the Norwegian College of Fishery Science (NFH).

First and foremost, I would like to express my sincere appreciation to my main supervisor Associate professor Terje Vasskog for being the most inspiring lecturer and giving me the opportunity to work on this project. Amidst a very hectic workday, you always found time to meet with me to discuss ideas, theories and challenges. Your extensive knowledge, patient guidance and calming personality have been invaluable, steering me in the right direction. Secondly, I which to thank my co-supervisor Dr. Jon Brage Svenning for introducing me to the field of marine biology. Your indispensable advice, practical suggestions, scientific and non-scientific discussions as well as lab assistance throughout this year are deeply appreciated.

I would also like to thank everyone form the Natural Products and Medical Chemistry Research Group for providing a friendly and supporting environment throughout this project, with a special thanks to PhD candidate Torbjørn Myhre for sharing your extensive software knowledge with patience and great humor.

My gratitude also extends to my fellow students and friends that have encouraged me through the study. I especially must thank Nima, Kristine and Vegard for making these last two years a whole lot more enjoyable. And to Marte Mari, thank you for all the great memories and for always being there.

Finally, I would like to express my deepest gratitude and love to my family for their endless support and continuous encouragement throughout this entire process. To my partner, Henning, this achievement would not have been possible without you. And to our two beautiful daughters, Aurora and Tuva, for providing joyful distraction and unconditional love.

Tromsø, May 2022

Agnethe Hansen Bæverud

Abstract

Background: In 2015, UiT The Arctic University of Norway and a local smelting plant initiated a project aiming to reduce the carbon footprint by mass cultivation of microalgae. The ability of the microalgae to directly capture industrially emitted CO_2 and utilize wastewater as alternative nutrient sources to produce high value biomass, causes the bio-carbon recycling to represent both an environmental and economical feasible strategy. The produced microalgal biomass composes value-added products as lipids, proteins and pigments, and has the potential to ensure macronutrient quality as supplements in aquaculture fish-feed. The main goals of this thesis were to develop a method for pigment analysis and investigate the pigment composition in response to irradiance wavelength.

Method: The polar diatom *Porosira glacialis* was cultivated under three different wavelength irradiances, red, blue and white light. Pigments were extracted from lyophilized algal biomass by utilization of a developed pigment extraction protocol and analyzed through HPLC-MS with positive ESI ionization. Data dependent acquisition (DDA) methods were used in order to create an in-house AMRT database, acquire identification information and determine relative pigment abundance. The identification and relative quantification were performed both manually and with the assistance of the software Compound Discoverer™.

Results: High confidence identification of 10 pigments derived from the marine diatom *P.glacialis* was achieved, representing both the carotenoid and chlorophyll pigment classes. In addition, putative identification of the xanthophyll adonixanthin was obtained. The results demonstrated an alteration of pigment composition in response to different irradiance wavelength with a significant difference detected between the red and blue light regime in terms of both microalgae growth and pigment production.

Conclusion: Cultivation under blue light resulted in a statistically significant higher growth rate and accumulation of the analyzed pigments compared to red light cultivation, except chlorophyll *b*. The blue light regime was suggested to promote pigment production in *P. glacialis*.

Table of Contents

Abbreviations

DDA	Data dependent acquisition		PQH$_2$	Plastoquinol
AMRT	Accurate Mass Retention Time		PQ	Plastoquinone
H-ESI	Heated electrospray ionization		RF	Radio frequency
APCI	Atmospheric pressure chemical ionization		AUC	Area under the curve
HPLC	High performance liquid chromatography		HCD	Higher collisional energy
MS	Mass spectrometry		CID	Lower collisional energy
ICCP	Impressed current cathodic protection		AGC	Automatic gain control
Bio-CCU	Biological carbon capture and utilization		ACN	Acetonitrile
PBR	Photobioreactors		FA	Formic acid
VAP	Value added product		Qc	Quality control
SOFIA	State of the world fisheries and aquaculture report		ID	Identification
LC-PUFA	Long chain- poly unsaturated fatty acids		Chl *a*	Chlorophyll *a*
FO	Fish oil		SNCE	Stepped normalized collision
EPC	Excess photosynthetic capacity		XIC	Extracted ion chromatogram
CCM	Carbon concentrating mechanisms		v/v	Volume/volume
PSII/I	Photosystem II/I		ANOVA	Analysis of variance
ROS	Reactive oxygen species		m/z	Mass-to-charge ratio
ATP/ADP	Adenosine triphosphate/diphosphate		HR-MS	High resolution mass spectrometry
NADPH/ NADP	Nicotinamide Adenine Dinucleotide Phosphate Hydrogen/ Nicotinamide adenine dinucleotide		IC	Internal calibration
NPQ	Non-photochemical quenching		LIT	Linear ion trap
FWHM	Full width half maximum		DC	Direct current
S/N	Signal-to-noise ratio		AC	Altering voltage
PMF	Proton motive forces		SD	Standard deviation

x

1 Introduction

1.1 Background

The persistent increase in carbon dioxide (CO_2) emission presents a critical universal challenge emphasized by the Paris Agreement and as stated in the ICCP (1) climate report of 2022, requires immediate and deep emission reductions across all sectors as means to limit global warming. In this effort, UiT The Arctic University of Norway and a local smelting plant initiated a project based on biological capture and utilization of CO_2 (bio-CCU) by mass cultivation of microalgae.

In an effort to meet the aim of climate change mitigation, industrial byproducts such as CO_2 emission along with wastewater hold the potential to serve as alternative nutrient sources for microalgae cultivated in photobioreactors (PBR). The possibility of a simultaneous high value biomass production causes such a carbon reduction strategy to be both environmentally and economically feasible. Macromolecules such as specific lipids, proteins and pigments constitute value-added products (VAPs), contributing to biomass application, for instance its potential as supplements in aquaculture fish-feed.

In accordance with the trend of the past decades, a recent SOFIA report (2) stated a significant and growing role of the aquaculture industry in providing food and nutrition, with a production projected to reach 109 tonnes in 2030. Fish meal and fish oil (FO) derived from capture fisheries are considered uniquely valuable in aquafeed formulation, containing a high protein level and abundant long-chain polyunsaturated fatty acids (LC-PUFAs) (3). An expanded demand for these products resulting from the growing aquaculture production, combined with a relatively stagnant supply, lead to a high raw material cost, plant-based substitution and ultimately an uncertain sustainability of the aquaculture industry (4). As a green and sustainable alternative replacement/supplement to aquaculture nutrition, the biomass produced by microalgae is seen as a promising strategy to ensure the macronutrient quality (5).

The photosynthetic microalgae recycle CO_2 efficiently, with a 10-50 fold enhanced fixation potential compared with terrestrial plants (6). Although efficient, the amount and value of the biomass produced will depend on the microalgae species, cultivation system and growth conditions. In this project, the polar diatom *Porosira glacialis* was investigated because of its robustness towards condition alterations, high growth rate under limited light availability and

low temperatures and a large surface to volume ratio. In addition, previous studies on the particular diatom have showed a lipid composition characterized by a high content of LC-PUFA (7).

As a result of the projects thorough emphasis on lipid composition, minor attention has been assigned to pigment characterization. Although the concentration of pigments per unit dry mass is lower than for other macromolecules, pigments possess a significantly higher commercial value (8). As part of the development of an industrial mass cultivation of marine diatoms, the project now seeks to develop a method for pigment analysis utilizing "state of the art" analytical instruments.

1.2 Marine diatoms

Life at sea depends on the primary producers, which establish the base of the marine food chain and comprise the photoautotrophs with the ability to convert inorganic carbon dioxide into organic carbon through photosynthesis (9). The microalgae constitute some of the world`s most important primary producers and are characterized as a diverse group of photosynthetic, small, unicellular organisms. As a result of each microalgal cell being photosynthetically active, the primary production efficiency is high compared to terrestrial plants. Although they only comprise 1% of the Earths estimated photosynthetic biomass, these photoautotrophs account for approximately 45% of the global primary production (10). A class of microalgae which constitute one of the dominant species of eucaryotic phytoplankton, is the diatoms. The marine diatoms are ubiquitous and the number of diatom species are estimated to be as high as 100 000(11). According to fossil records of diatoms, the spices has existed for more than 150 million years (10), with an origin believed to derive from two (or debatably three (12)) endosymbiotic events composed of the primary endosymbiosis of a an ancestral non photosynthetic eukaryote and an ancient cyanobacteria (todays red and green algae), and a second endosymbiosis of the resulting latter species and a heterotrophic eukaryote (10). Through this merging and evolutional reduction in cellular structure, the diatoms chloroplast has developed a distinct structure with unique features suggested to be of importance for the diatom's high adaptation capacity and survival in fast changing environments (12).

The diatoms are considered relatively large with a cell size ranging from 20 to >1000 µm (13) and a morphology separated in two main categories; the centric diatoms and the pennate diatoms (9). The centric diatoms are characterized as radially symmetrical with a spherical form, while the pennate diatoms are bilaterally symmetrical. Both centric and pennate diatoms tend to form dense blooms with their golden appearance caused by pigment reflection via fucoxanthin, as well as other carotenes and xanthophylls (10). A feature of the diatoms distinguishing them from other microalgae, are their encapsulation in a silica cell-wall, the frustule. The frustule consist of two silica heterovalvar shells (9), in which the geometry of the two diatom valves differs in radius creating a box-shape with the smallest valve (hypotheca) as the bottom and the bigger half (epitheca), constituting the lid. The epitheca and hypotheca are held together by grindle bands with a valve structure composed of silica lines, costae. The latter diverges from a nucleation site and divides specially shaped chambers. This structure provides

3

the diatom with functions as mechanical strength, movement, molecular sieving for nutrition uptake and photonic properties for light and energy harvesting (10).

The inherited ability of diatoms to reproduce both asexual and sexual is an essential characteristic, in which the vegetative cell division is the promotor for rapid cell-growth(9). In vegetative cell division, the cell divides into two daughter cells, which are clones of the ancestor cell. The new frustule valves are created inside the valves of the parent cell, resulting in a decreased cell-size for each cell division. At a certain point, the division stops. Original cell-size is reestablished by sexual cell division through the formation of a larger auxospore, enabling the relatively faster vegetative reproduction to proceed.

Diatom growth is dependent on the availability of sunlight, dissolved CO_2, inorganic nutrients and trace metals. Aside from carbon, hydrogen and oxygen, stored in the carbohydrates, as well as silicon for the silicification progress of the frustules, the diatoms require additional macro- and micronutrients to grow. These nutrients are often limited and comprise, among others, nitrogen, phosphorus, sodium, iron and magnesium (9), making the diatoms ideal for wastewater treatment (14). Compared to other phytoplankton taxa within its size range, the diatom growth rates are faster. Under optimal growth conditions, the latter combined with cell size and carbon-fixation ability through photosynthesis, enables a great biomass production (9) and simultaneously decrease carbon emission or increased carbon capture.

1.2.1 *Porosira glacialis*

Porosira glacialis is a marine centric cold-water diatom with a diameter of 30-40 µm and is commonly abundant in Norwegian coastal waters, constituting one of the main phytoplankton species at the beginning of the spring bloom (15). *P. glacialis* is characterized by its unique valvae, with areolae organized in wave-shaped striae and a weak silicification. The natural environment of polar diatoms is described as extreme, represented by permanently low temperatures, intense vertical mixing or stratification by ice, and in general, low light availability with occasional severe variations (16). As a result, through evolutionary adaptation or acclimatization strategies, the polar diatoms possess unique features such as a low light saturating parameter for photosynthesis (E_K estimated to 33 µmol photon $m^{-2}s^{-1}$), a high excess of photosynthetic capacity (EPC), a high number of photosynthetic pigments (17) and being psychrophilic (18). Additionally, the diatoms have a high adaptation capacity (see section 1.2)

and possess special characteristics such as a Rubisco enzyme with a relatively high CO_2 affinity, as well as carbon concentrating mechanisms (CCM) enabling utilization of the more biologically abundant bicarbonate as inorganic nutrient and protective mechanisms against alterations in pH or toxic elements (17). Although the latter characteristics are not unique to polar division, the natural high degree of environmental alterations, suggest these mechanisms to be crucial for their survival.

P.glacialis displays high growth rates under limited light availability and low temperatures, high tolerance towards condition alterations, maximizing of photosynthetic activity by reducing self-shading through a high surface to volume ratio and an high content of marine omega-3 fatty acids (18). This species is therefore studied as a candidate for mass cultivation in so-called carbon capture and utilization (CCU).

1.3 Photosynthesis

Photosynthesis is a biochemical process which results in the production of molecular oxygen (O_2), making life of aerobic organisms possible (9). In the biochemical process, energy from the sun is absorbed by photosynthetic pigments and converted into chemical energy (ATP), which is used to synthesize organic carbohydrates from inorganic carbon dioxide (CO_2). The organisms that are photosynthetic are called autotrophs and compose the primary producers, including the microalgae. In microalgae species and higher plants, photosynthesis takes place in the chloroplasts, which are chlorophyll containing plastids with a single layer lipid membrane enclosing the stroma and stacks of thylakoids, grana (17). The structure and composition of the diatom chloroplasts is composed of a four layered chloroplast membrane with circular unstacked thylakoids located at the periphery of the stroma, surrounding a diffuse pyrenoid and a genome (12). The conversion of light into chemical energy occurs in the membrane of the thylakoids (17), close to the stromal membrane and the CO_2- fixation/reduction at the stroma with the pyrenoid possessing a crucial role of the CCMs (12).

1.3.1 The biological role of pigments in the process of photosynthesis

Photosynthesis is a redox process, in which carbon dioxide is reduced to carbohydrates by electrons derived from water. Since water has a lower redox potential than sugar or NADPH, the process requires energy (17). This energy is provided by the photon energy of light and captured by the photosynthetic pigments as illustrated in Figure 1. The photon energy absorbed by the photosynthetic pigments results in electron excitation, producing an unstable molecule. The instability causes a spontaneous de-excitation, releasing energy. The orbital level reached by the electron is determined by the initial photon energy, in which absorption of shorter wavelengths equals more energy released by de-excitation (17).
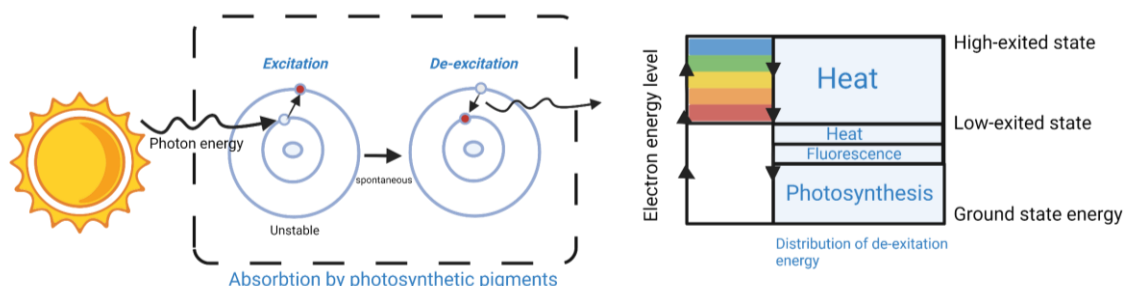

Figure 1:Simplified schematic of the light absorption part of the photosynthesis. Created with BioRender.com

Although more energy is released from high-excited states, only the energy generated from the low-excited state, the red-energy level, is transferred to the photosynthetic process. Released energy from de-excitations beyond the low-exited state, produces heat. The quantum yield of the overall photosynthetic process, defined as the amount of photosynthesis performed per photon(17), is for this reason independent of the photon energy-level absorbed. The excess energy, or by-product, from de-excitations requires dissipation mechanisms. These are performed by the photoprotective abilities of the diatom pigments (further described in section 1.6). An overview of the photosynthetic process is given in Figure 2, showing its complexity by interaction between the major multisubunit protein complexes of the diatom photosynthetic apparatus; PSII, cytochrome (Cyt) b_6f, PSI and the ATP synthase (10). In the next section, the role of the photosynthetic pigments in this process is described more thoroughly, followed by a brief description of the remaining steps towards the resulting carbohydrates.
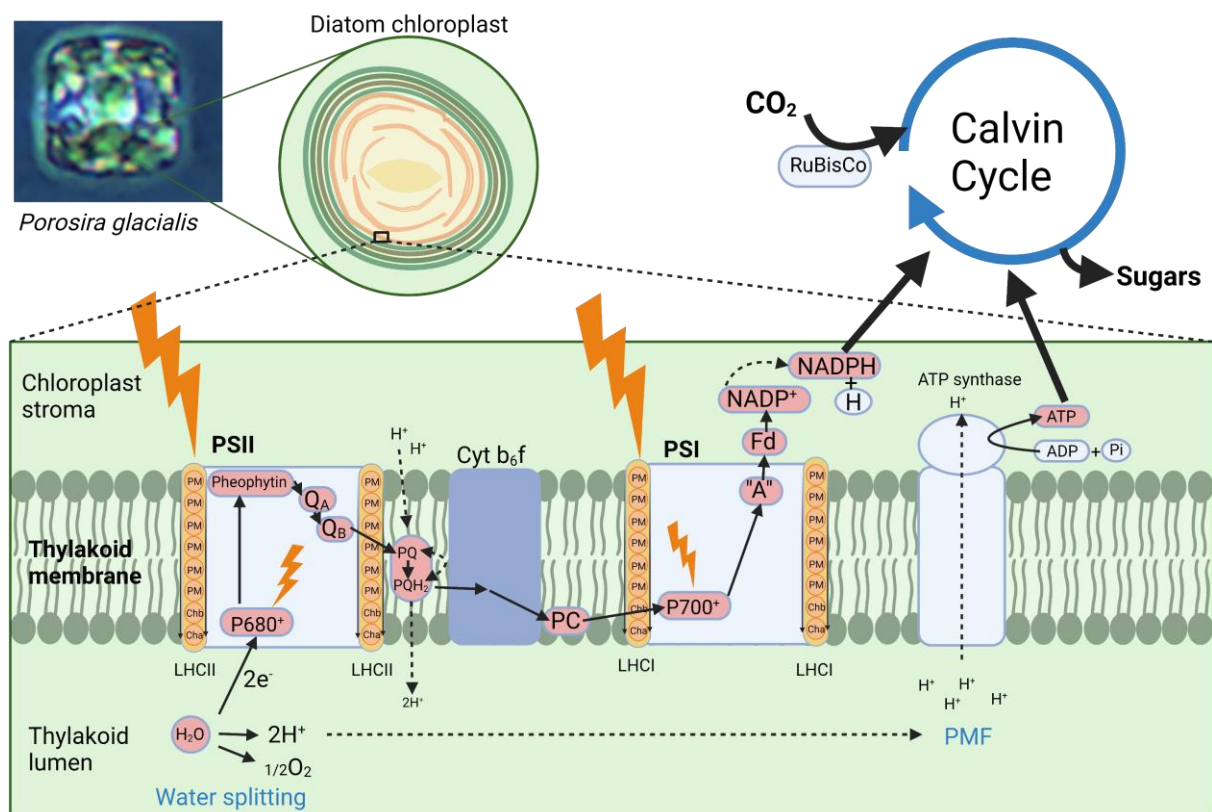

Figure 2: Simplified overview of the light absorption and charge separation by photosynthetic pigments, followed by the CO₂-fixation. Created with BioRender.com

The linear electron transport pathway from water to NADPH is initiated by photon absorption and primary electron transfer in the reaction center of PSII (17). The reaction center consists of a special pair of chlorophyll *a* molecules forming a chlorophyll dimer, with the ability to, instead of conducting electron transfer to a higher orbital upon irradiation, move the electron to an electron acceptor outside the molecule itself. The resulting reduced electron acceptor further catalyzes the series of reduction reactions and the remaining positively charged pair of chlorophyll *a* regain electrons from an electron donor, water.

The chlorophyll dimer at the reaction center absorbs photons, and is thereby capable of starting the reduction process itself, but due to speed limitations of photon absorption combined with the narrow absorption range of chlorophyll *a*, the construction of a complex pigment funneling system increases the extent and efficiency of the light harvesting part of photosynthesis (17). This funneling system, called the photosynthetic antenna, is comprised of several hundred pigment molecules, and is located around the reaction center. The organization of pigments is done in order of wavelength absorption, with the pigments absorbing shorter wavelengths located at the antenna end and the pigments absorbing wavelengths in the red band close to the reaction center. The antenna widens the absorption range and resonance transfer of energy absorbed by its constituting pigments, feeding the reaction center directing charge separation.

The reaction center consists of two photosystems, PSII and PSI, interconnected in the reduction pathway and fed by their own photosynthetic antenna (17). In PSII, the chlorophyll *a* dimer has an absorption peak at 680 nm and is therefore denoted P680. Correspondingly, the PSI chlorophyll *a* dimer has an absorption peak at 700 nm and is denoted P700. The interconnecting point between the systems is plastocyanin (PC), which function as an oxidizing agent for the positively charged P700 after primary electron transfer in PSI and the reduced form can be considered the end product of PSII.

The overall combined result of the two photosystems is the reduction of ferredoxin, which can further reduce $NADP^+$ to generate NADPH (17). Two systems are required because pheophytin, the first electron carrier intermediate in the electron transfer pathway of PS II, does not carry enough reducing power to directly reduce ferredoxin. Additionally, the generation of chemical energy in the form of ATP is dependent on these systems, in which both the water-splitting and the proton-gradient are created by reduction of plastoquinone (PQ) to plastoquinol (PQH_2),

accumulating protons in the thylakoid lumen. This accumulation of protons constitutes the proton-motive force (PMF) and creates a chemical and electric potential difference between the lumen and the stroma, due to energy loss when delivering electrons to PSI. The subsequent gradient flow of protons through the ATP synthase generates ATP from addition of a phosphate group to ADP.

The NADPH and ATP formed through the light-reactions are used in the fixation and reduction reaction, known as the Calvin cycle, in which CO_2 is reduced to form carbohydrates (17). The photosynthetic pigments thus have important roles in photosynthesis, as well as generation of primary building blocks for the synthesis of crucial compounds for cell function, energy formation utilized in metabolic processes, and other synthesized products such as lipids and proteins.

1.4 The algal photosynthetic pigments

Photosynthetic pigments in algae are divided into three major classes, namely the chlorophylls, the carotenoids and the phycobiliproteins. In the microalgae the most common photosynthetic pigments are the chlorophylls and the carotenoids, whereas the phycobiliproteins are present in cyanobacteria and red algae (19).

1.4.1 Chlorophylls

Chlorophyll is the most common photosynthetic pigment in phytoplankton. In microalgae, the chlorophylls are located at the chloroplast stroma, in which the chlorophylls transport electrons across the thylakoid membrane at a high speed and constitute the primary electron donor and acceptor (19). Chlorophyll *a* is present in all plants and consist of a porphyrin-like head-group and a lipophilic hydrocarbon chain tail (17). The head-group is comprised of four pyrrole rings retained by a magnesium atom and together with the phytyl-tail, the structure is characterized as hydrophobic.
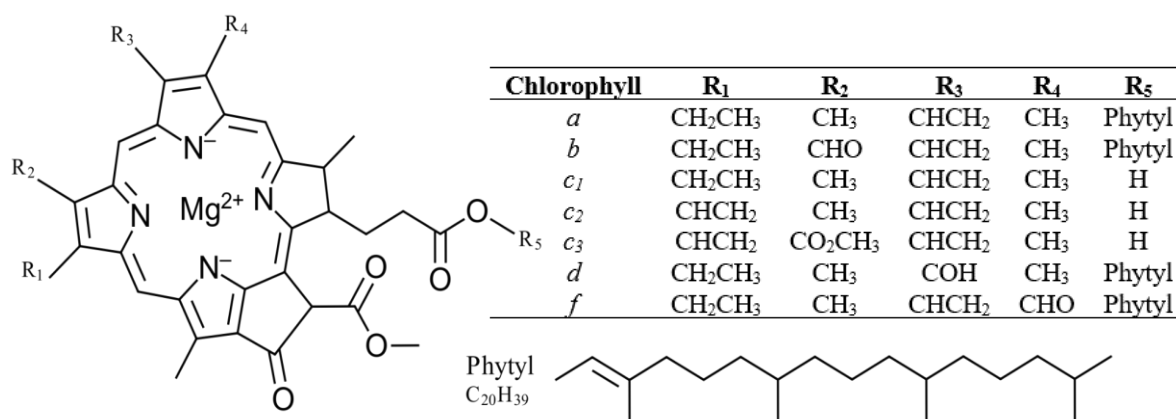
Chlorophyll	R_1	R_2	R_3	R_4	R_5
a	CH_2CH_3	CH_3	$CHCH_2$	CH_3	Phytyl
b	CH_2CH_3	CHO	$CHCH_2$	CH_3	Phytyl
c_1	CH_2CH_3	CH_3	$CHCH_2$	CH_3	H
c_2	$CHCH_2$	CH_3	$CHCH_2$	CH_3	H
c_3	$CHCH_2$	CO_2CH_3	$CHCH_2$	CH_3	H
d	CH_2CH_3	CH_3	COH	CH_3	Phytyl
f	CH_2CH_3	CH_3	$CHCH_2$	CHO	Phytyl

Phytyl $C_{20}H_{39}$

Figure 3: The structure of chlorophyll a, b, c₁, c₂, c₃, d and f.

The redox chemistry and the absorption by chlorophylls occurs at the aromatic tetrapyrrole macrocycle (19), in which the range of absorption is depending on the sub-structures of the head-group (17). Generally, chlorophylls absorb mainly blue light (approx. 430 nm), as well as some red light (660-665 nm) and reflects green light (9). While the head-group structure comprises the absorption and redox-reactions, the lipophilicity of the tail functions as an anchor in the lipid-based membranes of the thylakoids. Furthermore, the central magnesium ion (Mg^{2+}), influences the excited-state kinetics of tetrapyrroles, maximizing the excited-state lifetime (19).

In addition to chlorophyll *a*, several forms of chlorophylls have been identified: Chlorophyll *b*, chlorophyll $c_1/c_2/c_3$, chlorophyll *d* and chlorophyll *f* (19). Their structure mainly differs in functional groups attached to the head-group (Figure 3). An exception is the chlorophyll *c*, which is lacking the phytyl-tail, making these molecules more polar. The latter has yet no defined function, other than passing resonance energy towards chlorophyll *a* (20). In some species, chlorophyll *a* is exchanged with chlorophyll *d* or *f* at the reaction center (21). The presence and quantity of the different forms of chlorophylls are species specific, and hence used as taxonomic tools. The identified chlorophylls of the diatom includes chlorophyll *a* and chlorophyll *c* (*c*1,*c*2 and *c*3) (10, 19).

1.4.2 Carotenoids

Carotenoids are present in all plants and absorbs irradiance in the blue-green spectrum (400-550 nm) (17). By incorporating carotenoids in their photosynthetic antenna, the light spectrum utilized by the algae expands. As part of the resonance transfer funnel, the carotenoids are considered a group of accessory pigments with their backbone structure consisting of linear hydrocarbon polyenes (Figure 4), in which some are oxygenated derivates (19).
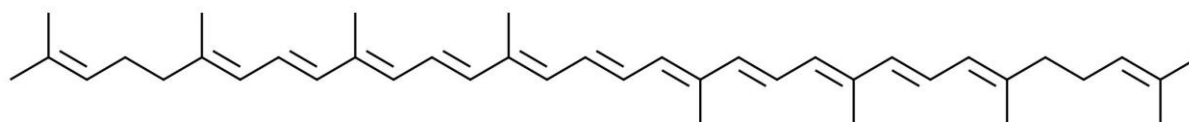
Figure 4: Chemical structure of lycopene, representing the branching-point in the biosynthesis of carotenoids.
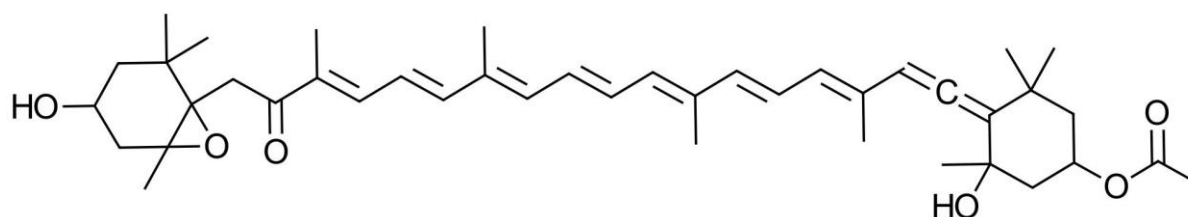
Figure 5: Chemical structure of fucoxanthin, an oxygenated derivate and the dominant carotenoid in diatoms.

The carotenoids are further divided into two subclasses depending on whether the backbone molecular structure is the non-oxygenated hydrocarbon polyenes or the oxygenated derivates, representing the carotenes and the xanthophylls, respectively (22). In addition, the carotenoids can be divided based on their function, in which primary carotenoids (i.e., β-carotene, lutein

and violaxanthin) act as energy harvesters that expand the light-absorbing spectrum of the cells, while the secondary carotenoids (astaxanthin and canthaxanthin) are involved in the photoprotection of the chlorophylls and are located outside of the chloroplast. All carotenoids have antioxidant functions that enables them to scavenge reactive oxygen species (ROS), and thereby protect the cell form free radical attacks and oxidation. The mechanism of neutralization of free radicals is attributed to the donation of electrons and hydrogen atoms from the electron-rich polyene chain (19). Moreover, the carotenoids affect the membrane fluidity with a reported increase in carotenoid content as temperature decreases, leading to a higher level of rigidity (23).

The photosynthetic antennae of microalgae typically contain one dominant carotenoid, which for the diatom species constitutes fucoxanthin (Figure 5). A previous study on *P. glacialis* also identified the carotenoids diadinoxanthin, alloxanthin, diatoxanthin, zeaxanthin, lutein and carotene (24).

1.4.3 Phycobilins

The phycobiliproteins pigments, phycobilins, are the main photosynthetic pigments in red algae species and are also present in most cyanobacteria (19). Unlike chlorophyll, the phycobilins are not embedded in the stromal membrane but form a complex with the membrane, phycobilisomes (17). Irradiance of 450-650 nm is harvested by these pigments and thereafter transferred to anchored chlorophylls in the membrane, and thus function as accessory pigments, enhancing the light collection for photosynthesis (19).

The molecular structure of the phycobilins consists of a tetrapyrrole chromophore covalently bound to the apoprotein (25). Within the phycobilisome, they are ordered in a manner so that the excitation energy is transferred between them, towards the reaction centers of photosynthesis. Thus, the phycobilisome can be seen as a light-harvesting antenna similar to the photosynthetic antenna of chlorophyll and composes the phycoerythrobilin, phycourobilin, phycoviolobin and phycocyanobilin (Figure 6).
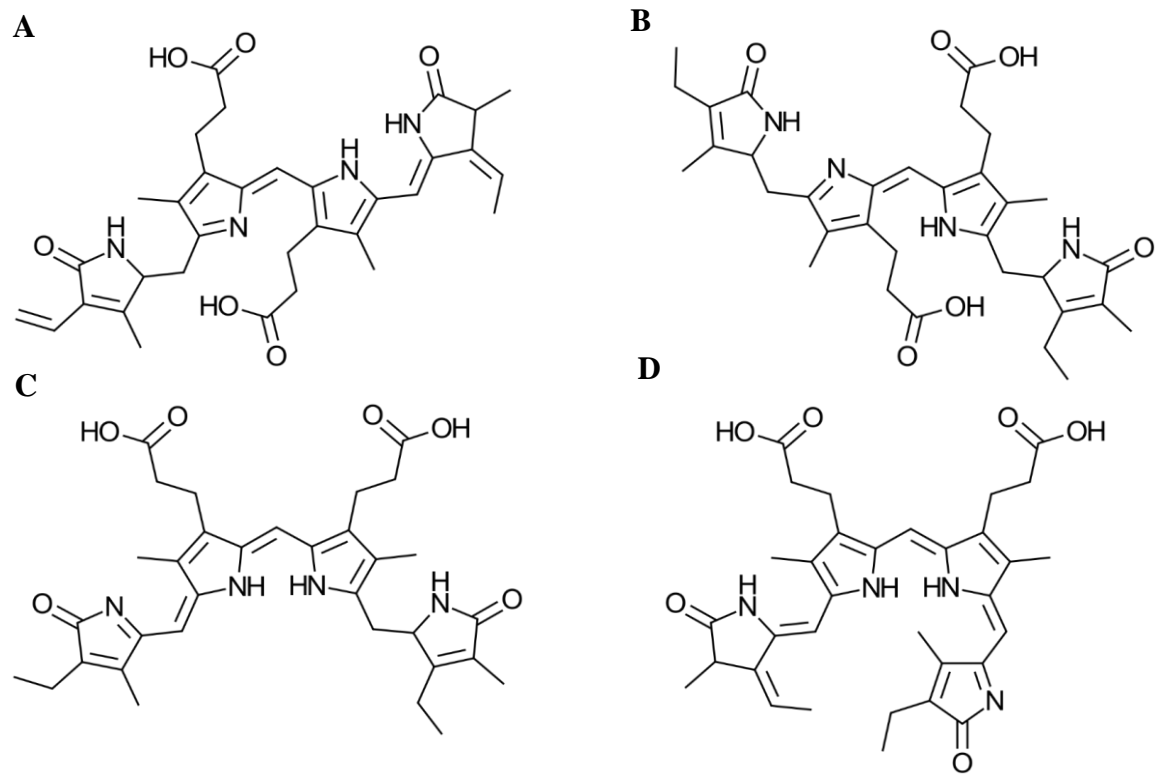
Figure 6: Chemical structures of the four groups of phycobilins; phycoerythrobilin (A), phycourobilin (B), phycoviolobin (C) and phycocyanobilin (D).

1.5 The established commercial applications and future possibilities of pigments derived from microalgae

Pigments are valuable natural products and their application in various industries is well established, including food, feed, cosmetics and nutraceutical industries (26). In all mentioned industries, pigments are utilized as natural colorants. Examples include the addition of lutein in animal feed, enhancing the color of egg yolk or promote the pink/red color of farmed salmonids by addition of astaxanthin in fish feed. Due to their antioxidant properties, pigments are also utilized to prevent quality degradation in food products as well as benefiting human health. In the cosmetic industry, the supplementation of pigments as antioxidants in ointments and creams protects the skin from UV-light damage, and thereby reduces the risk of skin cancer (26). The potential of improving the human health by pigment utilization is extensive, and studies have indicated benefits such as lower risk of inflammation, heart disease, type-2 diabetes, obesity and cancer (26, 27). Furthermore, pigments have shown to improve eye-health and protect neurons, the latter is of importance in diseases like Alzheimer, Parkinson and amyotrophic lateral sclerosis (ALS).

The carotenoids possess a high market value with astaxanthin being the most expensive pigment, followed by beta-carotene and lutein (26). Together with lycopene and zeaxanthin, these carotenoids already have established applications, although fucoxanthin and canthaxanthin have been gaining more attention with their potential to, respectively, reduce the risk of skin-cancer and reduction in body weight (22) and thereby rise their economic significance. Today, most of the pigment production is performed by chemical synthesis due to a faster and cheaper production compared to the relatively more costly and comprehensive derivation from microalgae (26). For instance, only 1% of the commercially available astaxanthin is algal derived, whereas 95% is synthetically produced (22). The high synthetic production of pigments stands in contrasts to consumers preferences, in which a biological origin is desirable (22) due to being perceived as a "healthier" product.

1.6 The effect of different light regimes on pigment content

Environmental factors affect both microalgal growth and pigment composition and in order for microalgae to survive in strong conditional variance, protective mechanisms are required. One of the these environmental factors is light availability (10). In low light exposure or shading, which resembles the winter season for polar diatoms, an increase of the pigment cellular quota occurs as means to prohibit impairment of the photosynthetic process by enhancing the funneling antenna. On the other hand, there exists an optimal light intensity for maximal photosynthetic efficiency (19). After reaching saturation, additional illumination leads to formation of excess energy which is dissipated through fluorescence and heat, or the unfavorable conversion of singlet chlorophylls to triplet state chlorophylls (10). In order to prevent the formation of chlorophyll triplets, the biosynthesis of photosynthetic pigments in response to light environments is tightly controlled.

A consequence of overloading the photosystems (PSII and PSI), is the accumulation of reactive oxygen species (ROS) through reactions between triplet state chlorophylls and oxygen (10). The ROS formed includes superoxide radical (O_2^-), hydrogenperoxide (H_2O_2) or hydroxyl radical (*OH) (19). These ROS have the potential to cause cell damage, for instance cleave a protein (D1) in PSII, resulting in photoinhibition of photosynthesis. To prevent damage caused by ROS formation, the microalgae has developed photoprotective mechanisms as, for instance, the xanthophyll cycle (28, 29). In green algae and land plants the violaxanthin cycle composes the major xanthophyll cycle (30). However, for diatom species, an additional xanthophyll cycle is reported to perform the main photoprotective operations, namely the diadinoxanthin cycle (Figure 7). In addition, the beta-cryptoxanthin cycle has been proposed as a third protective carotenoid cycle (28).
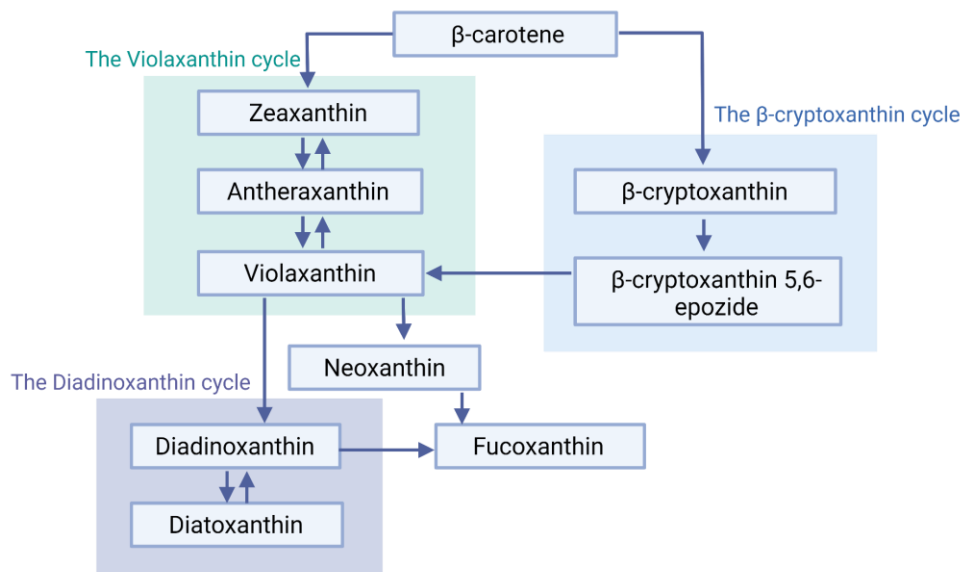
Figure 7: Selected part of a proposed pathway for carotenoid biosynthesis in marine diatoms adapted from (28, 29), highlighting the violaxanthin, beta-cryptoxanthin -and diadinoxanthin cycle. Created with BioRender.com

When exposed to high-light, both cycles, accepts excess light energy from chlorophyll *a* and dissipate it as heat (26). This mechanism is called non-photochemical quenching (NPQ) and is one among several dissipation-mechanisms involving enzymatic regulated conversions of different pigments in the cycles. Illustrated in Figure 7, an alteration in biosynthesis due to high-light protective mechanisms will affect the pigment composition of the diatom, in which the alteration occur schematically upwards in the violaxanthin cycle and descending in the diadinoxanthin cycle in response to irradiation with high-light (26, 30). Thus, developing an optimal light regime in mass cultivation could contribute to an efficient production of valuable carotenoids.

1.7 Cultivation

The establishment of an efficient cultivation system designate a fundamental step towards the application in question (31), for instance mass production of high-value microalgal biomass and footprint reduction. The main cultivation systems include the open systems, in which the surface-to-volume ratio is low, and closed systems, in which the latter parameter is high.

The open systems can be established as lakes and natural ponds or artificial ponds composed as circular- and raceway basins (31). Open systems are characterized by their technical simplicity, ease of operation and relatively high endurance. On the other hand, the requirement of a significant installation surface, the low volumetric productivity, relatively high contamination risks and difficulty in operational control makes this technique less preferable in many industrial applications.

Closed systems utilize photobioreactors of different shapes and sizes. These systems enable a greater operational control compared to the open systems (31). Depending on the design of the photobioreactors, the latter are divided into the tubular photobioreactors or the flat-plate photobioreactors, consisting of transparent tubes or rectangular panels, respectively. Separating the bioprocess of cultivation from the surrounding environment reduces the risk of contamination, facilitates better control of the cultivation conditions, and compared to the open systems, provide an increase in surface-to-volume ratio, biomass production and CO_2-fixation capacity. The main downside is associated with high construction and operation costs.

Operational conditions of cultivation are key-parameters for optimal CO_2-biofixation and high-value biomass productivity, depending both on the intrinsic characteristics of the algal species and the design of cultivation system (31). These parameters include light, temperature, pH, salinity, nutrient concentration, the present of toxic elements and hydrodynamic behavior. A change in one, or more, of these parameters can lead to a drastic alteration in both CO_2-fixation capacity, resulting in lower growth-rates, and composition of the biomass produced. Subsequently, the cultivation system of choice in terms of achieving high operational control is the photobioreactor.

1.7.1 Operating modes, growth curve and quantification of diatom biomass

From an industrial perspective, a continuous mode of operation with full control of the operating parameters is favorable, in which the simultaneous supplement of new growth media and harvesting of biomass occur (31). Although this is the preferred operation mode, the method requires species dependent optimization. To minimize time-consumption, technical challenges, and high expenses, most experiments are conducted in pilot scale operating in batch mode.

In batch mode the system is closed and the inoculum is introduced once into the culture media, containing all nutrients required for growth (31). The concentration of microalgal cells increases as a function of time until the limiting substrate is drained. Under these conditions, the microalgae growth follows a sigmoidal curve, composing the latency phase, the exponential growth phase, and the stationary phase. The latency phase is characterized by no cell growth and represents the acclimatization; the cells adaptation to a new environment, of which the capacity is species dependent. At the end of the latency phase, the cell is typically initiated by an acceleration phase prior to the exponential growth phase. In the latter phase, the growth rate is constant, and a maximum specific growth rate can be calculated. As the culture grows, the nutrients availability decreases, and at the end of this phase the cell concentration reach a limit value before entering the stationary phase. Other than nutrients (and other operational parameters), the high cell density can lead to self-shading and light penetration decreases and becomes the limiting factor.

To monitor the growth-state (phase) of microalgal cultures and fluctuations in microalgae biomass, optical density measurements are conducted using conventional methods including hemocytometry, through microscopy and chlorophyll *a* fluorescence spectroscopy (32) . From section 1.3.1, energy from chlorophyll de-excitation was dissipated/utilized as heat, fluorescence and photochemistry, and an inverse relationship between photosynthesis and fluorescence was stated (estimate for photosynthetic performance). Chlorophyll fluorescence is a weak red light, and since there exists a dependance between fluorescence intensity and concentration of the fluorescent substance (33), quantitative measurements can be determined by utilizing a fluorometer.

1.8 Harvesting

Following the cultivation is the harvesting of the produced microalgae biomass, which represent the costliest step in the production due to a high cost-cell concentration ratio (31). The aim of harvesting is to separate the microalgal cells from their growth medium and thickening the sludge obtained. There are multiple techniques in use for this purpose depending on the amount of biomass and culture volume. For small volumes, the traditional technique of gravity filtration utilizing a plankton net is a simple alternative, in which the culture is harvested by filtration through a filter with a specific pore size (9). Thereafter the algal biomass can be collected for further analysis. This method will be a challenge with large scale harvesting due to filter clogging, resulting in high time consumption. To overcome these challenges employing a centrifuge has been a success, where the biomass is separated from the growth medium by centrifugal forces (34).

1.9 Sample preparation for pigment analysis

The pigment extraction is a part of the sample clean-up and reduces the complexity of biological samples by minimizing the number of components in the mixture and thereby matrix effects are less prone (33). In addition, the concentration of the analyte of interest might be under the detection limit, which require a pre-concentration. Conversely, the analyte concentration might be too high, causing an overload of the chromatographic column, yield squared top-shapes and hence, require dilution. Some samples are even non-compatible with the instrument, and if not modified, might contaminate or damage the instrument.

Generally, the microalgal cell wall has a great structural strength, functioning as a formidable defense (19). The rigid wall structure requires a cell-disruption step to ensure access to the analyte in a subsequent extraction step. Regarding the microalgae *Porosira glacialis*, a recent study found that a cell-disruption step prior to extraction did not affect lipid extraction yields (35), suggesting that solvent choice and the number of re-extractions are the determining factors for lipid extraction yield. The results comply with the fragile cell wall morphology of *P. glacialis* (15), leading to generalize the finding to not only concern the lipid extraction yields, but to all product yield, including pigments.

Despite freeze-drying is considered a mechanical cell-disruption mechanism, its main role of application in pigment sample preparation from *P. glacialis*, is the removal of water, and thereby increasing the quantification accuracy. Additionally, with the removal of water, an inhibition of enzyme activity occur which enhances the pigment stability (36). Considering the obtention of a greater surface area generated by lyophilization, higher extraction efficiencies are reached, but the expanded surface also cause pigments to be more prone to oxidation (37). The duration, as well as storage facilities, from lyophilization to analysis should thus be evaluated and preferably kept to a minimum.

Unlike the existence of more or less standardized lipid extraction protocols from microalgae (i.e., Folch method and Bligh and Dyer method), a conventional protocol for the extraction of pigments is not present. The physiochemical differences both between pigment subclasses and pigment of the same class contributes to the challenge of making an ideal all pigment extraction protocol. For this reason, the selection of extraction method is dependent on the pigments of interest. In addition to an evaluation of targeted pigments, parameters as compatibility with

chromatographic technique, production scale, pigment stability and extraction duration should be considered (36).

Microalgal pigments are intracellular and require a solvent able to recover the pigments from the biomass (19). The extraction solvents utilized are therefore dependent on the polarity of the targeted pigments and variations in hydrophobicity between pigment subgroups necessitate a choice of extraction solvent appropriate to the pigment(s) of interest. The non-polar characteristics of chlorophylls and carotenoids interact with organic solvents, making them ideal extraction solvents for these pigment classes (19). In contrast, the phycobilins are water soluble and do not require organic solvents for pigment extraction. Acetone, methanol, ethanol and hexane are widely used extraction solvents for pigment analysis with high extraction recoveries for multiple pigment classes (36).

The extraction itself includes the addition of extraction solvent to the microalgae biomass, mixing, a solid/liquid separation step and a distillation step (19). Mixing ensures sufficient solvent-pigment contact and the solid/liquid separation provides a solvent phase with minimal cell debris. The last distillation step facilitates crude lipid extract containing targeted pigments and recycles organic solvents. The necessity of the latter step is dependent of the extraction solvent utilized. The extraction process is often repeated to increase extraction yield.

1.10 Ultra-high-performance liquid chromatography (UHPLC)

1.10.1 Liquid chromatography

The Russian scientist Mikhall Semenovich Tswett is considered the "Father of the Chromatography" as a result of his extensive study on pigment separation, thereby developing the term chromatography. Accordingly, chromatography is the process of separating components of a mixture (38). In liquid chromatography (LC) the separation technique constitutes a stationary phase of solid matter and a liquid mobile phase containing the dissolved analyte of interest. The separation is achieved by interaction differences of the compounds, leading to different transmission velocities.

If the flow pressure of the mobile phase is increased, the technique is called high performance liquid chromatography (HPLC). A high flow pressure combined with a uniform low particle size solid phase, yield a high resolving power and a capability to run fast analysis. By combining the HPLC-system with a detector, a chromatogram can be obtained. The detector signal is plotted as a function of time and the resulting peaks are utilized to identify and quantify contents of a complex mixture. The HPLC coupled to a detector establishes an important tool in the field of analytical chemistry.
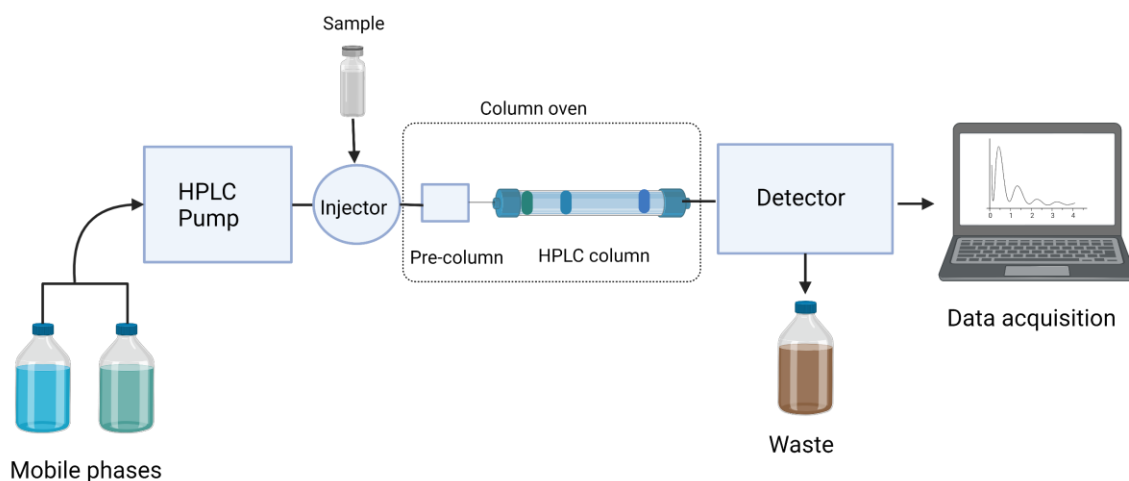
1.10.2 HPLC Instrumentation

Figure 8:Schematic of the HPLC-setup. Created with BioRender.com

A simplified HPLC-setup is illustrated in Figure 8, starting with the filtering and blending of an appropriate modified mobile phase flowing towards the HPLC-pump. To prevent potential

harm to the system, residues of dissolved gas are removed by a degasser prior to reaching the solvent delivery system (33). Due to the elevated backpressure developed as the mobile phases are introduced into the column, the HPLC pumps are required to handle a high amount of pressure to be capable of delivering a steady flow of mobile phase. The latter is further ensured by the employment of a pulse dampener. A sample to be analyzed is placed in an injection system and at a given time, the sample is injected into the mobile phase flow, by a leak-proof injection valve. A pre-column protects the HPLC column from particles and at the HPLC column, analytes are separated according to their distribution constant. Both the pre-column and the HPLC-column are placed in a column oven to provide optimal analyzing parameters and reproducibility. A detector at the column outlet registers signals for eluting analytes and the data generated are interpreted by a computer software which generates the chromatogram.

1.10.2.1   The column

In the HPLC-system, the separation of compounds is performed by the column. The general separation principle is based on interaction differences between analytes with the sorbent particles inside the column and the liquid mobile phase running through the column (38). This difference in affinity for the two phases creates a distribution constant, in which a higher distribution constant equals a stronger interaction between the analyte and the stationary phase, compared to the interaction between the analyte and the mobile phase (33). The stronger the analyte interact with the column sorbent, the longer the analyte is retained on the column, and accordingly, the retention time increases.

The sorbent inside the column consists of chemically modified silica particles with functional groups on the surface, facilitating the analyte-sorbent interaction (33). The separation ability of a column depends on the particle size and shape, the pore size, and the attached functional groups. By decreasing the particle size and ensuring a uniform spherical particle shape, the band broadening is minimized, leading to an enhanced separation ability. Additionally, both the diameter and length of the column affects the separation capabilities of the column(38). A longer column will increase separation, but at the same time the elution time is increased, resulting in longer time of analysis. A column with smaller inner diameter will have the same separation properties as a column with a bigger inner diameter, but with a lower solvent consumption. A smaller diameter, together with the particle size and flow-rate determines the back pressure generated in the HPLC-system. If the particle size is reduced to 2 µm the LC-

system is called ultra-high performance liquid chromatography, UHPLC (38). The UHPLC enables faster analysis, by being capable of utilizing a higher mobile phase flow without loss of efficiency. A higher amount of pressure and reduced particle sizes, provides a better signal to noise ratio due to reduction in band broadening, which also decreases ion suppression, since co-elution is less pronounced.

The reversed phase column consists of a non-polar silica based stationary phase (33). The silica particle is modified with an alkyl chain as the functional group, in which the length varies. A longer carbon chain equals a more hydrophobic column and increases the Van deer Vaal's interactions with lipophilic analytes, for instance carotenoids. The C30 column was in fact developed to separate carotenoid isomers, as an increase in alkyl chain length results in a deeper cavity for pigment interaction, and thereby shape selectivity increases (37). However, the currently most used column for pigment analysis is the C18 column which has shown similar separation abilities as the C30, but with a decreased time of analysis. In addition, the C8 column possesses selectivity towards compounds with slight differences in polarity and is accordingly employed for analysis of pigment with polarity distinctions.

1.10.2.2 Mobile Phases

The mobile phases utilized in reversed phase chromatography consist of one or multiple organic solvents miscible with water, and water (38). Since the retention mechanism on a reversed phase column is hydrophobic, the eluting strength of water is weak, thereby a higher degree of water in the mobile phase prolongs analyte retention time. In opposition, an increase in hydrophobic characteristics of the solvents leads to an elevated eluent strength and the analytes are less retained on the column. In addition to eluent strength, parameters as pH, flowrate and temperature also affect the retention time of the analyte, and controlling these parameters are therefore of importance (33, 38). The pH in the mobile phase solution together with the inherited pKa value of the analyte of interest determines whether the analyte is ionized. In a reversed phase column, an ionized analyte will interact with the sorbent to a lesser degree than the non-ionized form, resulting in a shorter retention time. More importantly, when the HPLC is coupled to a mass spectrometer, the ionization of an analyte will increase ionization efficiency. To control the pH, organic acids or bases are often added, usually ammonium formate and/or formic acid.

The temperature on the column oven, affects the viscosity of the mobile phase (38). A lower temperature increases the viscosity, leading to a higher back pressure in the column, requiring reduction in flowrate and ultimately slows down the time of analysis. On the contrary, a higher temperature facilitates higher flowrates, but requires control of boiling point and stability of the mobile phase components. To ensure reproducibility the column temperature is normally set to temperatures either above or below room temperature, in which the former is most common.

For complex samples, the manipulation of separation through a gradient elution might be required. In contrast to isocratic elution, the composition of the mobile phases is altered during the analysis ranging from a weak mobile phase composition to a stronger one (33). By implementing a gradient, existing co-elution combined with empty gaps in the chromatogram might be time efficiently solved, yielding both sufficient separation of analytes and a short duration of the analysis. A drawback with gradient elution is the requirement of equilibration between each run which in turn increases the time of analyses.

1.11 Mass spectrometry (MS)

Mass spectrometry is an analytical technique based on the motion of charged particles in an electric or magnetic field- aiding the measurement of mass to charge ratio (m/z). The mass spectrometer consists of several basic elements depicted schematically in Figure 9. In order for an analyte to enter the mass spectrometer, the analyte must be ionized (39). After ionization/vaporization performed in the ion source, the ion beam in gas phase is guided under vacuum through the analytical instrument under the influence of an applied electric field. The mass analyzer separates the heterogenous ion beam according to their respective m/z values and a detector converts quantum ion current into electrical current. The acquired data is handled by a data processing system, in which the detected intensity of ion signals are plotted as a function of m/z values, displaying a mass spectrum (40). Thus, the mass spectrometer provides formation of molecular ions and their related fragments, separation of ions according to their m/z value, and intensity measurement of the individual ions.

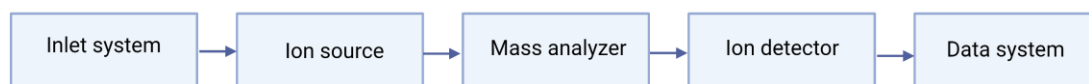| Inlet system | → | Ion source | → | Mass analyzer | → | Ion detector | → | Data system |

Figure 9: Schematics of the mass spectrometer components. Created with BioRender.com

The mass spectrometer ensures high sensitivity, relatively high speed of analysis, simultaneous analyses of compounds of a mixture, compound quantification and the ability to acquire information regarding the compound structure, aiding in structural elucidation and identification (39).

1.11.1 Ion source

Prior to passage into the mass analyzer, the analytes are required to be present as ions, which is facilitated by an ionization process located in the ion source of the mass spectrometer (40). Additionally, the ion source must be capable of handling a steep pressure drop with the LC-system operating at high pressure and the MS under vacuum. For both pigment analysis and lipidomics, the electrospray ionization (ESI) technique is one of the most prominently employed (19, 40). Moreover, the positive ionization mode has shown to ionize pigments more

efficiently compared to negative polarity (37). Accordingly, the ion source utilized in this study was the ESI in positive mode and is discussed further in the next section (1.11.1.1).

1.11.1.1   Electrospray Ionization

The electrospray ion source ionizes sample constituents under atmospheric pressure, enabling substances in solution, without extensive pretreatment, to be analyzed by the mass spectrometer (39). Generally, the ionization prosses can be viewed as to facilitate two parts, firstly the production of charged droplets and secondly formation of gaseous ions from these droplets. At the (often heated) inlet capillary, the solution containing the analytes of interest is introduced into the ion source. High voltage is applied at the inlet capillary along with at the entrance of the mass analyzer and for the positive- ion mode, the polarity of the employed electrical potentials are positive and negative, respectively. The generated electric field in the ion chamber, supported by addition of heated sheath gas, causes solvent reaching the capillary tip to form the Taylor cone, which polarize the solution and allows the release of sprayed droplets containing solvent and analyte molecules carrying a net electrical charge equal to the polarity of the applied capillary potential (38, 39). As the charged droplets travel through the chamber towards the orifice of the mass analyzer, the droplets evaporate until reaching the Rayleigh limit. At the present limit, the Coulombic repulsive forces exceed the surface tension, resulting in a Coulombic explosion, splitting droplets into smaller droplets. The iterative splitting process leads to gas phased charged analyte molecules, which is guided into the analyzer by the counter electrode and higher vacuum of the internal part of the ion source (39).

The most common adduct formed through electrospray ionization (in positive mode) is the proton adduct $[M+H]^+$ (38), however, dependent of multiple factors such as mobile phase composition, sample matrix, solvents and compound characteristics, formation of other adducts might occur (i.e., $[M+Na]^+$, $[M+NH_4]^+$ and $[M+K]^+$) (39). The chlorophylls exhibit abundant protonated molecule ions under ESI conditions, whereas the carotenes have been shown to form radical molecular ions only $[M]^+$ (37). The latter is believed to be associated with the conjugation extension, generating radical cations. The xantophylls are observed to form both radical ions and protonated molecular ions with an estimated ionization efficiency higher than carotenoids. Although, electrospray ionization is considered a "soft" ionization method with a reduced unwanted fragmentation (39), in source decay is still prominent under pigment analysis (41).

1.11.2   Mass analyzers

Subsequential to the ionization of analytes, the ions are guided to the mass analyzer, which operates by separating a mixture of ions according to their m/z values by subjecting them to electric and/or magnetic fields under conditions which minimize collisions with background gas molecules (38). Generally, mass analyzers are sorted in two groups, ions beams and ion traps. Which mass analyzer to choose is dependent on both availability and figures of merit required for the analysis. The mass spectrometer utilized in this study is the Orbitrap ID-X Tribrid MS, which combine three mass analyzers, the quadrupole, the linear ion trap and the orbitrap. In addition, the instrument is equipped with two different dissociation techniques, allowing fragmentation. Accordingly, these mass analyzers and modes of dissociation will be described more thoroughly in the following sub sections. In conclusion, a summary of the Orbitrap ID-X Tribrid MS workflow is provided.

1.11.2.1   The quadrupole

The separation of ions according to their m/z is achieved by the quadrupole through exploiting the stable oscillatory trajectory of ions in an electric field (39). The quadrupole mass analyzer consists of four cylindrical metal rods, parallel to each other as well as to the trajectory of the ion beam. Electrical voltage is applied to the rods with opposite rods retaining the same polarity, generating an electric field. In the quadrupole ions move with a constant speed parallel to the z-axis by applying a direct current (DC). The movement along the x-and y-axis is dependent on the voltage and frequency applied on the cylindrical rods (42). The alternating voltage of defined frequency applied to the rods together with adequate values of DC, decide which m/z-values getting stable fluctuations and thereby passing the analyzer, leaving the rest to be selected in an unstable pathway discharged during collisions with the rods. This allows monitoring of a particular m/z value or scanning a m/z range by varying the voltages (37). Quadrupoles are often referred to as transmission quadrupoles, owing to their function as mass-selective filters (40).

1.11.2.2 The linear Ion trap

The linear quadrupole ion trap (LIT) is constructed with the same physical principles as the quadrupole, modulated by further addition of electrodes at the trap exits (39). The former focuses ions between the rods as described in section 1.11.2.1 controlling the movement in the x and y direction and the added electrodes enables the control of movement along the z-axis. The combined result is the ability to trap ions at the center of the trap, between the rods. The ejection of ions from the trap transpires by two means of operation, axial ejection mode and radial mass selective ion ejection. The former occurs by changing an alternating voltage (AC) on the rods, in addition to the applied RF voltage, resulting in certain m/z values leaving the trap through small holes in the end cap. As the applied voltage increase, the higher m/z values become unstable and are ejected into a detector, which subsequently generates the mass spectrum. For this reason, the ejection acquiring the mass spectrum is performed in order of descending m/z (42). The mode of radial mass selective ion ejection is operated by changing the voltage applied on the rods, letting ions with a particular m/z through slits in one pair of rods positioned parallel to each other and thereby leaving in x and y directions (39). By altering the voltage configuration, all ions outside a certain range can be forced to leave the trap, constituting the ion isolation mode (42). Helium gas aids the trapping of the ions and through frequent collisions with helium gas molecules, the kinetic energy of the trapped ion is dissipated and cools the ions down. Additionally, helium gas molecules can be utilized for fragmentation, making MS^n a possibility.

In the commercial tribrid orbitrap by Thermo Fischer Scientific, an additional C-shaped quadrupole Ion trap co-functions with the orbitrap, retaining ions, cools them before injecting them into the orbitrap in a pulsed manner (42). The ion trap is equipped with a control function, which consist of performing micro scans of its ion content and is utilized in the orbitrap scan, aiding better signal to noise ratio (S/N).

1.11.2.3　　Orbitrap

The orbitrap is one of the newest mass analyzers and as the name suggest, is classified as a ion trap mass analyzer (39). Opposed to the linear quadrupole ion trap, described in section 1.11.2.2, the orbitrap belongs to an assemble of mass analyzers with high-resolution, namely high-resolution mass spectrometry (HR-MS). The ability to measure m/z values with high accuracy, significantly decreases the number of possible elemental compositions, and thereby composition elucidation is achieved with high reliability (39). Additionally, the high resolution power enables separation of near isobaric mass peaks, which is eminently beneficial/required for analyses of complex samples. The orbitrap operate at high vacuum and consists of a central spindle shaped electrode and an outer cylindrical bottle structure, in which the latter also constitute an electrode (40). The central spindle is kept at a very high voltage and creates an electrostatic field in the space between the outer and inner electrode. Ion packages of selected m/z are sent into the orbitrap from the c-trap through an opening in the outer electrode and directed perpendicular to the central electrode. The ions are affected by the electrostatic field and given the right velocity, forced to rotate around the central electrode in an ion specific orbit. Furthermore, a quadrupolar field between the orbitrap endcaps is generated, resulting in harmonic oscillations in the z-direction. The special construction of the orbitrap makes the potential generated from the movement in the z-direction independent of the ion transit around the central electrode, and thus the m/z relate to the ion oscillation frequency along the z-axis (38). The ion pathway facilitates a longer acquisition time, thereby more measure points are achieved and an increase in the orbitrap resolution is obtained (42).

Instead of utilizing an external detector, the orbitrap ions are sensed by plates (or the outer electrode) as they move in their specific oscillation (39). At proximity to one of the plates, a voltage is created which can be measured. The time-domain signal is converted to a frequency spectrum by Fourier transformation, and further to a mass spectrum. The possibility to precisely measure the oscillation frequency combined with the utilization of internal calibration (IC), leads to obtention of high mass accuracy (39).

1.11.2.4 Fragmentation

Conducting a MS^1 scan performed by an instrument with high mass-accuracy and resolution, facilitate compound separation (38). Adequate m/z separation combined with the related retention time of the peaks, enables compound identification. The validity of the latter statement will depend on the purity of the sample analyzed, and accordingly the presence of isobaric interference. Considering complex biological samples, the possibility of isobaric interference is increased, and an identification solely based on m/z and retention time might origin from both the analyte of interest and interfering isobaric compounds, or entirely constitute interference. Therefore, to ensure high quality identification and/or structural elucidation, compounds are required to be fragmented. The sequential MS^2 procedure is schematically depicted in Figure 10.
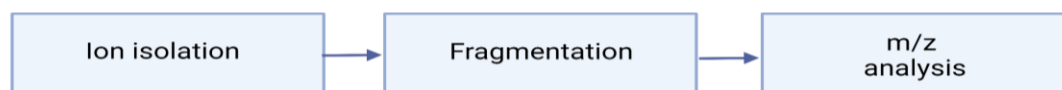

Figure 10: Simplified schematic of the MS^2 procedure. Created with BioRender.com

To assure the acquired fragment spectrum representing the specific fingerprint of the chosen molecule ion, the spectrum is required to be derived exclusively from the particular ion (39). Hence, the first step constitutes isolation of the latter from all other ions present in the sample. Subsequential to the isolation, is the fragmentation process, in which additional external energy provides dissociation of the most labile/all covalent bonds within the molecule before detection by a mass analyzer. The acquired fragment mass spectrum (MS^2 spectrum) holds structural information of the precursor ion and detection of qualifier ions confirm the identification of known compounds, along with structure elucidation of unknowns. The theoretically most labile bonds where fragmentation is most likely to occur, is between carbon and heteroatoms or carbon-carbon bonds in the alpha-position of a functional group (42). Two commonly utilized fragmentation techniques in omic-studies are the low-energy collision induced dissociation (CID) and the high-energy collisional dissociation (HCD). As the names of the dissociation mechanisms vary between vendors, the following descriptions are specific for the mass spectrometer utilized in the current thesis (Thermo Scientific orbitrap ID-X Tribrid mass spectrometer).

1.11.2.4.1   Low energy Collision induced dissociation (CID)

Collision induced dissociation, CID, occurs in the ion trap and is aided by an inert collision gas, for instance, helium (He). As the analyte ion collides with collision gas molecules, accumulation of internal energy occurs (42). A single collision is usually insufficient for ion decay and at least a few collisions are required. After a certain number of collisions, a maximum energy level is reached and the most labile bonds in the compound are fragmented. The latter is a result of redistribution of the internal energy between the collisions. In the ion trap, only the precursor ions are accelerated, leaving product ions to fall out of resonance with RF and cool. The result is a limited secondary fragmentation. After CID fragmentation, the daughter ions are sent to either the orbitrap or to the second ion-trap for detection.

1.11.2.4.2   High energy Collision activated dissociation (CAD/HCD)

Collision activated dissociation, CAD, occurs in the ion routing multipole/HCD-cell and, as the CID dissociation, involves frequent collisions with inert gas molecules, for instance, nitrogen gas. As opposed to CID dissociation, the energy applied to the ions under CAD dissociation is increased. Subsequently, a single collision is adequate for dissociation (39, 42). Additionally, the CAD dissociation technique are considered stochastic, resulting in fragmentations of weak bonds, as well as bonds of higher strength (39). After the collision, product ions retain kinetic energy and can repeatedly collide with collision gas molecules, and thereby undergo further fragmentation(42). Detection of fragments formed in the HCD cell occurs in the orbitrap or the second ion trap, and the resulting fragmentation spectrum is a result of multiple generations of dissociation.

1.11.2.5   Thermo Scientific orbitrap ID-X Tribrid mass spectrometer

Analyzing small molecules in complex biological samples constitute a great challenge for the mass analyzing techniques and has driven the development of novel technologies toward instrumentation capable to increase the amount of quality data at higher speed without compromising the mass accuracy and resolution (39). One of the more recently developed mass spectrometers is the Thermo Scientific Orbitrap ID-X Tribrid mass spectrometer, which combines tree mass analyzers, the quadrupole, the linear ion trap and the high resolution orbitrap (Figure 11).
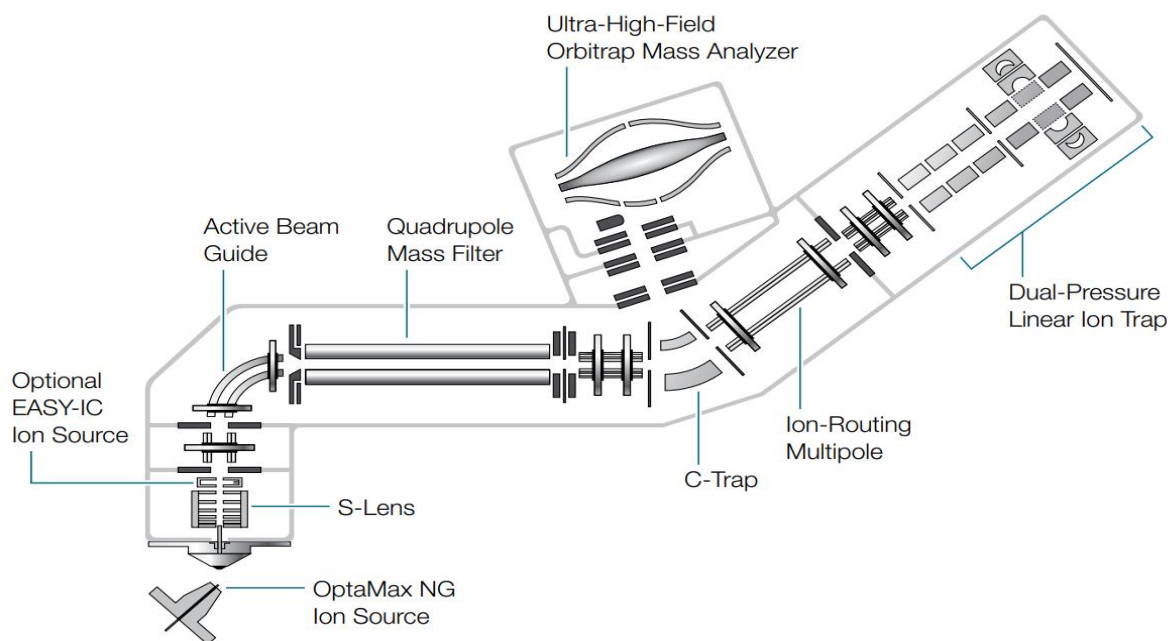
Figure 11: Thermo Fischer ID-X orbitrap schematic(43)

From the ion source ions are guided through the instrumentation by different lenses and bended pathways, constructed to alter the direction of ion movement(43). Subsequently, neutral molecules and high-velocity clusters are prevented entrance into the mass analyzers and thus, prohibits compromising the analysis. The ability to apply an internal lock-mass aids to assure mass accuracy, and at a set-time frequency, lock-mass ions are sprayed into the instrument for measurements in the orbitrap. The difference between the theoretical mass and the measured mass of the lock mass is used to correct any other masses measured by the instrument.

At the quadrupole mass filter, depending on the selected mode, scanning of the m/z range or precursor ions selection are performed before entering the c-trap. The c-trap cools down the ions, conducts microscans and prepare ion packages, prior to injection into the orbitrap for MS^1 (39). The velocity of the entering ions is of great importance for the obtention of stable ion trajectories in the orbitrap and must be sufficient tangential, or the ions will collide with the inner electrode (42). By applying high voltage on the exit lens from the c-trap and distance minimizing, a fast injection is obtained.

A previous weakness of the orbitrap has been the slow scan rate, which results in few measuring points over a chromatographic peak, leading to difficulties in accurate quantification (39). The scan rate has been greatly improved in the ID-X by lowering the diameter of the central

electrode, while keeping the voltage at the same high level. The reduced path around the high voltage electrode, reduces the distance between the central electrode and the ions, leading to a decreased risk of ions colliding with outer instrumental parts. Additionally, the risk of colliding with residual gas molecules also decreases with shorter transient path, as well as the measuring time. The outcome is less signal decay and shorter analyzing time, and ultimately better information at faster rates.

Aside from sending the ions from the c-trap directly into the orbitrap and generating MS^1 spectrums, ions can be guided to the ion routing multipole or/and the dual-pressure linear ion trap for HCD- and CID-fragmentation, respectively(43). If desirable, the daughter ions resulting from the fragmentation can be fragmented repeatedly (MS^n) before they are sent to either the orbitrap or the second ion trap that constitutes the dual-ion trap for detection, depending on where the fragmentation occurred. The ability to generate data from multiple fragmentations of compounds and different fragmentation techniques, enables informative MS^n spectrum, which in theory could be unlimited, but often is restricted by sensitivity and the usefulness of the data generated.

1.12 Data processing and identification of pigments

As the field of technology has developed, the possibility to acquire a remarkable amount of complex and multidimensional data from analysis, performed by hyphenated analytical instruments, has commenced (39). Considering an untargeted analysis, the achievement of successful characterizations of unknown molecules depends on the comprehensive acquisition of full scan and fragmentation data and subsequently, the interpretation of the acquired data for identification (44). In pursuance of the automatization of these characterization requirements acquisition tools are encountered, including the software AcquireX (Thermo Fisher Scientific, Waltham, MA, USA) and Compound discoverer (Thermo Fisher Scientific, Waltham, MA, USA).

1.12.1   AcquireX

The data acquisition software AcquireX increase the obtained data quality by implementation of a background removing exclusion list, an inclusions list, and creation of dynamic and real-time exclusion lists to the method (45). In deep scan mode a sequence acquisition workflow is defined by the operator and compose solvent blanks/background matrix samples, a representative pooled sample (a combined sample of all samples to be analyzed) and all samples of the study. Firstly, the acquired MS data from solvent blanks/background matrix samples generates the initial exclusion list. In a similar manner, an injection of a sample representing an average of all samples to be studied (representative study sample), establishes the initial inclusion list. Subsequently, a user defined iterative injection cycle of MS^n data acquisition is performed, in which the first replicate is compared with the initial inclusion/exclusion list to determine precursors for fragmentation. The resulting data are possessed, and the software relocate the fragmented precursors from the inclusion list to the exclusion list, creating the dynamic and real-time exclusion before proceeding to the second injection. The employment of exclusion and inclusion lists and their dynamic real-time updating result in a MS^2 acquisition time spent on sampling unique features of the sample of interest, and thereby detecting low-level compounds for further data processing.

1.12.2   Compound discoverer

The data processing tool Compound Discoverer conducts automated library searches for identification, tentative annotation and structural characterization. The software allows post-acquisition data to be imported, defined and processed through template workflows or customized workflows. The outcome consists of identification, annotation and structural elucidation by integration of multiple tools for gathering identification information such as compound detection, compound grouping, retention time alignment, prediction of elemental composition, removal of chemical background with data from blank samples, matching with on-line databases and/or local databases(46). Creating local databases and including them in a compound discovered workflow, enables automatically generated identifications of compounds at a high confidence level. A software which allows a development of such a database is the MzVault software (Thermo Fisher Scientific, Waltham, MA, USA).

2 Aim of the thesis

The main aim of this master thesis was to develop a method applicable for pigment profiling and investigate the pigment composition in response to irradiance wavelength of the marine microalgae *Porosira glacialis*. To achieve these goals, the following subgoals were set:

- ¤ Development of an efficient extraction protocol for pigments derived from *P.glacialis*
- ¤ Optimize the UHPLC method regarding separation and peak-shape
- ¤ Develop suitable MS methods for the "in-house" pigment library and algal pigment analysis
- ¤ Create an "in-house" pigment database
- ¤ Develop workflows in compound discoverer for automatic pigment annotation

3 Materials and methods

3.1 Chemicals

Table 1: List of chemicals

Chemicals	Purity (%)	CAS-number	Supplier
Acetone	≥99.5	67-64-1	VWR Chemicals, France
Methanol	≥99.9	67-56-1	VWR Chemicals, Netherlands
2-propanol	≥99.9	67-63-0	VWR Chemicals, United Kingdom
Milli-Q® water			Merc Millipore, Darmstadt, Germany
Acetonitrile	≥99.9	75-05-8	VWR Chemicals, Etats Unis
Ammonium formate	≥99%,	540-69-2	VWR Chemicals Leuven, Belgium
Formic acid (FA)	≥99%,	64-18-6	Merck KGaA, Darmstadt, Germany
Easy-IC;fluoranthene			Thermo Scientific™ Pierce™, Rockford, USA

3.1.1 Pigment standards

The pigment standards were purchased from DHI (Hørsholm, Danmark) and composed a total of 17 pigments derived from plants and phytoplankton; fucoxanthin, diatoxanthin, peridinin, violaxanthin, pheophytin a, zeaxanthin, lycopene, chlorophyll c_2, chlorophyll c_1, chlorophyll a, chlorophyll b, diadinoxanthin, canthaxanthin, β-carotene, antheraxanthin, astaxanthin and alloxanthin. In general, the chloro-pigments were dissolved in 90% acetone and the carotenoids in 100% acetone or ethanol, with a concentration range between 0.5 and 3.2 mg/L. The pigment standards were stored in sealed brown vials placed in a freezer with a temperature below -20°C.

Pigment structures, molecular formula and standard properties are listed in Appendix A: DHI pigment standards.

3.2 Materials

Table 2: Materials utilized for pigment extraction

Equipment	Specifications	Supplier
Analytical Balance	Sartorius Entris 2241-1S	Sartorius, Göttingen, Germany
Lyophilizer	Labconco FreeZone® 2.5L benchtop freeze dry system (-50°C)	Labconco Corporation, Kansas City, MO, USA
Shaker	Orbital Shaker PSU-10i	Grant Instrumentation Ltd, Cambs, England
Centrifuge	Jouan, MR 22i, rotor no. AM2.19	Saint Nazaire, France
Brown glass vials	Amber Vial, Screw Top 7 mL	Supelco®, Bellefonte, PA, USA
Glass Pasteur pipettes	Glass Pasteur pipettes 230 mm, No.567/2	Assistent, Germany
Eppendorf tubes	Eppendorf tubes® Safe-Lock Tubes 1.5mL	Eppendorf AG, Hamburg, Germany
LC-MS vials	12x32 mm glass screw neck vial, Quick Thread, LectraBond cap, PTFE/silicon septa	Waters, Milford, MA, USA
Pipettes	Eppendorf Research® plus pipettes, 10-100µL, 0.5-5 mL	PhysioCare Concept, Eppendorf AG, Hamburg, Germany
Finntip pipette tips	Finntip™ 250 Universal pipette tips	Thermo Fisher Scientific, Waltham, MA, USA
Eppendorf Tipps	epT.I.P.S.® Standard/Bulk 0.1-5 mL	PhysioCare Concept, Eppendorf AG, Hamburg, Germany

3.3 Cultivation and harvesting of *Porosira glacialis*

3.3.1 Cultivation procedure

During a research cruise in May 2014, a sediment sample from the Barents Sea was collected (N76° 27.54`, E 033° 03.54`) and through isolation (manual retrieval), identification (47) and culture testing with regards to optimal cultivation characteristics, the monoculture of *Porosira glacialis* was selected and cultivated in this study.

The cultivation of the monoculture of *P.glacialis* was performed in 150-liter clear plexiglass columns placed in an open container outside, monitoring the temperature and pH. The experimental pH remained relatively stable around 8, however the average experimental temperature decreased during the cultivation from 4°C to -0.8°C. An attempt to prevent/minimize the temperature drop by insertion of an oven was tested, which had limited success due to abnormally low ambient temperatures. The culture medium was composed of filtered and pasteurized seawater, ≥98% sodium metasilicate nonahydrate (Sigma Aldrich, St. Louis, MO, USA) and Guillard`s F2 Marine water enrichment solution (50x) (Sigma Aldrich, St. Louis, MO, USA). To avoid sedimentation, all columns were mixed by aeration.

The cultures were cultivated in three triplicates, to a total of 9 cultures, in which each triplicate was illuminated with white, blue or red light, respectively. Constant illumination was provided by LED light (Eurolight LED IP FL-10 COB RGB, Eurolite®, Germany) calibrated to an average scalar irradiance of 22 µmol photon m^{-2} s^{-1}. Recordings of peak wavelengths for the white, blue and red light, were achieved by using a BLACK-comet Fluorescence Spectrophotometer (StellarNet, Tampa, FL, USA), displaying 454 nm for blue light, 627 nm for red light and 453, 520 and 627 nm for white light.

Prior to the start of the experiment, three cultures were acclimatized to the experimental light regimes for one week (white, blue or red) and subsequently the cultures were divided into triplicates and diluted to a start volume of 45L with an average concentration of approximately $3*10^5$ cells/L for the red light triplicate, $6*10^5$ cells/L for the white light triplicate and $5*10^5$ for the blue light triplicate.

3.3.1.1 Chlorophyll *a* measurement, cell counts and estimation of biomass

The growth of the cultures was monitored daily by *in vitro* chlorophyll *a* – extraction and quantification, following the method of Holm-Hansen and Riemann (48) substituting methanol with 96% ethanol (Merck KgaA, 64271 Darmstadt, Germany), and cell-counting in 2 mL Nunc-chambers (Nunc A/S, Roskilde, Denmark). Measurements of *in vitro* chlorophyll *a* were used as an estimation tool for the biomass produced and the specific growth rate (μ; doublings hour^{-1}) were calculated utilizing both cell-counts and *in vitro* chlorophyll *a* measurements, ensuring the cultures not to enter the latency phase.

3.3.2 Harvesting procedure

On the 4th day, the cultures were harvested in the exponential growth phase by filtration trough a 10 µm plankton net (KC Denmark AS, Silkeborg, Denmark), into 50 mL Falcon tubes (Corning Science, Reynosa, Mexico). Prior to the filtration, the tubes were washed with 96% ethanol to minimize the possible interfering signal/ion suppression associated with plastic leakage into solution when using an ESI-interface. Thereafter the Falcon tubes, containing the filtrated sample, were centrifugated at 2576 G for 5 minutes (VWR Mega Star 600R, Germany) and the supernatant was discarded. The remaining algal biomass was then stored at -80 °C in the dark until further sample-preparation and pigment analysis.

3.4 Method development and optimization

3.4.1 Development of the pigment extraction protocol

During the development of an efficient extraction protocol for pigments derived from the marine microalgae *Porosira glacialis*, parameters such as extraction solvents, requirement of re-extractions and extraction time were investigated. All preliminary analysis on extraction configurations were performed on a Waters Acquity™ UPLC (Waters, Milford, MA, USA) coupled to the Orbitrap ID-X Tribrid MS (Thermo Fisher Scientific, Waltham, MA, USA) with configurations as described in segment 3.7.1 and 3.7.2. The final extraction procedure is specified in section 3.5.1

3.4.1.1 Extraction solvents

The extraction solvent of the study was chosen by exploratory testing extraction efficiency of pigments from residual samples of *P.glacialis* from previously conducted studies (November-21), utilizing five different extraction solvents. The examined extractants were selected based on literature searches and are listed in Table 3. Extractions were carried out in triplicates for each extraction solvent and the resulting extraction efficiency was measured by peak area.

Table 3:Extraction solvents tested to establish an extraction protocol of pigments from P.glacialis

Extraction solvent	Acetone (%)	Methanol (%)	2-propanol (%)	Milli-Q® water (%)
1	90			10
2		90		10
3			90	10
4	50	50		
5	50		50	

3.4.1.2 Extraction duration

Extraction duration was experimentally tested, alternating between four extraction times as listed in Table 4. Each treatment was performed in triplicates.

Table 4: Extraction time configurations tested for the development of an extraction protocol for pigments derived from P.glacialis

Extraction time (min)
5
15
30
60

3.4.1.3 Number of extractions needed

To evaluate whether a single extraction was sufficient for a high pigment recovery, a second extraction of the same algae pellet was conducted. Since only a part of the extract resulting from the first extraction was analyzed, the removal of solvent residue prior to the following extraction, was required. To avoid heat exposure of the algae samples through solvent evaporation, the latter was accomplished by pipette decantation and subsequently, visual examination of pellet desiccation. The necessity of a second extraction was determined based on peak area.

3.4.2 UPLC-MS method development

Prior to analysis of algae samples and creation of the "in-house" pigment spectral database, chromatographic conditions were optimized, and MS parameters were tuned. Unless otherwise stated, samples from the optimization experiments were analyzed on a Waters Acquity™ UPLC connected to the Orbitrap ID-X Tribrid MS with electrospray ionization.

3.4.2.1 Preliminary optimization of UPLC-configurations

The acquired data from initial test runs on pigment standards, revealed a high degree of unwanted peak-shape. In an effort to enable quantitative analysis, different columns were evaluated for the applicability of pigment profiling. In addition, separation conditions were optimized by examination of mobile phase compositions and gradient profiles. The columns, mobile phases and gradient profiles are listed in Table 5, Table 6 and Table 7, respectively. The assessment of peak shape quality was conducted by visual inspection of symmetry.

Table 5: Chromatographic columns tested for UPLC-condition optimization.

	Chromatographic columns
1	Waters Acquity UPLC® HSS T3 1.8µm 1.0 x 100 mm
2	Waters Acquity™ Premier Peptide BEH C18, 130Å, 1.7µm 2.1 x 100 mm
3	Waters Acquity UPLC® BEH C18 1.7µm 2.1 x 50 mm
4	Waters Acquity UPLC® BEH C18 1.7µm 2.1 x 100 mm
5	Waters Acquity™ Premier 100 mm x 2.1 mm 1.7 µm C18

Table 6:Mobile phases tested for UPLC-condition optimization.

	Mobile phases
1	**A:** Milli-Q® water and acetonitrile (50%/50%) with 1 mM ammonium formate (NH$_4$FA) and 0.01% formic acid (FA) **B:** 2-propanol and acetonitrile (49.5%/49.5%) with 1% Milli-Q®water, 1 mM NH$_4$FA and 0.01% FA.
2	**A:** Milli-Q® water with 0.01% FA. **B:** Acetonitrile with 0.01% FA.

Table 7:Gradient profiles for UPLC-condition optimization. Mobile phase consisted of A: Milli-Q® water and ACN (50/50) with 1 mM ammonium formate (NH₄FA) and B: 2-propanol and ACN (49.5/49.5) with 1% Milli-Q® water, 1 nM NH₄FA and 0.01%FA

Gradient profiles

Gradient 1

Time (min)	Flow (ml/min)	%A	%B
Initial	0.5	70	30
7	0.5	5	95
10	0.5	5	95
10.1	0.5	70	30
13	0.5	70	30

Gradient 2

Time (min)	Flow (ml/min)	%A	%B
Initial	0,.5	65	35
8	0.5	5	95
10	0.5	5	95
10.1	0.5	65	35
13	0.5	65	35

Gradient 3

Time (min)	Flow (ml/min)	%A	%B
Initial	0.5	60	40
9	0.5	5	95
10	0.5	5	95
10.1	0.5	60	40
13	0.5	60	40

Gradient 4

Time (min)	Flow (ml/min)	%A	%B
Initial	0.5	70	30
1.5	0.5	53.8	46.2
2.5	0.5	53.8	46.2
7	0.5	5	95
9	0.5	5	95
9.1	0.5	70	30
12	0.5	70	30

3.4.2.2 Preliminary tuning of MS conditions

Preliminary testing of ionization polarity, dissociation method and collision energy on pigment standards were performed with the evaluated parameters summarized in Table 8. Owing to time constraints, no further tuning was carried out.

Table 8: Summary of ion source and MS conditions examined in the optimization process.

MS method development	
Conditions	**Settings**
Ionization polarity*	Positive
	Negative
Dissociation method*	HCD
	CID
Collision energy	Stepped 15, 30,45
	Stepped 30, 45, 60

* Analysis performed on a Vanquish Horizon UPLC (Thermo Fisher Scientific, Waltham, MA, USA) coupled to the Orbitrap ID-X Tribrid MS with electrospray ionization.

3.5 Pigment extraction

The extraction protocol was developed in accordance with previous studies on pigment extraction (49, 50), and parameters as re-extractions, extraction solvents and extraction duration were optimized to establish a pigment extraction method from *Porosira glacialis*. Prior to the extraction, the biomass was freeze-dried and homogenized by spatula mixing. Considering the unstable nature of pigments, all experiments were conducted under dimmish light and minimizing elevated temperatures. Additionally, all plastic equipment utilized was pre-washed with 100% acetone to minimize introduction of plastic to sample solutions.

3.5.1 Extraction method

Approximately 20 mg of freeze-dried algal biomass was weighed into brown vials and the exact mass was noted. Acetone 90% was then added to a concentration of 5 mg/mL and the samples were shaken (250 rpm) for 30 minutes at 5°C. After the extraction approximately 1.5 mL of the extract was pipetted out with a glass pipette into Eppendorf tubes. The Eppendorf tubes were thereafter centrifuged at 1100 G for 5 minutes at 5°C. Subsequently, the supernatant was transferred to LC-vials pre-wrapped with aluminum tape in order to avoid light exposure. All samples were re-extracted by first removing solvent residue followed by repeating the extraction protocol on the same biomass. The pigment extracts were stored in the freezer until analysis, keeping the storage time to a minimum.

3.6 Preparation of samples for analysis

All samples prepared for analysis are followingly described with an illustration of the sample preparation workflow provided in Figure 12.

Algae samples: The extract from each parallel of the associated light regime was split in triplicates. Due to low yield, the three biological replicates cultivated under red light were combined into a single replicate in order to obtain sufficient biomass for analysis. The total number of extracted parallels was 7, resulting in 21 samples prepared for analysis.

Re-extracted algae samples: After the first extraction, the 7 parallels were re-extracted. During the re-extraction, parallel 2 of the blue light regime was destroyed and subsequently removed from the analysis. As for the first extraction, each parallel was transferred to three LC-vials, producing a total of 18 samples for analysis.

Blank sample: A system blank was created by adding 4 mL of extraction solvent to an empty 8 mL brown vial and subsequently follow the same extraction procedure as for the algae samples (section 3.5.1).

Qc/ID-sample: The Qc/ID-sample was produced by transferring 200 µL of all algae samples into a HPLC-vial, resulting in a pooled sample representing an average of all samples to be analyzed.
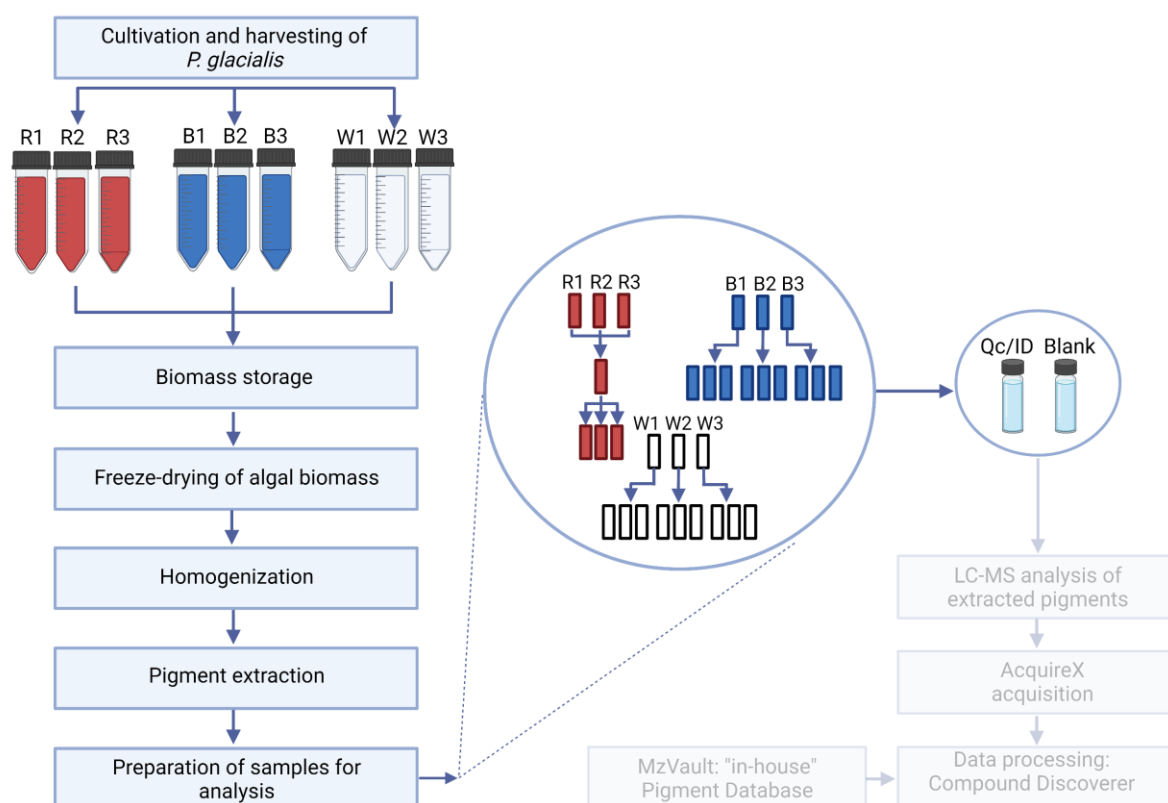

Figure 12: Sample preparation workflow. Created with BioRender.com

3.7 UPLC-MS analysis

3.7.1 UPLC configuration

The liquid chromatographic separations were performed on a Waters Acquity™ UPLC (Waters, Milford, MA, USA) system equipped with a Waters Acquity™ Premier C18 reversed phase column with dimensions of 100 mm x 2.1 mm and 1.7μm particles. The injection volume was 2 μL, and the flow rate was set at 0.5 ml/min. The chromatographic system was composed of a binary pump (Binary Solvent Manager, Waters) and an autosampler (Sample Manager, Waters) set to maintain a temperature of 5°C. Mobile phase A consisted of 50:50 Milli-Q® water/ACN and mobile phase B of 49.5:49.5:1 2-propanol/ACN/Milli-Q® water. Both mobile phase A and B contained 1 mM ammonium formate (NH_4FA) and 0.01% formic acid (FA). The initial condition of the mobile phases were 65% phase A and 35% B and the employed gradient was: from 0-7 min, a linear gradient to 95%B and maintained at 95%B from 8 min to 10 min (Table 7, Gradient profile 2). The column temperature was set to 60°C ±2 and needle wash was performed with 10μL/s Milli-Q® water /MeOH (3:1, v/v) for 5 seconds.

3.7.2 MS configuration

All experiments were performed on an Orbitrap ID-X Tribrid MS (Thermo Fisher Scientific, Waltham, MA, USA) with a heated electrospray interface (H-ESI) operating in positive ionization. The H-ESI parameters in positive polarity were the following: static electrospray voltage of 3500V positive; sheat gas of 20 arbitrary units (arb); and auxiliary gas and sweep gas of 10 and 2 arb, respectively. The ion transfer tube operated at 300°C and the vaporizer temperature was set to 350°C. The mass spectrometer was calibrated using Easy-IC; fluoranthene calibration solution.

3.7.2.1 Full scan setup

Full scans were acquired by utilization of the orbitrap detector with a resolution of 120 000 FWHM, a scan range (m/z) of 150-1500 in positive polarity by quadrupole isolation, an automatic maximum injection time mode, a standard automatic gain control (AGC) target, 1 microscan and RF lens set to 60%. The source fragmentation was disabled, and a profile data type was selected. The full scan method was configured as master scans for the MS^2 acquisitions, further specified in the next segment.

3.7.3 MS^2 acquisition

For the MS^2 analyses, three different methods were utilized: 1) a standard HCD data-dependent MS^2 method, 2) a HCD data-dependent MS^2 method with a targeted mass list, and 3) an AcquireX experimental workflow for analysis of pigment extracts.

3.7.3.1 Data-dependent acquisition with HCD

Samples from preliminary optimization experiments were analyzed in triplicates, using a conventional DDA method. The configuration was set up to perform one master scan every second whereby ions over an intensity threshold of 2.0e4 was fragmented by HCD dissociation. After fragmentation, the precursor ion was excluded for 10 seconds (dynamic exclusion). The HCD fragmentation and scan configurations of the MS^2 method are listed in Table 9.

Table 9:Configuration of HCD fragmentation and scan in the ddMS^2 method.

ddMS2 OT HCD

Configuration	Setting
Isolation Mode	Quadrupole
Isolation Window (m/z)	1.6
Isolation Offset	Off
Activation Type	HCD
Collision Energy Mode	Stepped
HCD Collision Energy Type	Normalized
HCD Collision Energies (%)	15,30,45
Detector Type	Orbitrap
Orbitrap Resolution	60000
Scan Range Mode	Auto
AGC Target	Standard
Minimum Injection Time Mode	Auto
Microscans	1
Data Type	Centroid
Use EASY-ICTM	False

3.7.3.2 Targeted data-dependent HCD acquisition

The pigment standards were analyzed using a ddMS^2 method including a target mass list. The configurations of the master scan were equal to the settings described in section 3.7.2.1, except scan range (m/z), which was reduced to 500-1000. The HCD fragmentation and scan conditions were kept as described in Table 9 apart from the quadrupole isolation window and orbitrap resolution, which was lowered to 0.4 and 30 000, respectively. The development of the targeted acquisition of standard samples was a consequence of impurity and low pigment abundance, resulting in absence of fragmentation/lower fragmentation data quality. Thus, the development of the presented method was required in order to create the "in-house" spectral library. The targeted mass list of the acquisition composed the m/z-value corresponding to both the radical $[M^*]^+$- and proton adduct $[M+H]^+$ of the pigment standards, to a total of 34 m/z values. For the comprehensive target mass list see Appendix B.1 Target mass list for ddMS^2 HCD acquisition. The method workflow is illustrated in Figure 13.
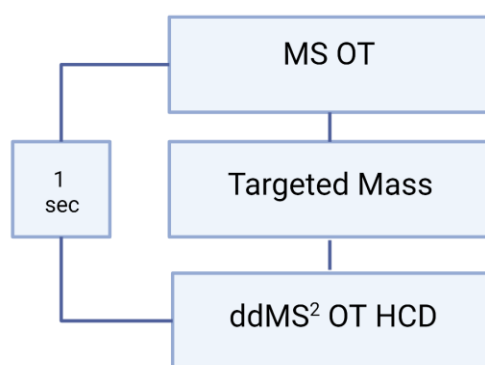

Figure 13:Workflow of the targeted MS2 method. Every 1 second the orbitrap mass scan (MS OT) checks the target mass list before HCD fragmentation occurs. Created with BioRender.com

3.7.3.3 Acquisition workflow for analysis of pigment extracts

Algae extracts were analyzed using the AcquireX Data Acquisition Technology (Thermo Fisher Scientific, Waltham, MA, USA) in Deep scan (DS) mode. The AcquireX workflow is illustrated in Figure 14, with a peak intensity threshold at 1.0e5. The acquisition was set to identify proton adducts. Ideally, radical adducts should have been included, but a corresponding setting option was not available. Configurations for the full scan and master scans were as described in section 3.7.2.1 and settings for MS^2 acquisition as listed in Table 9, except a decrease of resolution power to 30 000.
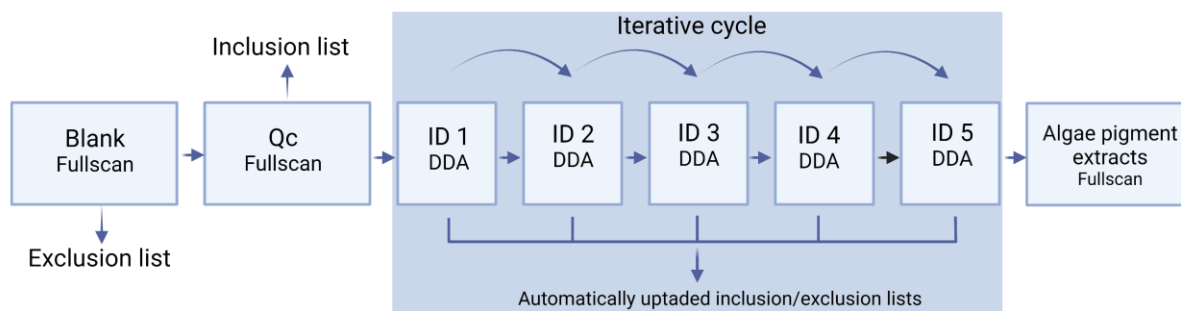
Figure 14:AcquireX acquisition workflow. The generation of an initial exclusion and inclusion list was disabled in the current study. Created with BioRender.com

From Figure 14, the injection sequence is initiated by running three blank samples (for sample preparation details see section 3.6). Normally, exclusion and inclusion lists are automatically generated after the injection of a blank and a pooled sample in full scan, respectively. As a result of software difficulties with connecting analytical instruments (UPLC-MS) from different vendors (resp. Waters, Thermo Fisher Scientific), the latter functions were disabled. Following injection of the blanks, the ID sample used to create MS^2 scans was injected, with an iterative cycle of 5. Lastly, the algae pigment extracts were injected in full scan mode. In between algae samples cultivated under different light regimes, an injection of the Qc sample was conducted. A total of 32 injections were analyzed, resulting in a runtime of approximately 7 hours. The complete injection sequence is listed in Appendix B.2 Injection Sequence of the Acquire X acquisition.

3.8 Spectral pigment library

To build an Accurate Mass Retention Time (AMRT) database, a pooled sample of the purchased pigment standards was analyzed utilizing the target $ddMS^2$ method (see section 3.7.3.2). The acquired RAW files were processed with MzVault (Thermo Fisher Scientific) for the creation of the fragmentation library. The most abundant adduct for each pigment standard was considered and the best fragmentation spectrum was automatically selected by the software`s algorithm. All spectra included in the library were manually reviewed. The following parameters were evaluated: Retention time in alignment with preliminary runs, presence of molecular ion, a sufficient number of fragments and signal intensity.

3.9 Data processing

Post-acquisition data processing was performed for identification/annotation and structural characterization of pigments/compounds of interest. Raw files were processed by Compound Discoverer 3.3 (Thermo Fisher Scientific) and identifications were achieved by spectral matching with data from the AMRT database developed in MzVault (Thermo Fisher Scientific). Subsequently, tentative identifications/annotations were performed by comparison with online libraries and databases such as mzCloud library(ddMS^2), LipidBlast in-silico library(ddMS^2), ChemSpider and LipidMAPS databases (formula or exact mass). The AUC of the identified pigments was extracted from Compound Discoverer and exported to R for further statistical analysis. The Compound Discoverer workflows and a description of each node are provided in Appendix C.1 Compound Discoverer parameters. Additionally, data from preliminary optimization experiments were manually analyzed in Freestyle (Thermo Fisher Scientific).

3.10 Statistical analysis

The data from preliminary optimization experiments was analyzed by Microsoft Excel® and are expressed as means ± standard deviation. In addition, the relative standard deviations are provided in the corresponding tables. One-way analysis of variance (ANOVA) was utilized to determine whether a significant difference in peak area for selected preliminary samples was present (<10). Significance level was set to 0.05.

Data on pigment content in response to irradiance wavelength obtained from Compound Discoverer were analyzed by R. Data were considered significantly different if $p<0.05$ using a pairwise Tukey test.

3.11 Visual abstract of the sample preparation and analysis of pigments derived from *P.glacialis*
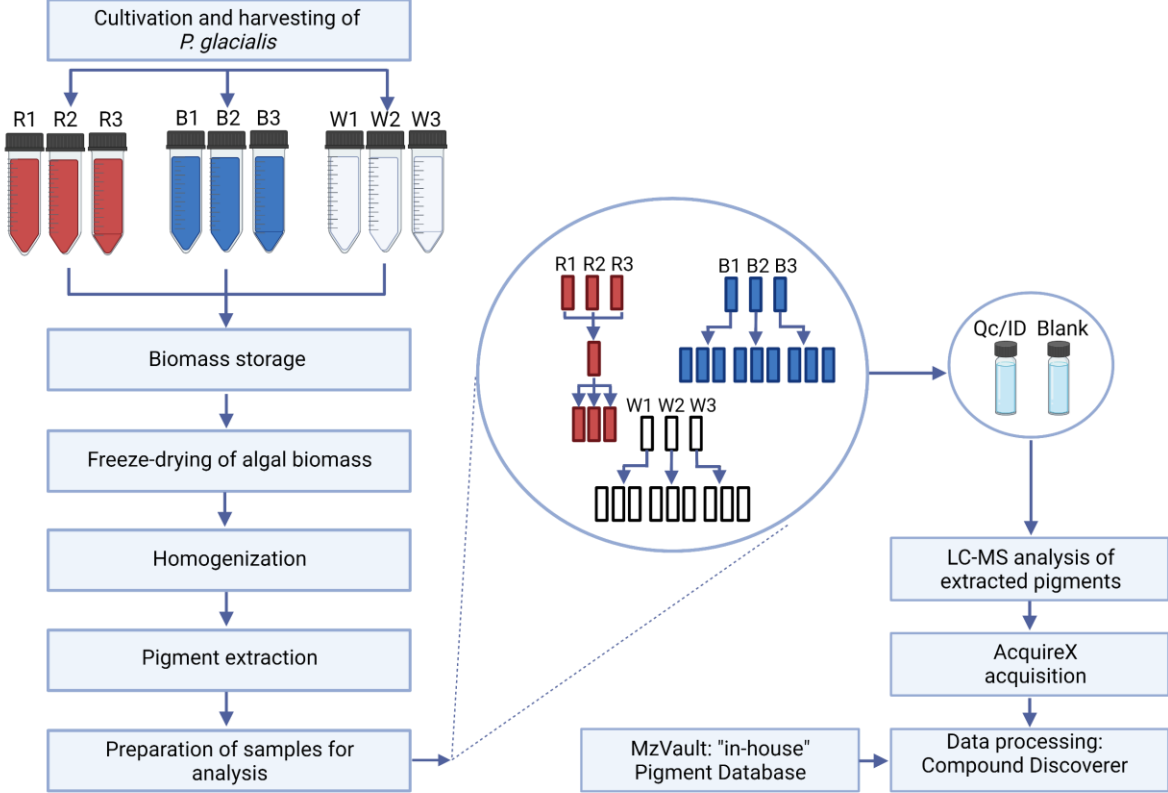

Figure 15: Flowchart of the sample preparation and analysis of pigments derived from P.glacialis. Created with BioRender.com

4 Results and discussion

4.1 Pigment extraction protocol

4.1.1 Effect of extraction solvent

The pigment content of *P. glacialis* was extracted with five different extraction solvents and compared with respect to peak area. Preliminary extractions were performed on residual *P.glacialis* biomass cultivated in November 2021 and pigments were identified by exact m/z and retention time equal to a reference standard. Aqueous acetone (90%) was found to give the highest extraction recoveries for most of the investigated pigment classes and selected as the extraction solvent in the present study. A total of 15 pigments, representing the xantophylls, carotenes and chlorophylls, were extracted by the extraction solvents listed in Table 10, hereupon referred to by their corresponding abbreviation.

Table 10:The extraction solvents tested for pigment recovery from P.glacialis, with the corresponding abbreviation utilized in this section.

Extraction solvent	Abbreviation
90% Acetone	E1
90% Methanol	E2
90% 2-propanol	E3
50%/50% Methanol/Acetone	E4
50%/50% Acetone/2-propanol	E5

Relative extraction yields, expressed as peak area, of β-carotene, fucoxanthin and chlorophyll *a* in different extraction solvent mixtures are depicted in Figure 16, representing the three pigment classes included in the study. Extraction efficiencies appeared similar in all five solvents with E1 returning the highest AUC for both fucoxanthin and chlorophyll *a* ($9.71e^8$ $\pm 1.89e^7$ and $1.41e^9$ $\pm 5.15e^7$, respectively). E5 returned the highest peak area of β-carotene ($6.38e^7 \pm 2.68e^6$) with E1 as the second highest ($6.19e^7$ $\pm 6.26e^6$). Mean peak areas for all pigments evaluated with standard deviation and relative standard deviation are listed in Appendix D.1.1 Effect of extraction solvent.
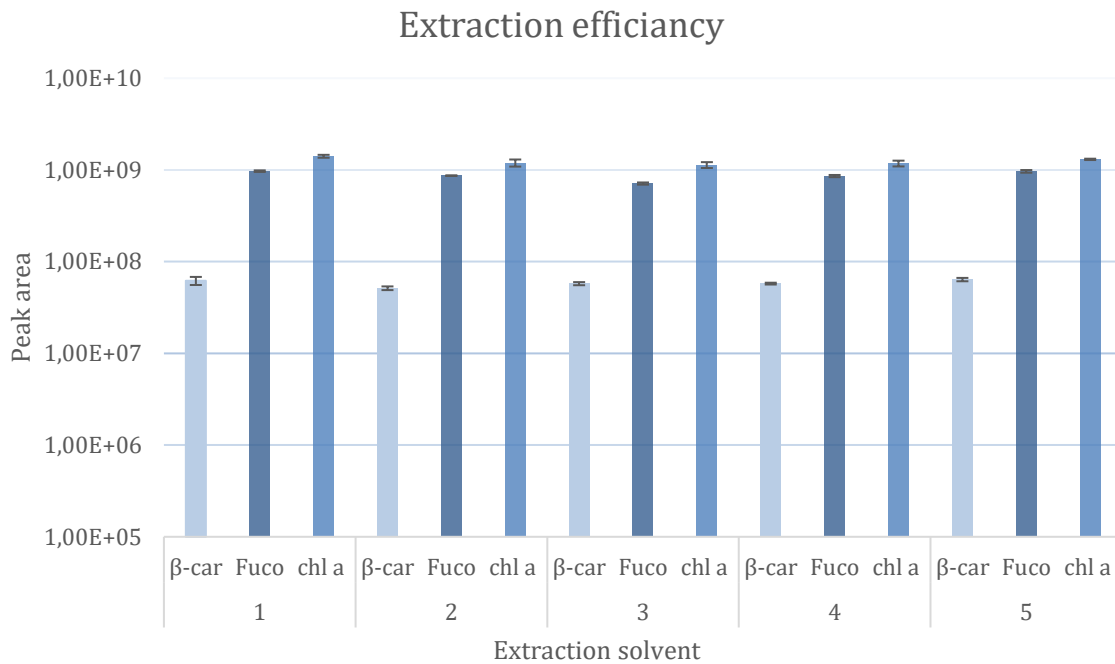
Figure 16:Extraction efficiency expressed as mean peak area with brackets representing the SD of β-carotene (β-car), fucoxanthin (Fuco) and chlorophyll a (Chl a) achieved by altering the extraction solvents listed in Table 10.

Several pigment class specific patterns were observed such as E1 and E5 giving the highest recoveries for the xanthophylls, followed by E1 and E4 for the chlorophylls. E2 and E3 had the lowest extraction efficiency for the xantophylls and chlorophylls, respectively. The lower yield of chlorophylls extracted by 2-propanol compared to the more polar extraction solvents could be attributed to the polar nature of chlorophylls, leading to an enhanced affinity for polar solvents and thereby an increased solubilization. Methanol has been reported to be superior to acetone in terms of extraction efficiency of xanthophylls (19, 51), which is inconsistent with the reduced extraction efficiency of the solvent found in this experiment. A suggested rationale for the latter finding is a decreased pigment stability in methanol, leading to xanthophyll degradation (52).

The peak area obtained for β-carotene extracted with E2 was $5.14e^7 \pm 2.36e^6$, which is significantly lower compared to the E5 extraction method, which yielded the highest β-carotene recovery (p<0.05). Applying the same principle as for the chlorophylls extracted with 2-propanol, non-polar carotenoids such as β-carotene favors a solvent of lower polarity. A study on solvent regimes for the extraction of pigments from higher plants found a low β-carotene

58

recovery utilizing methanol as extractant and suggested that methanol based methodologies for pigment extraction led to an underestimation of β-carotene content (53).

Overall, extraction with 2-propanol and methanol gave the lowest extraction efficiencies for chlorophylls and carotenoids, respectively. In comparison with the extraction solvent which yielded the highest extraction efficiency, a reduced recovery of approximately 20% was observed when utilizing the former solvents for β-carotene, fucoxanthin and chlorophyll *a* extraction. Other than methanol and 2-propanol, the choice of extraction solvent had a modest effect on total pigment recovery with aqueous acetone and acetone/2-propanol mixture showing the highest extraction efficiency for all pigments included. A slightly higher pigment yield was obtained by employing 90% acetone as extractant for most of the pigments compared to the latter solvent mixture. Accordingly, 90% acetone was selected as extractant for the current pigment profiling.

4.1.2 Extraction time effect

Aqueous acetone presented the most promising results concerning pigment extraction yield from *P. glacialis* (section 4.1.1) and accordingly, the effect of including a mixing treatment to increase pigment yield was examined applying this extraction method. Four treatments (5, 15, 30 and 60 minutes) were tested following solvent addition, using an orbital shaker placed in the dark at 5°C. Treatment length was found to influence the pigment yield of all pigment classes and an extraction duration of 30 minutes was established as the optimal time to ensure maximal pigment recovery.

Table 11: Mean peak area of β-carotene, fucoxanthin and chlorophyll a obtained at different extraction durations. The corresponding standard deviation (SD) and relative standard deviation (RSD) are displayed.

Extraction time				
Time (min)		β-carotene	Fucoxanthin	Chlorophyll a
5	Mean area	4.63E+07	8.89E+08	1.17E+09
	SD	1.44E+06	1.99E+07	8.14E+06
	RSD%	3.10	2.24	0.69
15	Mean area	4.94E+07	9.47E+08	1.18E+09
	SD	3.53E+06	7.45E+07	4.86E+07
	RSD%	7.16	7.87	4.13
30	Mean area	5.21E+07	9.59E+08	1.21E+09
	SD	1.80E+06	3.70E+07	3.15E+07
	RSD%	3.45	3.85	2.59
60	Mean area	5.06E+07	9.34E+08	1.21E+09
	SD	2.90E+06	3.22E+07	4.05E+07
	RSD%	5.72	3.44	3.35

The extraction yields expressed as peak area of β-carotene, fucoxanthin and chlorophyll *a* are displayed in Table 11, representing the different pigment classes. Thirty minutes was sufficient to achieve maximum yield for all three classes. The enhanced recovery during the interval of 5-30 minutes was seen for all pigments included, except zeaxanthin which reached the maximum peak area after 15 minutes.
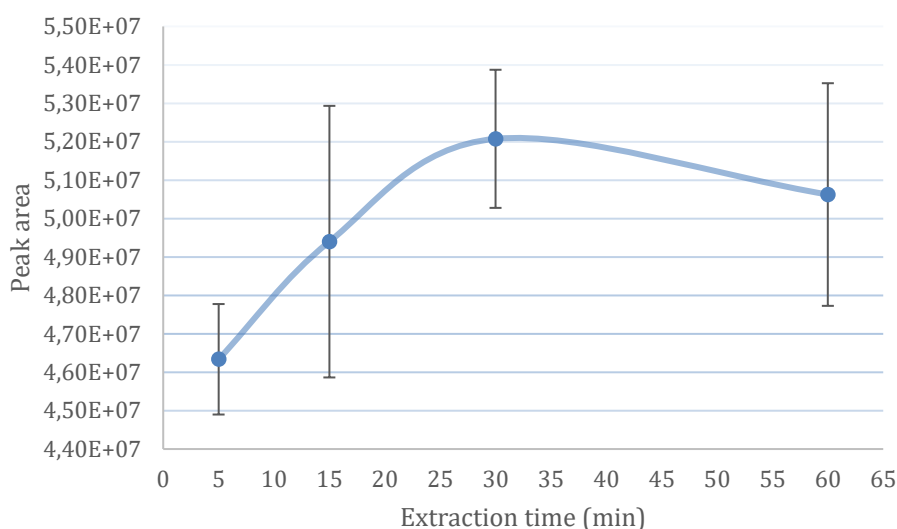
Figure 17:Mean peak area of β-carotene in relation to extraction time utilizing 90% acetone as the extraction solvent. The brackets represent the SD for each duration set-up.

The extraction efficiency of β-carotene displayed by peak area as a function of extraction time is showed in Figure 17, visualizing the trend of an initial increased yield followed by reaching the curve peak and thereupon for β-carotene, a decrement in yield. As the contact time between pigments and solvent increases, the extraction yield is expected to increase correspondingly until reaching saturation, which is consistent with the initial enhanced peak area upon reaching a 30-minute extraction duration (54). The observed reduction in peak area for some pigments at 60 minutes might imply degradation, either by the solvent utilized (55) or external factors (i.e., increased temperatures or light exposure).

Based on these results, 30 minutes of mixing was chosen as the optimal treatment for pigment extraction. However, statistical analyses revealed, for instance, an insignificant difference in extraction yield for β-carotene, fucoxanthin and chlorophyll *a* between the extraction durations of 15 and 30 minutes (p>0.05). Although this finding might have been affected by imprecise extraction performance owing to a relatively small amount of extracted microalgae biomass (20 mg), omitting internal standard and a low number of included parallels (n=3), further investigation is of interest to minimize the cost associated with increased time of analysis. Mean peak areas for all pigments relative to the time configurations with standard deviation and relative standard deviation are listed in Appendix D.1.2 Effect of extraction duration.

4.1.3 The influence of multiple extractions

The peak area of 13 pigments resulting from the first extraction was compared with peak area of a second extraction of the remaining pellet in order to evaluate the necessity of multiple extractions to the total pigment yield. The added peak area achieved by performing one re-extraction for pigments cultivated in blue light utilizing 90% acetone as extractant and a 30-minute extraction duration showed a minor increase for 9 pigments ($\leq 10\%$) and a greater contribution to the total peak area ($\geq 12\%$) for 4 pigments. Although a slight difference between the added peak area of multiple extractions among the cultivation regimes was observed, the results imply a pigment dependent effect of a second extraction. Subsequently, the finding suggests inclusion of multiple extractions to be based on pigments of interest.

The peak areas obtained from the initial extraction and a secondary extraction of fucoxanthin from microalgae cultivated in blue light are depicted in Figure 18, which were $9.20e^8$ ($\pm 4.67e^7$) and $2.14e^7$ ($\pm 5.38e^6$), respectively. The contribution of the mean peak area of the second extraction to the total peak area was 2.28%, indicating a high initial extraction efficiency and further extractions to be of minor importance for the total yield of fucoxanthin.
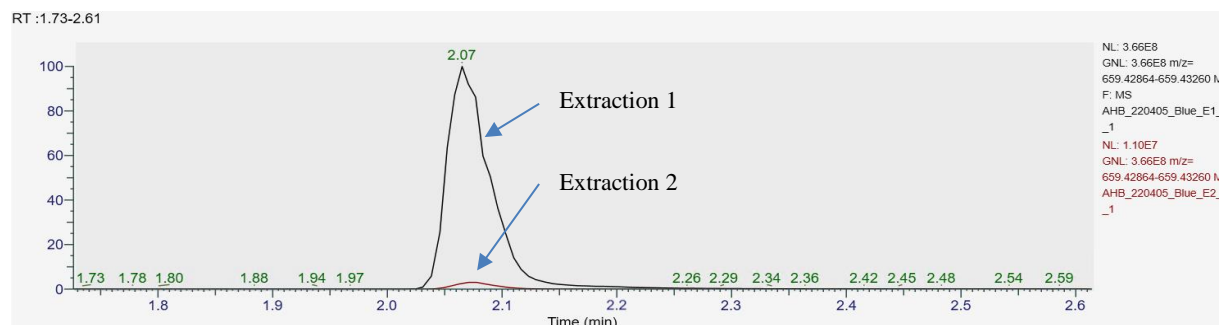

Figure 18: Extracted ion chromatogram (XIC) of fucoxanthin cultivated in blue light (parallel 2). The chromatogram overlays two XIC of fucoxanthin, in which the black peak represent the first extraction of fucoxanthin and the red peak, the second extraction. Extraction two is normalized to extraction one.

Although a single extraction was sufficient for the fucoxanthin recovery, the initial extraction efficiency of diadinoxanthin, zeaxanthin, chlorophyll *a* and β-carotene was observed to be lower compared to the majority of the included pigments under all employed light irradiances (results from the blue light regime is listed in Table 12). Considering the elution order from the RP column, these pigments interact stronger with the octadecane chain compared to most of the studied pigments, implying a more hydrophobic characteristic of these compounds. An enhanced lipophilicity might cause these pigments to possess a lower partition ratio in the

applied system and by replacing the saturated extract with additional extraction solvent, their recovery is expected to increase (33). An alternative is to perform the second extraction with an extraction solvent of lower polarity, which might further increase the extraction efficiency of more hydrophobic pigments. However, the amount of other lipids might increase by applying such a strategy and requires further examination.

Table 12: Mean peak areas obtained by the initial extraction (E1) and the second extraction (E2) from P. glacialis. Standard deviation (SD), relative standard deviation (RSD%) and the contribution of a second extraction to the total peak area (%) are displayed.

				Blue light			
	E1			**E2**			
Pigment	**Mean**	**SD**	**RSD%**	**Mean**	**SD**	**RSD%**	**%E2/total**
Fucoxanthin	9.20E+08	4.67E+07	5.08	2.14E+07	5.38E+06	25.1	2.28
Diatoxanthin	6.84E+06	7.69E+05	11.2	1.28E+06	4.60E+05	35.8	15.8
Violaxanthin	6.86E+06	1.61E+05	2.35	2.36E+05	4.97E+04	21.1	3.33
Pheophytin *a*	1.10E+09	1.92E+08	17.5	7.44E+07	9.48E+06	12.8	6.31
Zeaxanthin	8.00E+04	1.90E+04	23.7	1.14E+04	1.20E+03	10.6	12.4
Chlorophyll *c2*	1.12E+07	8.99E+05	8.02	1.25E+06	1.92E+05	15.3	10.1
Diadinoxanthin	6.75E+07	6.24E+06	9.25	4.79E+06	1.51E+06	31.6	6.63
Chlorophyll *c1*	7.06E+06	8.53E+05	12.1	7.61E+05	1.47E+05	19.4	9.74
Chlorophyll *a*	1.26E+09	2.97E+07	2.37	2.02E+08	4.63E+07	22.9	13.9
Chlorophyll *b*	3.39E+06	2.21E+05	6.52	8,09E+04	2.47E+04	30.5	2.33
β-carotene	3.09E+07	2.08E+06	6.74	6.65E+06	8.27E+05	12.4	17.7
Antheraxanthin	2.93E+06	9.49E+04	3.24	1.65E+05	3.22E+04	19.5	5.33
Alloxanthin	3.85E+06	3.69E+05	9.57	1.48E+05	4.48E+04	30.3	3.70

From Table 12 a relatively high standard deviation is seen for all pigments of the second extraction. This could be a consequence of the re-extraction performance, in which microalgae pellet desiccation was conducted by pipette decantation in order to avoid pigment degradation through solvent evaporization (for method description see section 3.4.1.3). The added yield achieved by a second extraction might therefore be a result of diluted residue extract from the former extraction. However, as the previous mentioned trend of an increased contribution of a second extraction for the same pigments in all light regimes was observed, an enhanced extraction efficiency by performing a second extraction is plausible. In addition, the standard deviations of the second extraction for samples cultivated in red and white light were comparatively lower. Mean extraction efficiency for all pigments evaluated with corresponding standard deviation and relative standard deviation are tabulated in Appendix D.1.3 Re-extraction requirement.

4.2 UPLC-MS method development

4.2.1 Performance comparison of different columns

The performance of five different columns was compared based on peak shapes of pigment standards revealed through initial test runs. Aside from a variation in pigment elution time, the comparative chromatograms showed an insignificant difference in peak quality. Consequently, the column selection was based on time of analysis and laboratory convenience and hence the Waters Acquity™ Premier 100 mm x 2.1 mm 1.7 µm C18 column was chosen.

Data from initial analysis displayed violaxanthin as one of the pigment standards with lowest peak shape quality (Figure 19), presenting chromatograms consisting of multiple peaks with an observed retention time range of approximately 3 minutes. Five different octadecyl UPLC columns were for this reason assessed for their ability to achieve, preferably, Gaussian peak shapes for the AMRT database creation, sensitivity enhancement, separation optimization and integration reproducibility. To limit both the time consumption and quantity of pigment standard utilized, only two selected pigment standards were tested on all columns, violaxanthin and β-carotene. The latter pigment standard was chosen due to possessing the highest retention time.

The acquired chromatograms of violaxanthin and β-carotene showed marginal differences in peak shape quality with regards to visual comparison of peak symmetry. However, the retention time of β-carotene increased by 1 minute on the Waters Acquity UPLC® HSS T3 1.8µm 1.0 x 100 mm column (data not showed), which is in line with previous studies comparing retention times of carotenoids between the BEH 18 and HSS T3 columns (56, 57). Consequently, the latter column was excluded from the pigment profiling of this project and the choice between the remaining four columns was conducted according to the most frequently used UPLC column for lipid analysis at the research laboratory of the study, namely the Waters Acquity™ Premier 100 mm x 2.1 mm 1.7 µm C18 column.
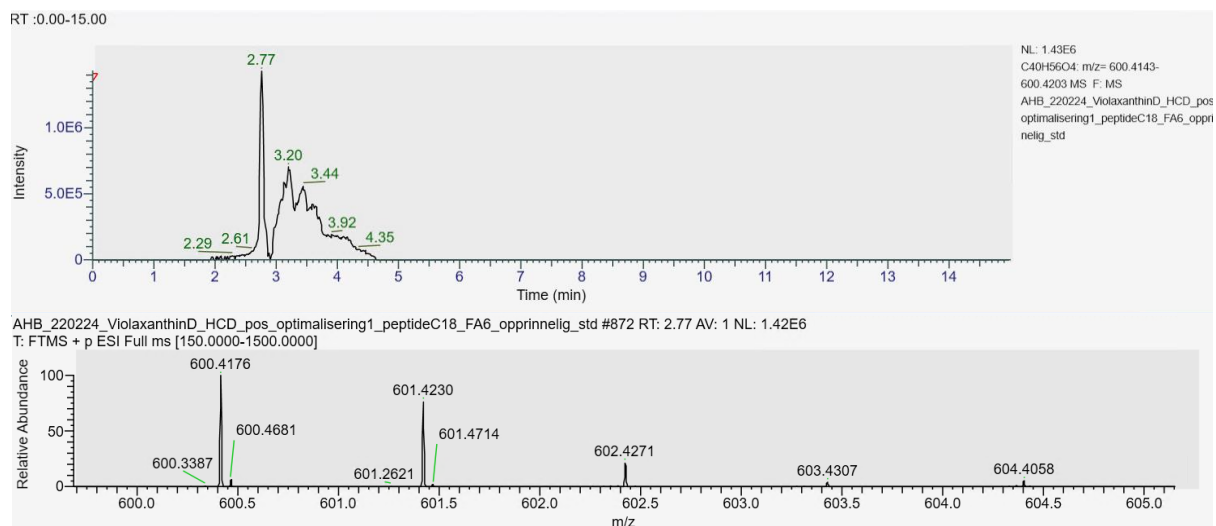
Figure 19:XIC of violaxanthin standard with the corresponding full scan spectrum at RT=2.77 min. Chromatographic column; Waters Acquity™ Premier Peptide BEH C18, 130Å, 1.7μm 2.1 x 100 mm, prior to gradient optimization.

The peak shape of violaxanthin displayed in Figure 19 shows a base peak presumably separated from the second shoulder peak and a full scan mass spectrum corresponding to the base peak of the XIC. The isotope distribution of violaxanthin at the base peak of the chromatogram was found to appear throughout the following shoulder peak and as means to investigate whether violaxanthin was present in the more retained peaks with lower intensity, the fragmentation pattern of the molecular radical ion at the corresponding retention times were considered and are displayed in Figure 20 and Figure 21.
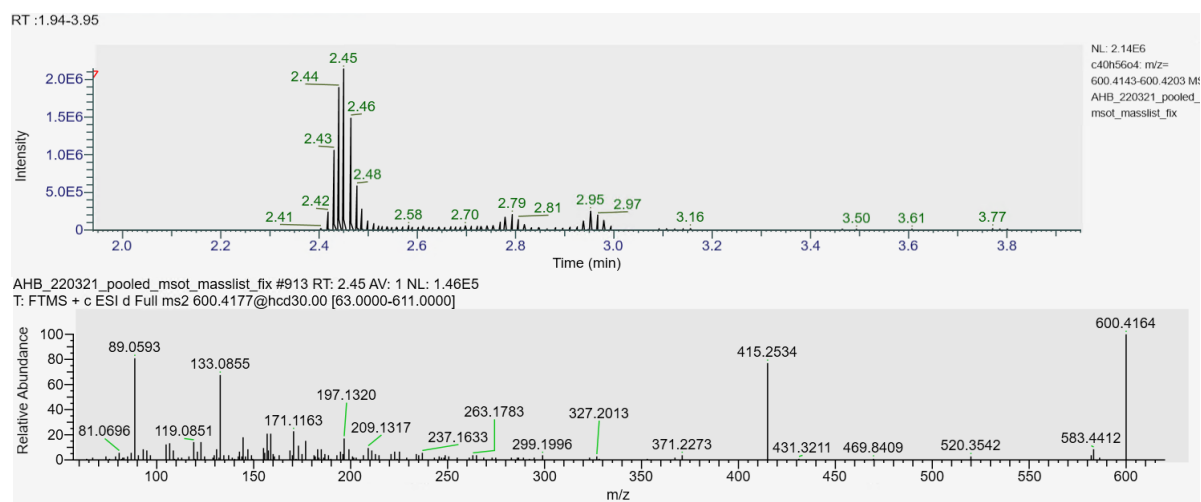

Figure 20:The upper chromatogram displays a XIC of the violaxanthin standard and the lower spectrum is showing the MS^2 scan of violaxanthin cation at RT=2.45. The fragmentation was obtained by utilization of the targeted ddMS^2 method.
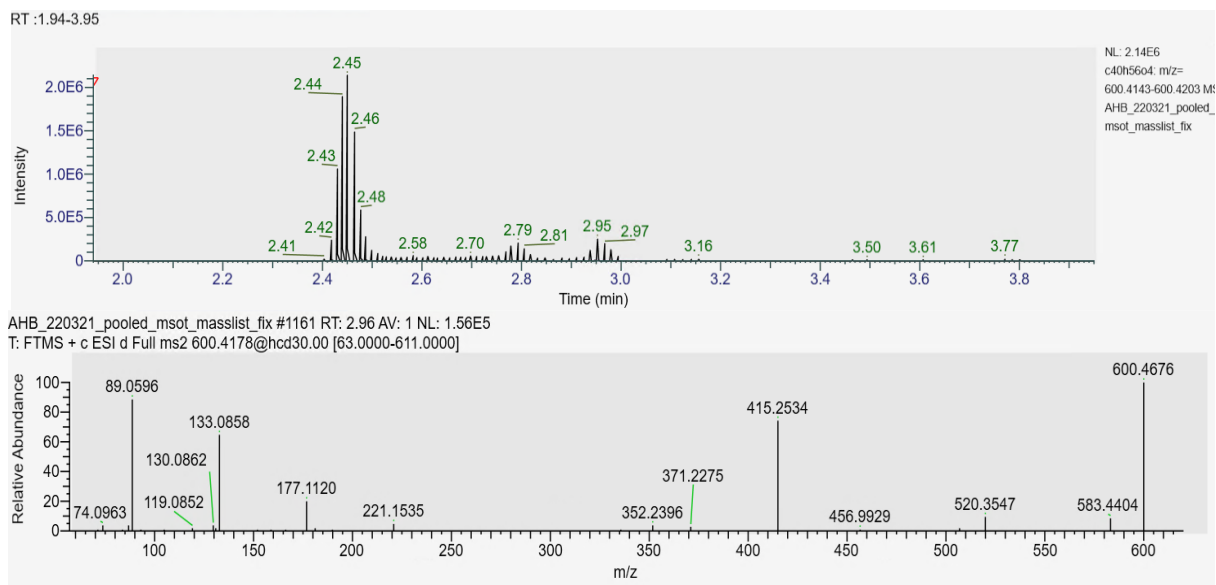
Figure 21:The upper chromatogram displays a XIC of the violaxanthin standard and the lower spectrum is showing the MS^2 scan of violaxanthin cation at RT=2.96. The fragmentation was obtained by utilization of the targeted ddMS^2 method.

The comparison of molecular ion (m/z=600.4178) fragmentation spectra of the peaks with distinct retention times revealed highly similar fragmentation patterns (Figure 20 and Figure 21). Although the lower intensity peaks displayed a decreased number of fragments, the most abundant daughter ions were present. The similarities of the evaluated MS^2 spectra led to a high probability of the observed peaks to represent violaxanthin. This finding implies the presence of multiple pigment isomers in the purchased carotenoid standards with their existence supported by the literature, stating the presence of optical and geometrical carotenoid isomers in addition to regio isomers (19, 58). A study of carotenoid profile of commercial fruit juice (57) found both the all-E violaxanthin and the geometrical isomer 9Z violaxanthin depicted in Figure 22.
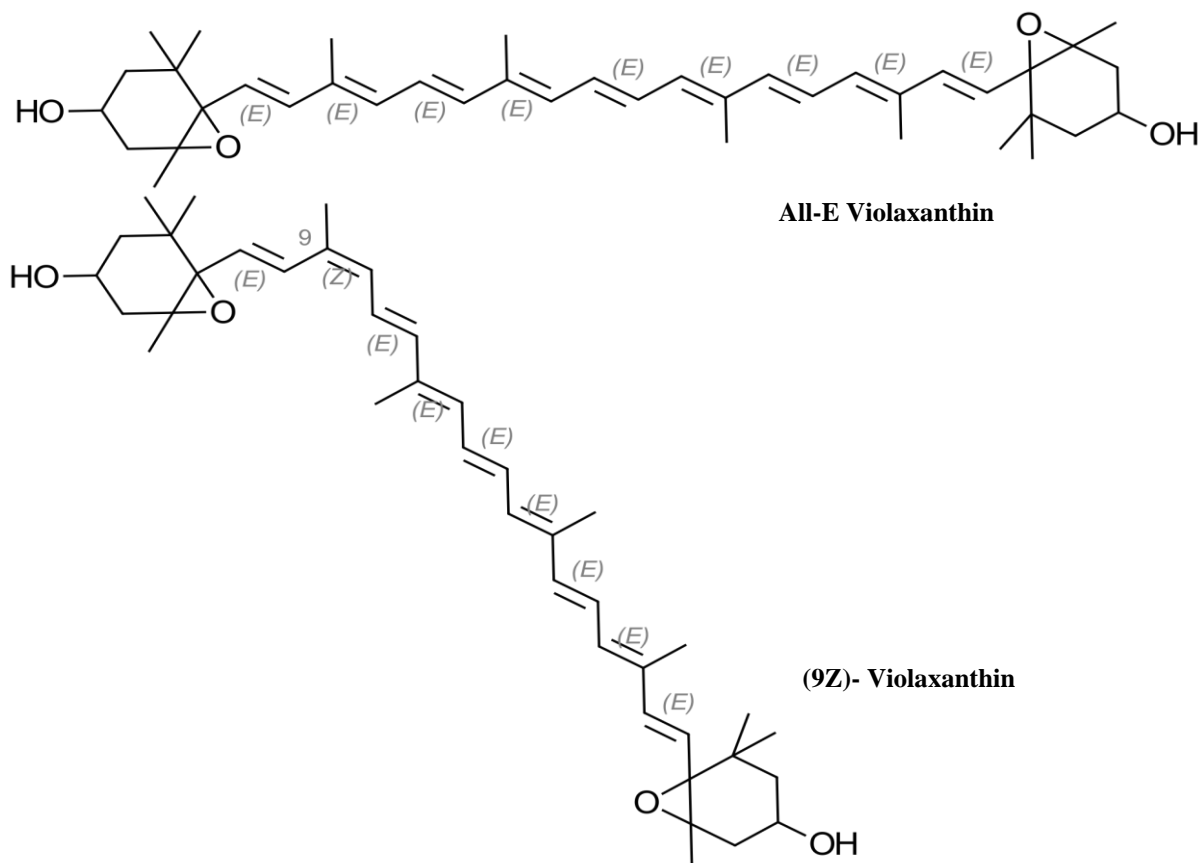
Figure 22: Geometrical isomers of violaxanthin

Isomerization of the carotenoid alkyl chain leads to a considerable alteration in pigment shape and accordingly, the interaction with column particles might vary between isomers of the same pigment. A study on elution order of carotenoids (58), including carotenoid isomers, revaeled a limited separation of geometrical isomers of carotenoid hydrocarbons on a RP C18 column. However, the separation of polar carotenoids was partly achieved with an increased retainment (in the dimension of several minutes) for the cis isomer compared to trans isomer, in addition to an inter pigment variability in successful separation of cis/cis isomers. To further add complexity to the isomer elucidation of pigments, central cis isomers are reported (59) to elute prior to the trans isomers, whereas not centrally located cis isomers are found to be more retained relative to the trans isomer. By making some assumptions, the findings of the aforementioned studies could be applied to evaluate the chromatography of the polar carotenoids of this study (Figure 23) and thus enable isomer trend detection accompanied by possible tentative isomer identifications.
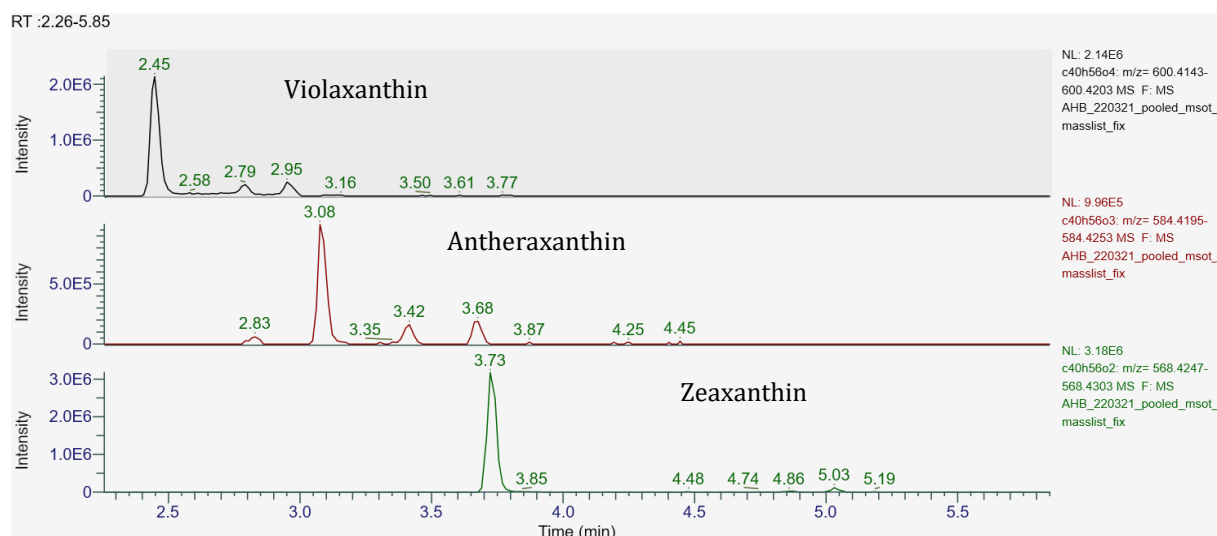
Figure 23: XIC of the polar carotenoids violaxanthin, antheraxanthin and zeaxanthin displaying multiple isomers

Illustrated in Figure 23, the XIC of selected polar carotenoids revealed a trend of multiple peaks with a relatively wide range in elution time. This trend was observed for all polar carotenoid standards, which constituted 12/14 of the included carotenoid standards of the study (listed in section 3.1.1). By considering the pigment standards to contain the all-trans isomer as the major form of carotenoid isomer combined with assuming a degradation of minor importance conducive to the trans/cis ratio difference, permitted a tentative identification of the base peak as the trans isomer. Furthermore, supposing the latter identification was valid, the more retained peaks might represent mono/poly-cis isomers. In addition, the peak eluting prior to the base peak for the epoxy carotenoids (e.g. antheraxanthin, Figure 23) might be explained by the presence of an optical isomer (58) or a not centrally located cis isomer (59).

Based on the discussion on pigment isomerization in this section, the observed peak shape of the pigment standards might imply standards composed of mixed pigment isomers. The impurity might potentially arise from processing (60) or derived from the natural isomer variation in plant and phytoplankton upon the manufacturing of the standards. Additionally, the findings support the UPLC C18 column as promising for polar carotenoid trans/cis isomer profiling.

4.2.2 Optimal chromatographic conditions

In order to improve carotenoid peak shape and optimize pigment separation, preliminary testing of two mobile phase compositions and four gradient profiles were performed. The most suitable chromatographic conditions found applicable for the current pigment profiling were a 10-minute gradient elution with a mobile phase composed of Milli-Q® water, acetonitrile, 2-propanol, ammonium formate and formic acid (detailed in section 3.7.1).

The most commonly utilized eluents for pigment analysis are low viscosity, polar organic solvents, which are modified to achieve better separation (57), hence the mobile phases examined consisted of a mixture of water/ACN and water/ACN/2-propanol. In the current literature on pigment analysis the inclusion of 2-propanol as a pigment eluent is less frequent, although commonly used in lipid analysis (40). As the initial objective was to obtain high quality peak shapes, analogous to the evaluation of column performance (see section 4.2.1), violaxanthin and β-carotene were selected for the assessment of mobile phases. The acquired chromatography showed negligible differences regarding peak shape quality and a shorter retention time according to the higher eluent strength of 2-propanol (data not shown). Thus, the selected mobile phase was composed of water/ACN/2-propanol.

The gradient was optimized by testing four mobile phase configurations (specifics in section 3.4.2.1) and evaluated based on pigment separation abilities. Due to time limitations the separation of the most abundant pigment isomers was addressed. The examined gradient parameters were the initial eluent strength and the linear gradient duration. The first gradient profile was set up with an initial eluent strength of 30%B and a linear gradient duration of 7 minutes, followed by a 3-minute hold (Figure 24).
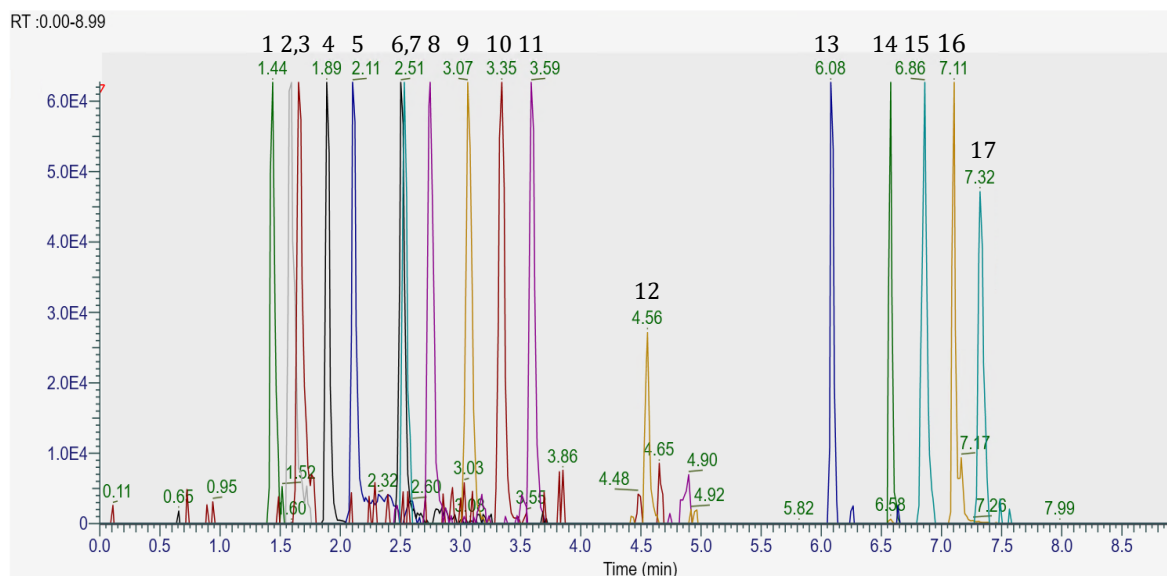
69

Figure 24:Chromatogram for gradient profile 1 described in Table 7, composing an overlaid XIC of all pigment standards. 1=Peridinin, 2=Chlorophyll c₂, 3=Chlorophyll c₁, 4=Fucoxanthin, 5=Violaxanthin, 6=Diadinoxanthin, 7=Astaxanthin, 8=Antheraxanthin, 9=Alloxanthin, 10=Diatoxanthin, 11=Zeaxanthin, 12=Canthaxanthin, 13=Chlorophyll b, 14=Chlorophyll a, 15=Lycopene, 16=Pheophytin a and 17= β-carotene.

Displayed in Figure 24, the separation was incomplete with co-elution of both chlorophyll c_1/c_2 and diadinoxanthin/astaxanthin (depicted in more detail in Figure 25). In addition, the first pigment standard eluted after approximately 1.5 minutes, leaving an empty gap in the chromatogram.
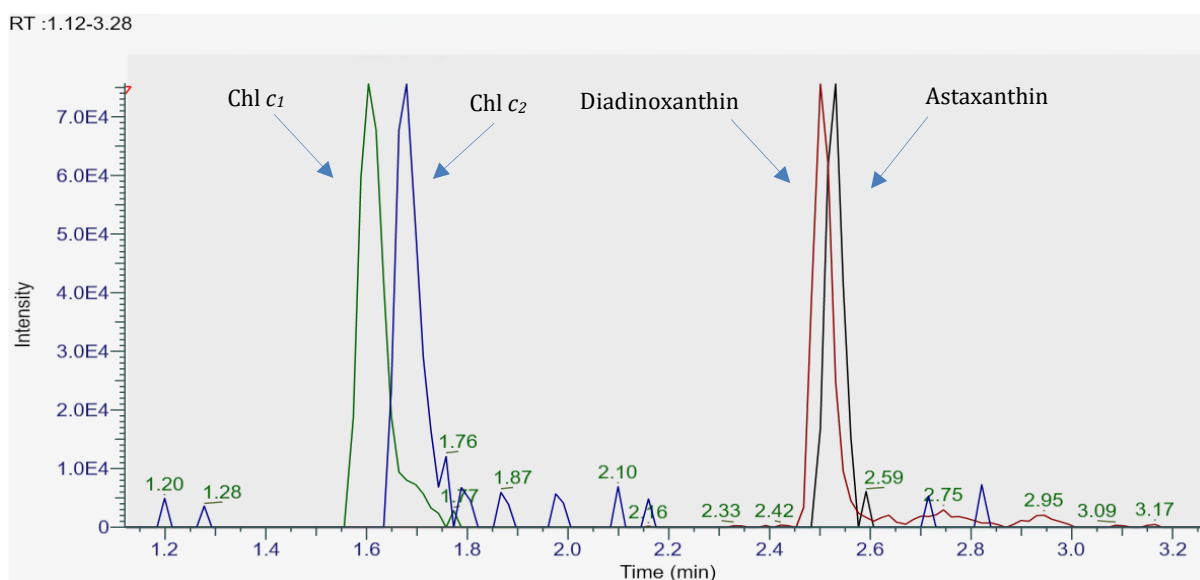

Figure 25:Gradient method 1; XIC of chlorophyll c₁ (Chl c₁), chlorophyll c₂ (Chl c₂), diadinoxanthin and astaxanthin.

70

In order to optimize the separation and simultaneously keep the time of analysis as short as possible, the initial eluent strength was increased to 35% and 40%B combined with altering the linear gradient duration between 7-9 minutes. Additionally, an isocratic hold was examined. The results showed a minor variance in pigment separation capability among the included gradient methods with time of analysis dependent on mobile phase strength. As the gradient with an initial start concentration of 40%B (gradient 3, Table 7) showed a slight decrease in separation ability compared to gradient 2 (initially 35%B, Table 7), the latter was selected with a linear gradient duration of 7 minutes (Figure 26).
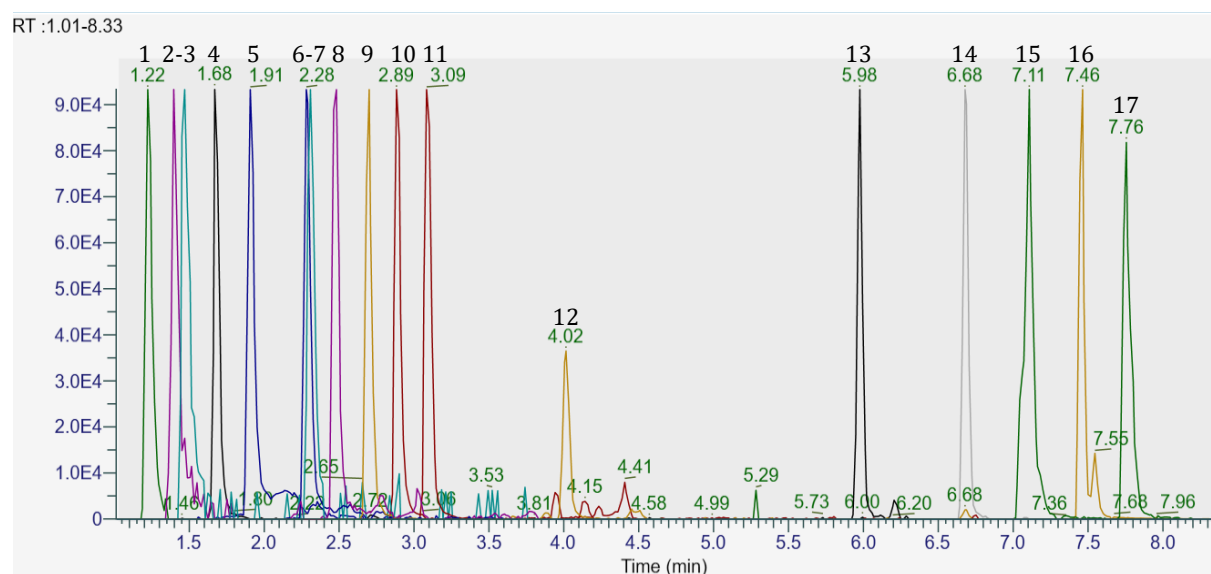

Figure 26: Gradient profile 2 of the study. 1=Peridinin, 2=Chlorophyll c2, 3=Chlorophyll c1, 4=Fucoxanthin, 5=Violaxanthin, 6=Diadinoxanthin, 7=Astaxanthin, 8=Antheraxanthin, 9=Alloxanthin, 10=Diatoxanthin, 11=Zeaxanthin, 12=Canthaxanthin, 13=Chlorophyll b, 14=Chlorophyll a, 15=Lycopene, 16=Pheophytin a and 17= β-carotene.

The final gradient allowed separation of the majority of the high-abundance pigment isomers within 8 minutes. Pigments which differed by only one double bond (Chl c_1/Chl c_2) and diadinoxanthin/astaxanthin were not separated. Exploring the effect of separation by altering the column temperature could have been a possibility, as a decreased temperature has showed an effect on alkyl chain rigidity (58), providing higher selectivity for longer molecules. Additionally, a lower column temperature has been found to reduce pigment allomerization (57). On the other hand, a reduction in column temperature leads to prolonged analysis due to the rising back pressure as the mobile phase viscosity increases. An optimal compromise in terms of efficiency, selectivity, analysis time and cost is therefore required. Preferably, the optimized chromatographic condition should provide separation of all pigment isomers,

however as already mentioned, time restriction and access to pure pigment standards led to no further separation optimization. The chromatograms displaying the separation ability of gradient 3 and 4, as well as the pigment elution order are provided in Appendix D.2 UPLC method development.

4.3 MS method development

The sensitivity of the employed MS method depends on several key parameters such as ionization polarity, dissociation method and collision energy, in which the applied configurations of the study were positive mode, HCD and stepped (15,30,45), respectively.

In compliance with the current literature (37, 61), the ionization polarity had a major impact on pigment ionization efficiency. Despite detecting molecular ions or deprotonated molecules of xanthophylls and chlorophylls in negative mode, the extent and quantity ionized by utilizing the positive polarity were superior (data not showed). Although, apolar pigments such as hydrocarbon carotenes were ionized by the ESI electrospray in positive mode, the ionization efficacy has been found to be lower for these pigments compared to the pigments of the polar region (62). An explanation might be that radical ion formation depends on the conjugation extension and that formation of proton adducts are highly influenced by the acid-base ionization of heteroatoms, which enables xanthophylls to utilize both mechanisms compared to only the former mechanism facilitating the ionization of hydrocarbon carotenes (37). As an alternative to the ESI interface, an APCI interface could be employed which is reported to possess a greater ability to ionize non-polar compounds and produce less in-source fragmentation (63). Additionally, the mobile phase composition utilized has been proven to highly affect the dominating form of the ionized molecule (64). The latter finding, was also established in this study with an increased presence of dominating proton adducts when employing a more polar mobile phase (data not showed). Although not assessed in the current study, an interesting notion is whether a polar mobile phase composition increases the ionization efficiency of, for instance, astaxanthin which has proven to favor protonation rather than radical formation.
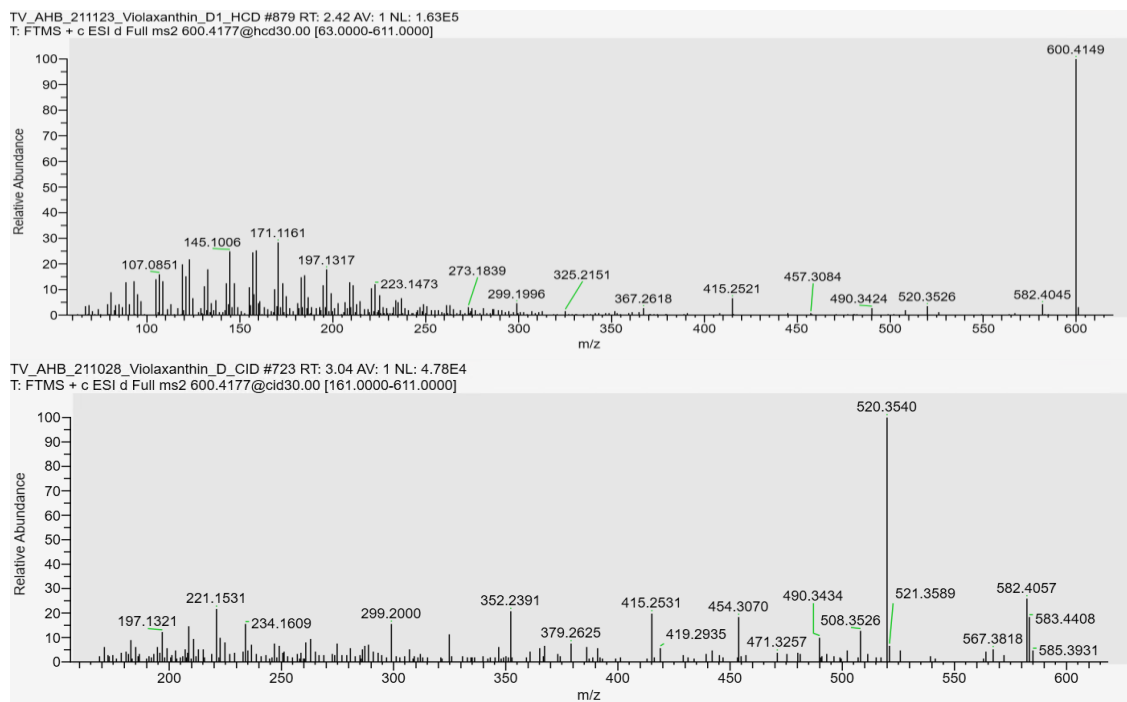
Figure 27: MS² spectrum of violaxanthin [M*]⁺ utilizing HCD fragmentation with a stepped collision energy of 15,30,45 (upper spectrum) and CID fragmentation with a collision energy of 30 (lower spectrum).

Obtaining optimal pigment fragmentation increases the quality of spectral information and accordingly, two dissociation mechanisms (CID/HCD) and collision energy levels were evaluated for their applicability for pigment identification. The comparison of the MS² spectra of the pigment standards achieved utilizing both dissociation mechanisms reveled a higher amount of fragments with a low m/z value obtained by HCD dissociation (Figure 27). The result complies with the 1/3 cut-off restriction for fragmentation in the ion trap (65) and as the difference in number of fragments with higher m/z values was limited (except intensity variation), the structural information obtained by HCD dissociation was better than with CID. This enhanced spectral information is of great importance for pigment identification as several pigment qualifier ions are present within the lower m/z range (66). Hence, the chosen dissociation mechanism was the higher energy collision dissociation.
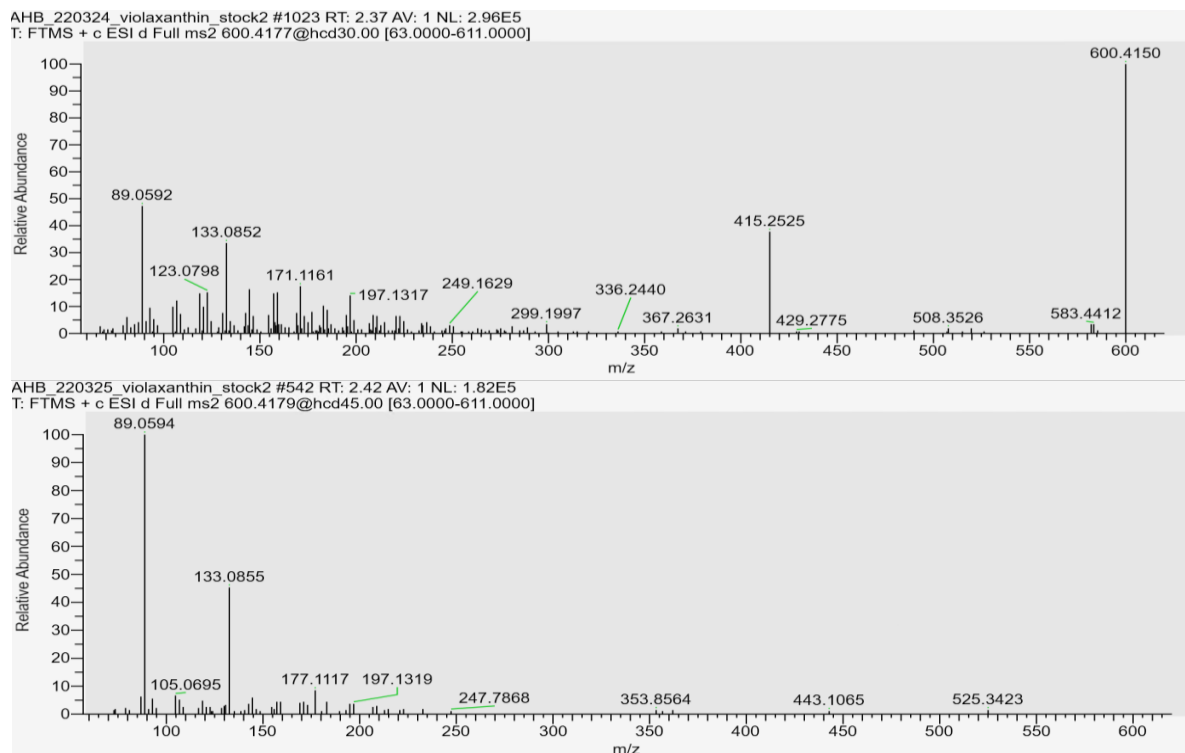
Figure 28: MS² spectra of violaxanthin acquired utilizing different collision energies, in which the upper spectrum corresponds to a stepped energy at 15,30,45 and the lower spectrum at 30,45,60.

The developed HCD method included stepped normalized collision energy (SNCE) as means to increase spectral information without tuning for each pigment. The applied energy range was altered to examine if an elevated stepped collision energy provided more informative data (SNCE 30,45,60). From the MS² spectra displayed in Figure 28, a definite reduction in fragments of higher m/z values was achieved by increasing the collision energy. Accordingly, a more informative spectrum was achieved at lower collision energy and SNCE at 15,30 45 was selected.

For the generic screening of pigments in algae samples the MS parameters yielding the highest ionization efficiency and most informative data were the positive polarity ionization, HCD dissociation and a SNCE of 15,30,45. Even though further tuning was desirable, additional optimization experiments was not conducted due to time limitations. For future references exploring the ion source temperature is a possibility, as a higher temperature has been reported to cause cis/trans isomerization in the ESI ion source (67). Even though the latter presumably results in the same fragmentation pattern and correctly identify the pigment, alteration in fragmentation intensities has been utilized as a diagnostic marker for isomer identification (68).

4.4 Identification of targeted pigments in algae samples

All raw data achieved from the acquireX acquisition were processed with compound discoverer (CD), utilizing the workflow specified in Appendix C.1 Compound Discoverer parameters. The selected workflow automatically annotated 3272 features, in which 10 of the most abundant adducts of the targeted pigments included in the AMRT database could be tentatively identified. All compounds tentatively identified presented a mzVault (MS^2) match score better than 70. However, an extensive variation in mass accuracy for the predicted composition (molecular formula), in addition to deviation of the retention time compared to the AMRT database were observed and most likely occurred as a result of radical ion formation, presence of pigment isomers and lack of robust pigment retention times.

Table 13: Tentative identification of the most abundant adduct of the targeted pigments processed by compound discoverer

Compound	ΔMass (ppm)	m/z	Rt (min)	mzVault Best Match (MS^2)	Reference ion
Pheophytin *a*	1.90	871.47490	7.677	92.2	$[M+H]^+$
Chlorophyll c_1	-0,78	611.21346	1.680	91.3	$[M+H]^+$
β-carotene	-1877.85	536.43813	7.961	91.3	$[M+H]^+$
Chlorophyll *a*	1.66	893.54407	6.939	88.6	$[M+H]^+$
Chlorophyll c_2*	1.01	1217.39116	1.603	89.4	$[2M+H]^+$
Fucoxanthin	0.55	659.43098	1.923	84.4	$[M+H]^+$
Chlorophyll *b*	-0,83	907.52110	6.940	79.3	$[M+H]^+$
Zeaxanthin	-1772.23	568.42792	5.940	82.7	$[M+H]^+$
Antheraxanthin	0.78	585.43073	4.565	71.1	$[M+H]^+$
Diatoxanthin	-1779.04	566.41199	3.227	89.1	$[M+H]^+$

*Tentatively identified in a separate CD analysis

The list of tentatively identified compounds matching the AMRT-database acquired from the CD analysis originally composed 18 hits. By closer examination several of the compounds detected were identified as already recognized pigments, reducing the number to a total of 10 unique pigments (Table 13). The detection of multiple peaks identified as the same compound

is in line with the previous discussed isomer formation discovered upon initial analysis of the pigment standards (see section 4.2.1). In Figure 29 the two peaks identified by CD as fucoxanthin are displayed, which might resemble the fucoxanthin trans(E) and cis(Z) isomer and, as expected, the mzVault match score decreased as the retention time deviance enhanced. Regarding fucoxanthin, the second peak eluting after approximately 3 minutes was provided a match score at 63.4 compared with the most abundant ion achieving a match score at 84.4 (Rt 1.918, Figure 29).
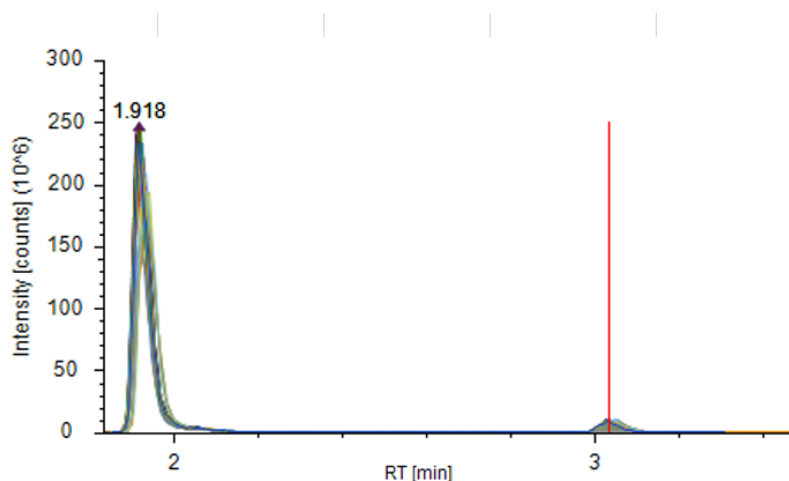
Figure 29: XIC of fucoxanthin acquired from compound discoverer (CD). The red line indicates the lower intensity peak which also was identified as fucoxanthin.

From the mass accuracy data presented in Table 13 a deviation interval of -1877.85 to 0.5 ppm (in order of increasing mass accuracy) is revealed with certain carotenoids constituting the lower range. The broad range in mass accuracy is a result of the carotenoids tendency to form radical cations instead of the proton adduct utilized by the software as reference ion. By replacing the reference ion with the molecular cation, the calculated mass accuracy is increased to 0.88, 0.74, and 0.34 ppm for beta-carotene, zeaxanthin and diatoxanthin, respectively.

Figure 30:MS^2 of the detected adduct $[2M+H]^+$ of chlorophyll c_2 by CD. m/z=1217.3914.
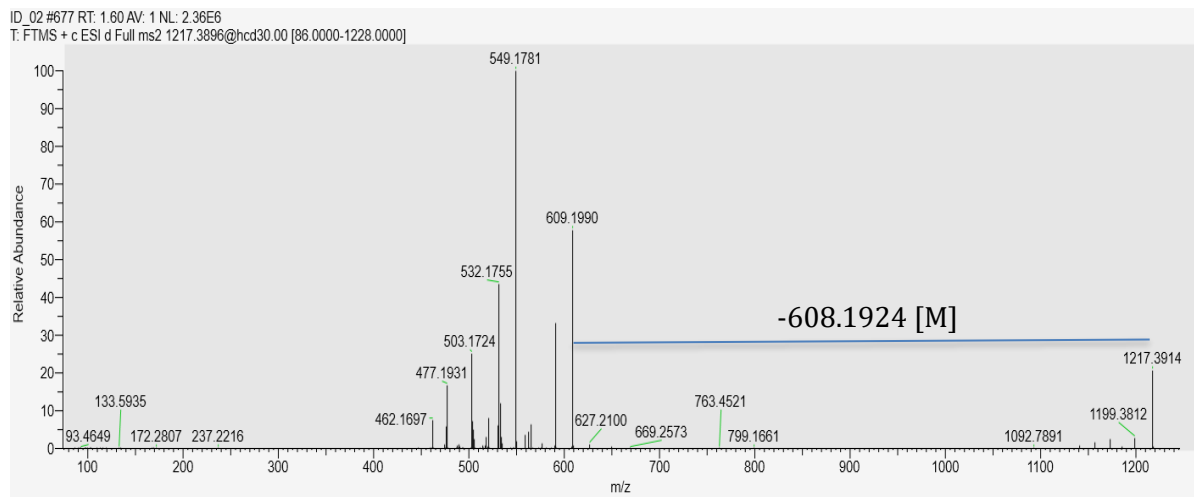
In addition to the high mass deviation for several carotenoids, the measured m/z of chlorophyll c_2 was at 1217.39116, corresponding to the protonated dimer $[2M+H]^+$. The latter adduct was the only adduct detected for chlorophyll c_2, which might indicate a high degree of complex formation. Illustrated in Figure 30, the loss of a chlorophyll c_2 molecule (m/z= 608.1910) from the measured m/z listed in Table 13 establish a fragment equal to the proton adduct of chlorophyll c_2 (ΔM=0.33 ppm). The cluster formation was also observed for chlorophyll c_1, however the protonated molecular ion for chlorophyll c_1 was detected at a higher abundance.

The pigments identified by compound discoverer possessed diverse levels of retention time accuracy compared to the elution times of the "in-house" pigment database with a shift variance of approximately 0.1-3 minutes. This observation could be explained by a microalgal pigment content with a high abundance of isomers not included in the AMRT database, either reflecting the true pigment profile of the species or as a result of degradation. An alternative suggestion is an unequal mobile phase composition between the creation of the library and algae analysis due to many instrument operators as the instrument was used for a multitude of different analyses in the project period.

Preliminary manual analysis of dated algae samples showed a higher number of tentatively identified pigments by comparison of exact masses and retention time with authentic pigment standards. Subsequently, an extensive effort was made towards tuning the compound discoverer workflow parameters by for instance increasing the adduct inclusion list, lower multiple threshold-settings and increase the retention time window. The outcome of the multiple CD

77

analyses was quite diverse with missing peak areas and reduced number of detected pigments. However, a positive result was the detection of chlorophyll c_2.

According to a study on identification confidence (69), the presented results correspond to a high level of confidence. The proposed minimum data requirements for a level 1 identification constitute a structure confirmation via a reference standard with MS, MS^2 and retention time matching. Despite certain retention time deviances, the mzVault match scores were high for all pigment identified (>70) which allowed a high identification confidence level. The assignment of specific levels was however debatable, in which pigments possessing the lowest retention time deviance might be annotated as a level 1 identification and pigments tentatively identified retaining a greater deviance, as a level 2 identification confidence.

Although the pigments identified returned a high confidence identification, the absence of a software function allowing the radical ion to be utilized as reference ion, a relatively large retention time deviation, software robustness deficiency combined with the potential presence of isomers not included in the AMRT database led to an uncertainty regarding whether the employed workflow was capable of detecting all pigments possibly present in the microalgae.

4.5 Identification of unknown substances

To avoid the identification of pigments to only concern the pigments of the reference standards, a second CD analysis was performed utilizing a non-targeting screening workflow (Appendix C.1 Compound Discoverer parameters) . The selected workflow detected 28379 items, in which 15423 features were filtered out as background interference, resulting in a dataset of 12956 compounds. For high confidence putative identification, the compounds were further filtered based on MS^2 matches with the spectral libraries included in the workflow (mzCloud, mzVault, LipidBlast). The resulting number of MS^2 matches was at 7733 (independent of match score), in which detection of pigments was unsuccessful. Hence, putatively identified pigments with a low confidence level (Level 3, (69)) and presence of MS^2 data were evaluated and subsequently selected for in-depth MS^2 examination.

Table 14: Putatively identified pigments (level 3) with presence of MS² data processed by compound discoverer

Compound	Molecular Formula	ΔMass (ppm)	m/z	Rt (min)	Predicted Composition (match)	Reference ion	Area (Max.)
*Adonixanthin/4-Ketozeaxanthin	C40H54O3	0.75	583.41501	2.603	Full	$[M+H]^+$	$6.94e^7$
Astaxanthin diglucoside	C52H72O14	2.44	921.50171	6.252	No	$[M+H]^+$	$8.25e^5$
Meso-Astaxanthin	C40H56O4	0.36	597.39405	1.152	Partial	$[M+H]^+$	$6.30e^5$
Zeaxanthin diglucoside	C52H76O12	3.42	893.54307	6.947	No	$[M+H]^+$	$9.12e^8$
Capsorubin	C40H56O4	-3.16	601.42219	1.809	Partial	$[M+H]^+$	$3.37e^5$
*Rhodoxanthin	C40H50O2	0.32	563.38861	1.932	Full	$[M+H]^+$	$7.69e^6$
Halocynthiaxanthin	C40H54O4	0.42	581.39917	2.831	No	$[M+H-H2O]^+$	$7.15e^6$
4-Oxomytiloxanthin	C40H52O5	0.17	613.38887	1.935	No	$[M+H]^+$	$1.34e^6$
Eschscholtzaxanthin	C40H54O2	0.42	567.41990	2.801	No	$[M+H]^+$	$2.77e^4$

*Natural loss of fatty acids: 18:2, 18:3, 20:4, 22:5, 22:6

The resulting pigments putatively identified by compound discoverer after filtering out compounds with absent fragmentation spectra are shown in Table 14. All compounds displayed were annotated by ChemSpider and/or LipidMAPS with a predicted composition match score at three levels, namely full match, partial match or no match. The glycosylated xanthophyll esters together with 4-oxymytiloxanthin, eschscholtaxanthin and halocynthiaxanthin presented a no match predicted composition and were therefore excluded from further investigation. Additionally, the meso-astaxanthin and capsorubin pigments with a partial match predicted composition were present at low abundances and correspondingly the obtained MS^2 spectral quality was insufficient for structure elucidation/identification conformation. The remaining pigments, adonixanthin/4-ketozeaxanthin (followingly referred to as adonixanthin) and rhodoxanthin presented informative MS^2 spectra, high mass accuracy and full match predicted composition. Consequently, the latter pigments were selected for a thorough structure evaluation with the intention of either allowing an increased identification confidence or potentially reject the proposed annotation.

Figure 31: MS spectrum at RT=1.90 with a scan number corresponding to the one utilized for identification of rohdoxanthin in CD.

The mass spectrum displayed in Figure 31 correspond to the scan number utilized by compound discoverer for the annotation of rhodoxanthin (m/z=563.3886). From the full scan spectrum, three signals were found present at higher abundances compared to the tentatively identified pigment within the same chromatographic peak (m/z= 581.3992, m/z= 641.4205 and m/z=659.4308). Considering the m/z at 659.4308 combined with the retention time at 1.90 minutes, the peak was suspected to represent fucoxanthin. By comparing the data obtained from

this analysis with findings from the previously conducted targeted pigment analysis (section 4.4), the identification of m/z 659.4308 as fucoxanthin was confirmed. In addition to the identification of fucoxanthin, the mass difference between the fragments (Figure 31) comprised 18.0103 (659.4308-641.4205), 60.0213 (641.4205-581.3992) and 18.0106 (581.3992-563.3886), which indicates the loss of a water molecule, acetic acid and a second water molecule, respectively.
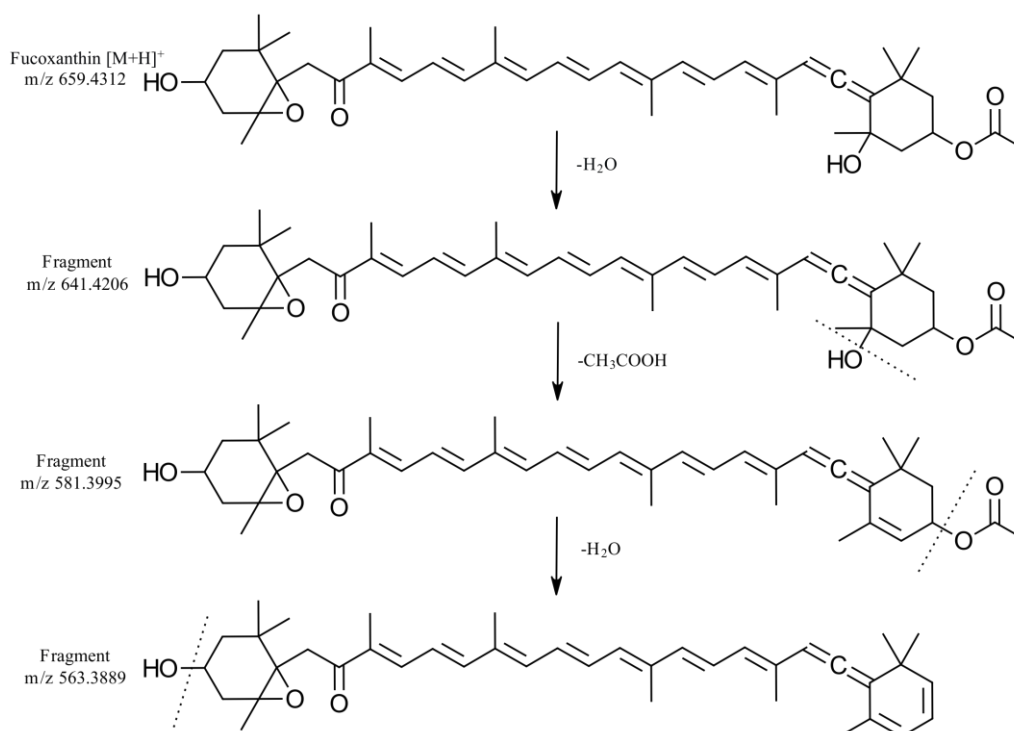
Figure 32:Schematic of the proposed fragmentation of fucoxanthin, in which the displayed m/z values corresponds to theoretical m/z

Figure 32 displays a proposed fragmentation pattern, in which the first step includes the removal of water with a measured m/z at 641.4205, deviating with 0.16 ppm from the theoretical m/z. Subsequently, the measured mass corresponding to the loss of a carboxylic group at the ε-terminal ring had a mass accuracy of 0.52 ppm and lastly, the loss of the second water molecule with a deviation of 0.53 ppm. The suggested fragments of fucoxanthin are in agreement with multiple studies (70, 71), and the reported fragments of rhodoxanthin are absent (72). Additionally, the MS^2 spectrum of m/z 563.3886 was visually compared with the MS^2 spectrum of the fucoxanthin reference standard, revealing undetectable differences. Accordingly, the putatively identification of m/z 563.3886 as rhodoxanthin was dismissed and recognized as in-

source fragmentation of fucoxanthin. The MS^2 spectrum of m/z 563.3886 and the fucoxanthin standard are provided in Appendix D.3 Identification of unknown substances.

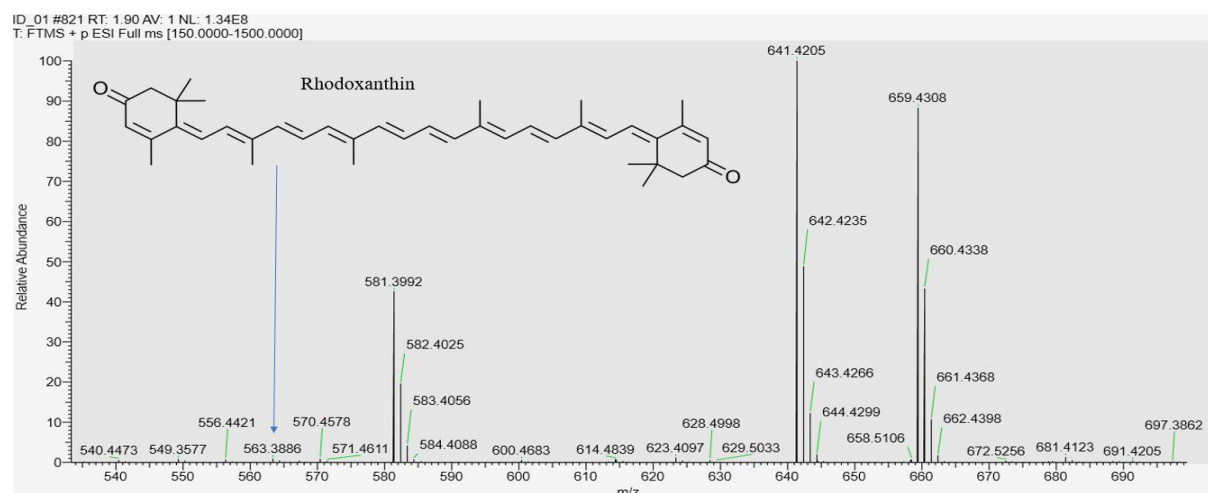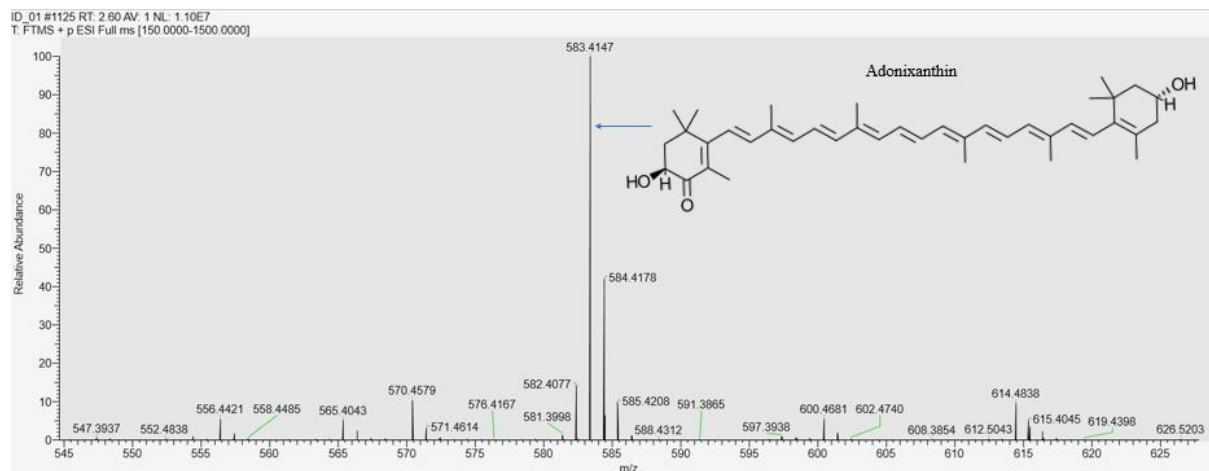*Figure 33: MS spectrum at RT=2.60 with a scan number corresponding to the one utilized for identification of adonixanthin in CD.*

An investigation of the detected pigment putatively identified as adonixanthin displayed in Figure 33 with an apparently high abundance (Table 14) was of great interest as the pigment represent a precursor in the metabolic pathway of astaxanthin (73) which is frequently added in fishmeal and thus precent a possible value added product (VAP).
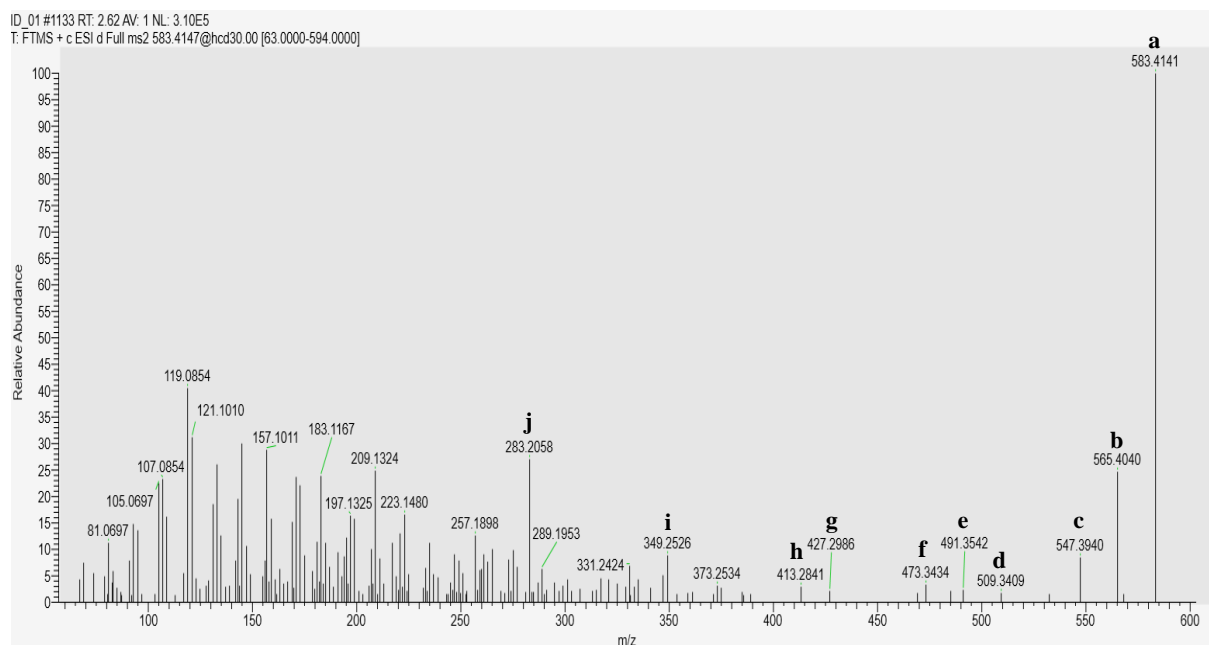
Figure 34:MS^2 of m/z=583.4147 at RT=2.62 identified by CD as adonixanthin. Fragments are denoted alphabetically, corresponding to structures proposed in Figure 35, Figure 36, Figure 37 and Figure 38.

The MS^2 spectrum of the precursor ion at m/z 583.4147 yielded the typical complex fragmentation spectrum seen for carotenoids with a relatively high number of product ions at low m/z, as well as several fragments at higher m/z-values (Figure 34). Prior to closer fragment elucidation, the obtained MS^2 spectrum of m/z 583.4147 was matched visually with both fragment spectra of the AMRT database and adonixanthin spectrum found in the Massbank database. The former matching was conducted in order to evaluate whether the identified pigment could represent a constitutional isomer of adonixanthin, namely the xanthophyll diadinoxanthin. The visual inspection revealed several differences between the fragmentation patterns of diadinoxanthin and the unknown substance. Additionally, the MS^2 matching with the adonixanthin spectrum of the Massbank database showed promising similarities and further structural investigation was performed.

The followingly proposed fragmentation pathways for adonixanthin are developed in accordance with current carotenoid MS^2 literature. Fragments are denoted alphabetically in order of decreasing m/z and corresponds to the annotation of peaks depicted in Figure 34. The loss of water molecules is characteristic for pigments that contain hydroxyl groups (66, 74, 75) and the signals at m/z 565.4040 (b) and 547.3940 (c) were accordingly assigned to the fragment ions after elimination of one and two water molecules, respectively (Figure 35). The fragment m/z 509.3409 (d) was proposed as the successive loss of isobutene by terminal ring decyclization (66), following the former dissociation of a single water molecule (m/z 565.4040).

Figure 35:Proposed fragmentation pathway for adonixanthin, showing theoretical monoisotopic masses for all substances (Part 1).

The product ion m/z 427.2986 (g) was attributed to the loss of the hydroxy end-ring through an intermediate fragment at m/z 566.4118 present in the MS^2 spectrum (Figure 36, Figure 34). The latter ion was thought to derive from the reported (70) characteristic dissociation of the carbonyl-carbon/oxygen bond from ketocarotenoids after an extensive electron delocalization, resulting in a proton transfer from the adjacent methyl group to the carbonyl oxygen prior to elimination (76). In addition, the adonixanthin qualifier ions at m/z 147 and 135.1 were detected (66), corresponding to dehydration of the keto terminal ring with cleavage between carbons 7 and 8 (data not shown). However, these characteristic ketocarotenoids fragments were found in low abundances.

Figure 36:Proposed fragmentation pathway for adonixanthin, showing theoretical monoisotopic masses for all substances (Part 2).

The presence of extensive conjugation within the molecule results in chain fragmentation(66). The mechanism proposed for the neutral loss of toluene (e) from the central polyene chain is involves an electro cyclic reaction, forming a stable tricyclic intermediate (66, 76) (Figure 36). A further elimination of water result in the fragment at m/z 473.3434 (f). By means of enhancing the structural elucidation of adonixanthin, a continuation of the fragmentation pathways proposed in Figure 35 and Figure 36 are shown in Figure 37 and Figure 38, focusing on in-chain fragmentation. Additionally, several of the low m/z fragments in the complex carotenoid spectra are attributed to smaller fractions of the hydrocarbon chain, for instance 119, giving rise to various chain cleavages and thereby product ions (66, 72). The proposed structures are inspired of studies on the astaxanthin fragmentation pathways (70, 77) and as a studied stated a 50% relative abundance of m/z 283.2056 detected for adonixanthin, a suggested structure of the latter product ion is also provided (Figure 37).

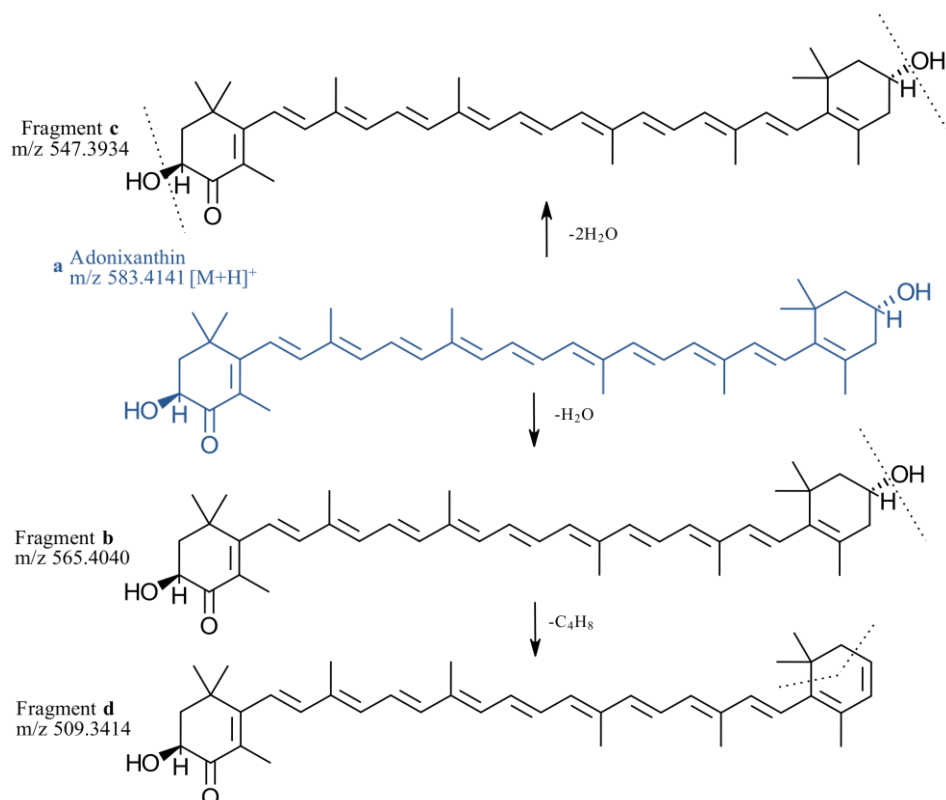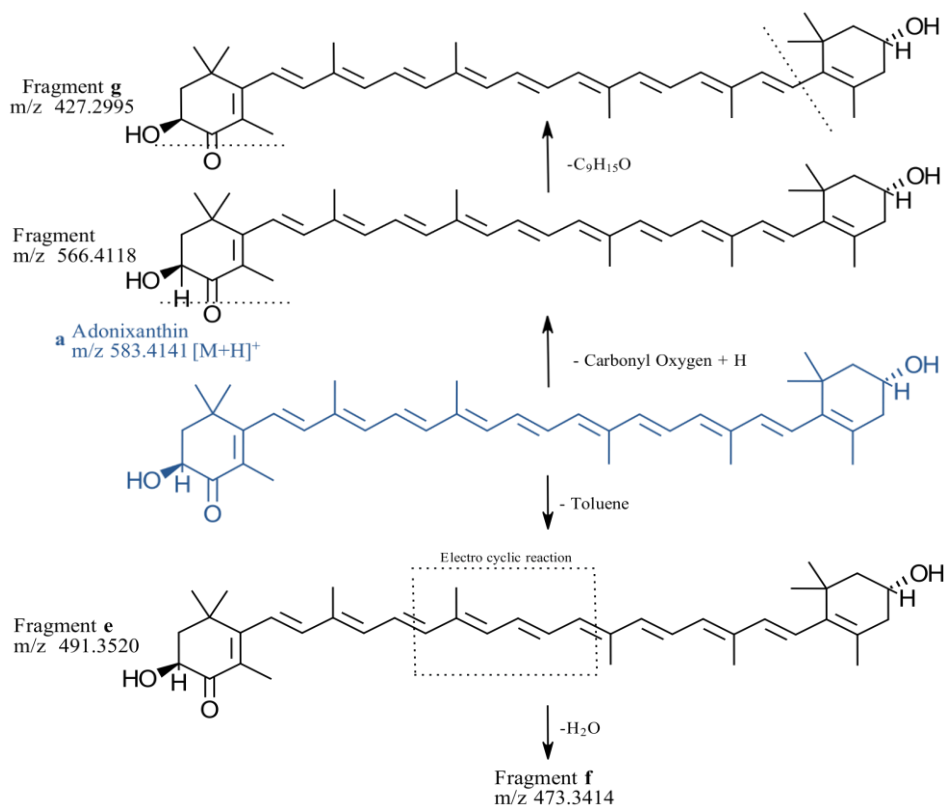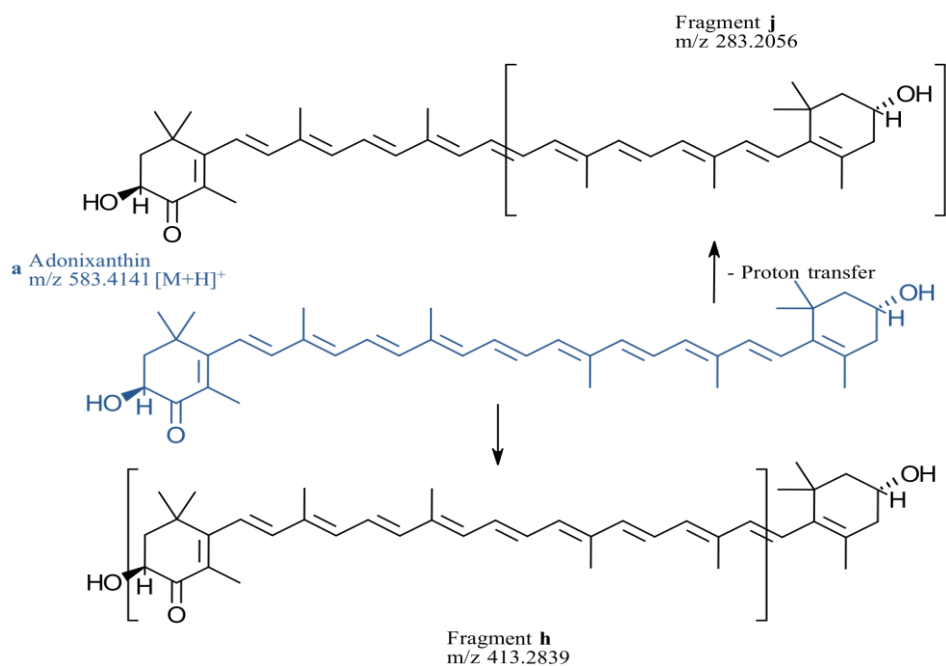*Figure 37:Proposed fragmentation pathway for adonixanthin, showing theoretical monoisotopic masses for all substances (Part 3).*
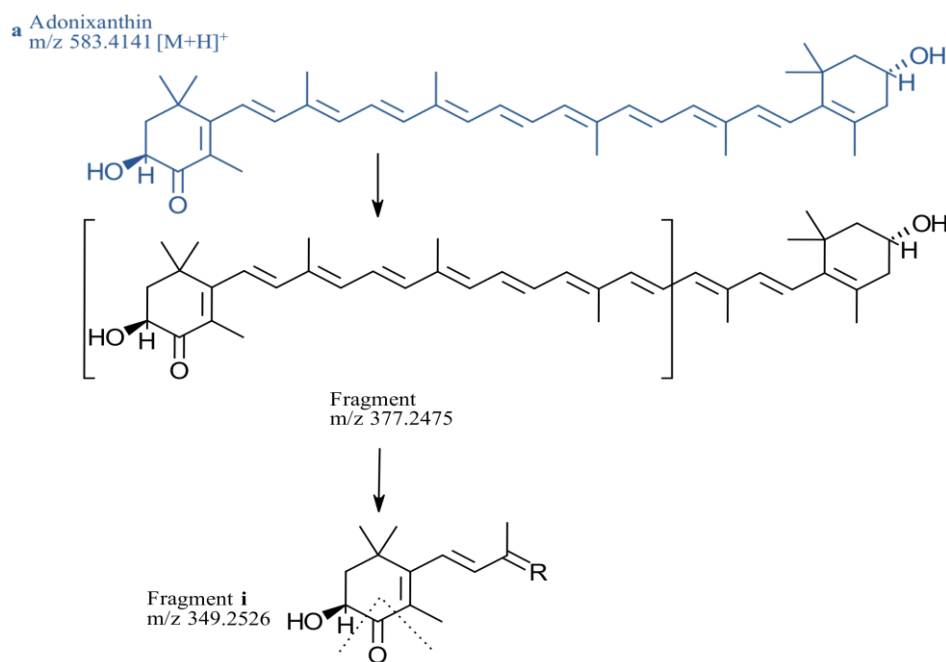
Figure 38:Proposed fragmentation pathway for adonixanthin, showing theoretical monoisotopic masses for all substances (Part 4).

In general, the analysis of unknown substances revealed a lack of currently available online MS^2 spectra for pigment profiling and highlights the value of obtaining an in-house pigment database. On the other hand, the untargeted analysis detected valuable information regarding in source fragmentation and presence of xanthophyll esters (Table 14). Lastly, a screening

approach enabled a putative low confidence identification of adonixanthin which, by conducting an in-dept fragment examination, might indicate the presence of adonixanthin in *P.glacialis*.

4.6 Relative amount of pigments in response to irradiance wavelength

The peak area of pigments identified by compound discoverer was exported and aggregated according to cultivation regime for statistical comparison of irradiance wavelength impact on pigment composition. Pigment specific distribution of peak area measurements grouped according to wavelength irradiance is displayed in Figure 39 and includes the pigments with a high confidence identification (described in section 4.4), except chlorophyll c_2 which was excluded due to detection in a separate CD analysis. Cultivation of *Porosira glacialis* under blue light resulted in a pigment profile similar to the composition obtained under white light. In comparison, red light resulted in a lower accumulation ($p<0.05$) of all included pigments. The results suggest that light color regulates pigment synthesis in *P. glacialis,* and that blue light promotes pigment production compared to red light.
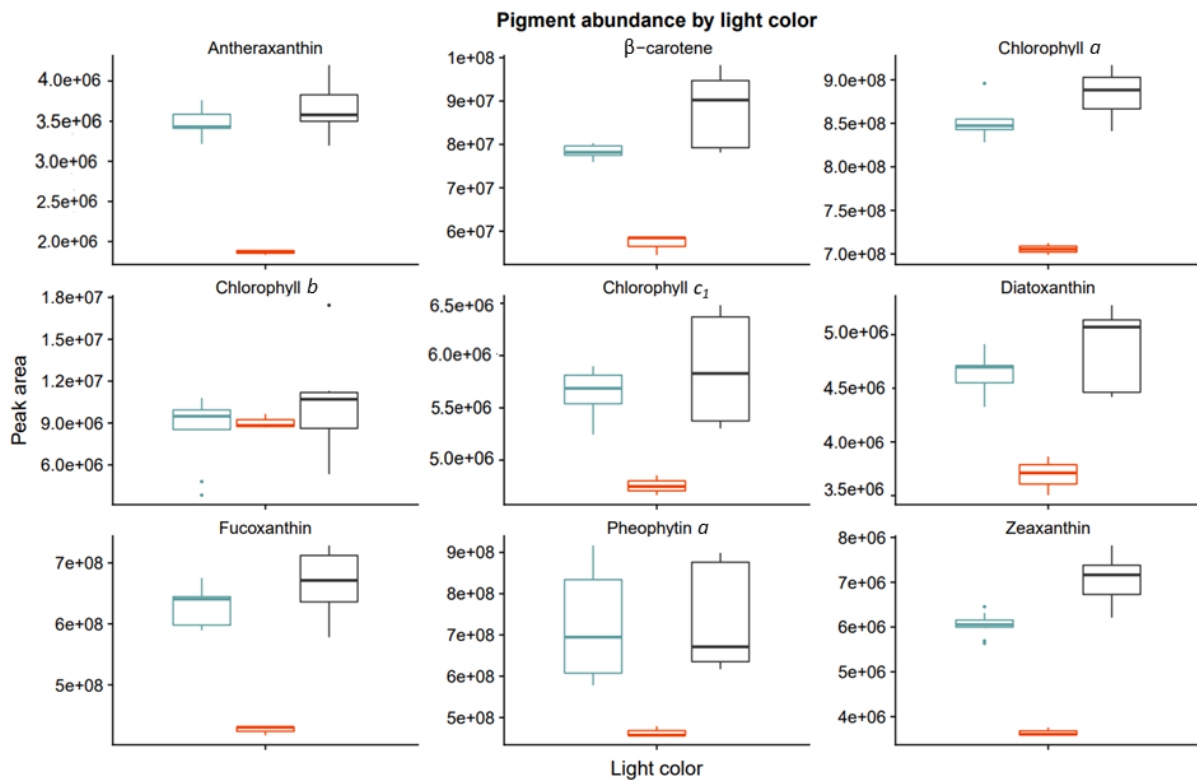
Figure 39:Boxplot of pigment abundance by light color. X-axis: light color represented by blue, red and black boxes, corresponding to cultivation in blue, red and white light, respectively. Y-axis: Peak area from data processed by compound discoverer.

Chlorophyll *b* deviated from these observed trends and did not show a significant difference between any of the employed light regimes ($p>0.05$). From the corresponding boxplot, multiple outliers for both blue and white light measurements are shown, revealing a wide data

distribution. Consequentially, chlorophyll *b* was removed from the overall analysis of light effects on pigment composition.

A higher pigment content of zeaxanthin and chlorophyll *a* was observed with white light irradiance compared to both blue and red light ($p<0.5$). The peak area measurements for both zeaxanthin and chlorophyll a were relatively symmetrical and tightly grouped compared to β-carotene, diatoxanthin, chlorophyll c_1 and pheophytin *a.* The comprehensive interquartile range with sections indicating uneven measurements might have caused an inability to detect a true difference between the blue and white light regimes. The natural variance in biological samples (40) and inter extract variations derived from sample preparation, as well as ion suppression, could explain the wide data distribution observed.

Interestingly, the growth rate measurements based on cell count revealed a statistically significant lower microalgal growth rate in red light compared to blue light and a seemingly decreased ($p>0.05$) growth rate in red light in comparison with white light (data not shown). The higher growth rate detected in blue light establishes an opposition to the optimal wavelength of 600-700 nm for most algal species (78) and might be ascribed to a higher amount of light harvesting pigments with an absorption in the blue-green range and/or a higher efficiency of photon absorption in the blue light spectrum by the chlorophyll *a/b* (79). The latter suggestion is supported by the identification of chlorophyll c_1 and c_2 dimers with rather high intensities (specified in section 4.4), which were dismissed in the current determination of relative quantity, due to pre-selecting the molecular ion in the AMRT database. Additionally, the detection of esterified xanthophylls (section 4.5) probably affected the quantification of this pigment class since only radical and/or proton adducts were included in the AMRT database.

Overall, the results implies that irradiance with wavelengths of blue light affects the production of the analyzed pigments to a higher degree compared to red light illumination of *P. glacialis*. The finding is in agreement with previous studies resulting in higher pigment content with blue irradiation on different algal species (80-82) with a suggested explanation of blue light having an ability to conduct transcriptional regulation in addition to activate enzymes directing metabolic pathways via photoreceptors (83). However, studies also find conflicting results with an increased influence on pigment composition with red light compared to blue light for certain species, indicating a variation of optimal light color among microalgae genus (84).

5 Limitations of the study

Although precautions were taken, the signal intensity of the pigment standards decreased through the time scope of this project. The degradation of pigment standards was presumably a consequence of the significant amount of time between breaking the reference seal and pigment analysis, as result of unexpected instrumental defects. The degradation of standards led to unknown pigment concentrations and accordingly, creation of calibration curves was unachievable. The absence of calibration curves successively caused an absolute quantification to be unattainable and the linear range was not determined. The latter might have impacted the relative estimation of pigment content. In addition, the signal intensity reduction led to difficulties in acquiring MS^2 data of high quality and as a result it became necessary to increase the pigment concentration in the standards by solvent evaporation. The exposure to increased temperature, light and air associated with solvent evaporation might have caused even further degradation of the pigment standards, which in turn might have led to a pigment database composed of multiple unidentified isomers of known pigments. Thus, pigment isomers which were not included in the database, but present in algae samples were probably discarded.

As previously stated, the software tools employed in this project lacked the function which allows radical ions to be chosen as preferred precursor ion. The following consequences on pigment analysis performance are uncertain, although a decreased sensitivity in pigment identification is likely. The high m/z deviation obtained when the proton adduct is incorrectly used as reference ion presumably decreases certain matching threshold settings for annotation and might exclude pigments present in the sample. Additionally, the robustness of analysis performed by compound discoverer were insufficient with unexplainable variations between runs.

The biomass resulting from cultivation of *P.glacialis* was limited, especially for the algae cultivated in red light, which required combining the original three parallels to yield one red light sample. Low cultivation temperature (below 0 degrees at day 4) and low light intensity ($22 \ \mu mol \ m^{-2}s^{-1}$) might have influenced the algae growth and resulted in lower growth than expected in red light. However, no explanation was found to why this only occurred for the red light cultivated microalgae. The resulting low biomass might partly be responsible for the high variance in pigment content of the same light parallel and the inclusion of an internal standard would have been advantageous.

6 Future perspectives

The findings from the current study provides valuable information regarding both the composition and relative abundance of pigments in the investigated microalgae, creating new future possibilities for marine pigment investigation. In addition, the presented method developed for pigment analysis constitute a foundation for future pigment profiling. Despite obtaining useful data, further improvements of methods as well as expanding the AMRT database could be explored. Enlisted below are several future perspectives suggested as means to enhance both pigment identification and abundance.

- As the biological activity of pigments depends on the geometrical isomer present, more attention should be granted to prevent pigment degradation (85). A suggested storage protocol composes light reflecting containers stored at -80°C with a minimization of time spent exceeding these conditions. Additionally, including stabilizers could be beneficial.

- Investigate a multiple stage extraction protocol in order to purify the obtained pigment extract and possibly enhance extraction and ionization efficiency. Reducing the amount of interferences eases the interpretation of chromatograms and mass spectra. Moreover, a reduced presence of lipids in sample extracts would decrease the esterification of xanthophylls and hence increase the quantification accuracy and pigment identification. Including a saponification step is therefore a possibility.

- Assess multiple mobile phase compositions, sample solvents and optimize the elution gradient to achieve sufficient separation of pigment isomers. The mobile phases and solvent utilized for pigment analysis has been shown to impact the adduct formation and peak shape quality (66) and in effort to obtain reproduceable data, these conditions should be considered.

- Expand the AMRT database with a higher number of pigment standards as well as including standards for their corresponding isomers. In addition, the library should contain MS^2 data of both the radical molecular ion and the proton adduct to enhance the probability of automatic identification by the currently available software.

- Further explore the parameter settings in compound discoverer to increase its applicability in pigment analysis.

7 Conclusion

A pilot scale cultivation of *Porosira glacialis* irradiated with different light regimes was conducted to investigate the pigment composition in response to irradiance wavelength. Cultivation under blue light resulted in a statistically significant higher growth rate and accumulation of the analyzed pigments compared to red light cultivation, with the exception chlorophyll *b*. Therefore, the blue light regime was suggested to promote pigment production in *P.* glacialis. The resulting pigment profile under blue light was comparable to the composition obtained under white light.

In the present study, a novel automatic approach was applied for both a targeted pigment analysis utilizing an in-house spectral database (MzVault) and a screening approach for pigment profiling. Intelligent data acquisition (AcquireX-DS-DD-MS^2) and automated data processing (Compound Discoverer^{TM}) including a developed pigment AMRT database, online spectral libraries and substance databases, allowed a high confidence level identification of 10 pigments derived from the marine diatom *P.glacialis*, representing both the carotenoid and chlorophyll pigment classes. In addition, the screening approach enabled pigment annotations, from which the putative identification of the xanthophyll adonixanthin was revealed. The latter identification was further supported by detection of adonixanthin diagnostic product ions as well as in-dept elucidation of possible fragmentation pathways. The potential detection of adonixanthin in the diatom species constitute an important finding, implying the presence of the metabolic pathway towards astaxanthin.

An extraction protocol was developed to recover pigments with a wide structure and polarity range, in which an extraction methodology composed of a 30-minute extraction with aqueous acetone (90%) was found to yield the highest extraction efficiency for the majority of the included pigments. Resulting from the UPLC-MS method optimization, the employment of positive polarity ionization and HCD fragmentation enhanced the ionization efficiency and provided the most informative data in terms of pigment profiling. In addition, the developed 10-minute gradient allowed separation of the most abundant pigment isomers with a few exceptions. The presented results from the pigment analysis method development of this study could serve as a starting point in the direction of a standardized protocol for pigment analysis.

References

1.   Shukla PR, Skea J, Slade R, Khourdajie AA, van Diemen R, McCollum D, et al. Climate Change 2022: Mitigation of Climate Change. Contribution of Working Group III to the Sixth Assessment Report of the Intergovernmental Panel on Climate Change. Cambridge University Press, Cambridge, UK and New York, NY, USA: IPCC; 2022. Report No.: AR6.

2.   FAO. The State of World Fisheries and Aquaculture 2020. Sustainability in action. Rome: Food and Agriculture Organization of the United Nations; 2020. Report No.: 1020-5489.

3.   Turchini GM, Trushenski JT, Glencross BD. Thoughts for the Future of Aquaculture Nutrition: Realigning Perspectives to Reflect Contemporary Issues Related to Judicious Use of Marine Resources in Aquafeeds. N Am J Aquacult. 2019;81(1):13-39.

4.   Zhang Y, Lu R, Qin C, Nie G. Precision nutritional regulation and aquaculture. Aquac Rep. 2020;18:100496.

5.   Shah MR, Lutzu GA, Alam A, Sarker P, Kabir Chowdhury MA, Parsaeimehr A, et al. Microalgae in aquafeeds for a sustainable aquaculture industry. J Appl Phycol. 2017;30(1):197-213.

6.   Onyeaka H, Miri T, Obileke K, Hart A, Anumudu C, Al-Sharify ZT. Minimizing carbon footprint via microalgae as a biological capture. CCST. 2020;18:100007.

7.   Artamonova EY, Vasskog T, Eilertsen HC. Lipid content and fatty acid composition of Porosira glacialis and Attheya longicornis in response to carbon dioxide (CO2) aeration. PLoS One. 2017;12(5):e0177703.

8.   Daneshvar E, Wicker RJ, Show P-L, Bhatnagar A. Biologically-mediated carbon capture and utilization by microalgae towards sustainable CO2 biofixation and biomass valorization – A review. Chem Eng J. 2022;427:130884.

9.   Townsend DW. Oceanography and marine biology : an introduction to marine science. Sunderland, Mass: Sinauer Associates; 2012.

10.   Gordon R, Seckbach J. Diatoms: Fundamentals and Applications. Newark: Newark: John Wiley & Sons, Incorporated; 2019.

11.   Mann DG, Vanormelingen P. An Inordinate Fondness? The Number, Distributions, and Origins of Diatom Species. J Eukaryot Microbiol. 2013;60(4):414-20.

12.   Nonoyama T, Kazamia E, Nawaly H, Gao X, Tsuji Y, Matsuda Y, et al. Metabolic Innovations Underpinning the Origin and Diversification of the Diatom Chloroplast. Biomolecules. 2019;9(8):322.

13.   Xiong Z, Li T, Algeo T, Doering K, Frank M, Brzezinski MA, et al. The silicon isotope composition of Ethmodiscus rex laminated diatom mats from the tropical West Pacific: Implications for silicate cycling during the Last Glacial Maximum. Paleoceanography. 2015;30(7):803-23.

14.   Gupta SK, Bux F, Editors. Application of Microalgae in Wastewater Treatment. Volume 2: Biorefinery Approaches of Wastewater Treatment Cham, Switzerland: Springer International Publishing : Imprint: Springer; 2019.

15.   Throndsen J, Tangen K, Hasle GR. Norsk kystplanktonflora. Oslo: Almater forl.; 2003.

16.   Lacour T, Larivière J, Babin M. Growth, Chl a content, photosynthesis, and elemental composition in polar and temperate microalgae. Limnol Oceanogr. 2017;62(1):43-58.

17.   Beer S, Björk M, Beardall J, Thompson S. Photosynthesis in the marine environment. Ames, Iowa: Wiley-Blackwell; 2014.

18.   Svenning JB, Dalheim L, Eilertsen HC, Vasskog T. Temperature dependent growth rate, lipid content and fatty acid composition of the marine cold-water diatom Porosira glacialis. Algal Res. 2019;37:11-6.

19.   Jacob-Lopes E, Queiroz MI, Zepka LQ. Pigments from Microalgae Handbook. Cham: Springer International Publishing : Imprint: Springer; 2020.

20.   Qiu NW, Jiang DC, Wang XS, Wang BS, Zhou F. Advances in the members and biosynthesis of chlorophyll family. Photosynthetica. 2019;57(4):974-84.

21.   Allakhverdiev SI, Kreslavski VD, Zharmukhamedov SK, Voloshin RA, Korol'kova DV, Tomo T, et al. Chlorophylls d and f and their role in primary photosynthetic processes of cyanobacteria. Biochem (Mosc). 2016;81(3):201-12.

22.   Cezare-Gomes EA, Mejia-da-Silva LdC, Pérez-Mora LS, Matsudo MC, Ferreira-Camargo LS, Singh AK, et al. Potential of Microalgae Carotenoids for Industrial Application. Appl Biochem Biotechnol. 2019;188(3):602-34.

23.   Lone SA, Malik A. Microbiomes and the Global Climate Change. Singapore: Springer Singapore Pte. Limited; 2021.

24.   Stokkeland IM. LC-MS characterization of pigments in microalgae from different cultivation regimes. Tromsø: UiT Norges arktiske universitet; 2019.

25.   Hudson P. Cyanobacteria biotechnology. Weinheim, Germany: Wiley; 2021.

26.   Novoveska L, Ross ME, Stanley MS, Pradelles R, Wasiolek V, Sassi J-F. Microalgal Carotenoids: A Review of Production, Current Markets, Regulations, and Future Direction. Mar Drugs. 2019;17(11):640.

27.   Pangestuti R, Kim S-K. Biological activities and health benefit effects of natural pigments derived from marine algae. J Funct Foods. 2011;3(4):255-66.

28.   Arora N, Philippidis GP. Fucoxanthin Production from Diatoms: Current Advances and Challenges. Singapore: Singapore: Springer Singapore; 2020. p. 227-42.

29.   Seth K, Kumar A, Rastogi RP, Meena M, Vinayak V, Harish. Bioprospecting of fucoxanthin from diatoms — Challenges and perspectives. Algal Res. 2021;60:102475.

30.   Bertrand M. Carotenoid biosynthesis in diatoms. Photosynth Res. 2010;106(1-2):89-102.

31.   Tebbani S. CO2 biofixation by microalgae : modeling, estimation and control. London, England,Hoboken, New Jersey: ISTE : Wiley; 2014.

32.   Santos-Ballardo DU, Rossi S, Hernández V, Gómez RV, del Carmen Rendón-Unceta M, Caro-Corrales J, et al. A simple spectrophotometric method for biomass measurement of important microalgae species in aquaculture. Aquaculture. 2015;448:87-92.

33.   Pedersen-Bjergaard S, Gammelgaard B, Halvorsen TG. Introduction to pharmaceutical analytical chemistry. Hoboken, NJ: Wiley; 2019.

34.   Najjar YSH, Abu-Shamleh A. Harvesting of microalgae by centrifugation for biodiesel production: A review. Algal Res. 2020;51:102046.

35.   Svenning JB, Dalheim L, Vasskog T, Matricon L, Vang B, Olsen RL. Lipid yield from the diatom Porosira glacialis is determined by solvent choice and number of extractions, independent of cell disruption. Sci Rep. 2020;10(1).

36.   Kuczynska P, Jemiola-Rzeminska M, Strzalka K. Photosynthetic Pigments in Diatoms. Mar Drugs. 2015;13(9):5847-81.

37.   Roy S. Phytoplankton pigments : characterization, chemotaxonomy, and applications in oceanography. Cambridge: Cambridge University Press; 2011.

38.   Boyd RK, Basic C, Bethem RA. Trace Quantitative Analysis by Mass Spectrometry. 1. Aufl.,1st ed. New York: New York: Wiley; 2008.

39.   Smoluch M, Grasso G, Suder P, Silberring J. Mass Spectrometry: An Applied Approach. Newark: Newark: John Wiley & Sons, Incorporated; 2019.

40.   Han X. Lipidomics : comprehensive mass spectrometry of lipids. Hoboken, New Jersey: John Wiley & Sons, Incorporated; 2016.

41.   Arrizabalaga-Larrañaga A, Rodríguez P, Medina M, Santos FJ, Moyano E. Simultaneous analysis of natural pigments and E-141i in olive oils by liquid chromatography–tandem mass spectrometry. Anal Bioanal Chem. 2019;411(21):5577-91.

42.   Ekman R. Mass spectrometry : instrumentation, interpretation, and applications. Hoboken, N.J.: John Wiley & Sons; 2009.

43.   Transforming small molecule identification and structure elucidation [Web Document]. Thermo Fisher Scientific; [cited December 10, 2021] Available from: https://assets.thermofisher.com/TFS-Assets/CMD/Specification-Sheets/ps-65188-orbitrap-id-x-tribrid-ms-ps65188-en.pdf.

44.   Yusà V, López A, Dualde P, Pardo O, Fochi I, Pineda A, et al. Analysis of unknowns in recycled LDPE plastic by LC-Orbitrap Tribrid HRMS using MS3 with an intelligent data acquisition mode. Microchem J. 2020;158:105256.

45.   Byeon SK, Madugundu AK, Pandey A. Automated data-driven mass spectrometry for improved analysis of lipids with dual dissociation techniques. J Mass Spectr Adv Clin Lab. 2021;22:43-9.

46.   Miralles P, López A, Dualde P, Coscollà C, Yusà V. Liquid chromatography‐Orbitrap Tribrid high‐resolution mass spectrometry using data dependent‐tandem mass spectrometry with triple stage fragmentation as a screening tool to perform identification and risk assessment of unknown substances in food contact epoxy resin. J Sep Sci. 2021;44(16):3020-30.

47.   Uradnikova M. Species validity of five common northern/Arctic spring bloom diatoms: a combined morphological and molecular study. Tromsø: UiT Norges arktiske universitet; 2020.

48.   Holm-Hansen O, Riemann B. Chlorophyll a Determination: Improvements in Methodology. Oikos. 1978;30(3):438-47.

49.   Kim SM, Kang S-W, Kwon ON, Chung D, Pan C-H. Fucoxanthin as a Major Carotenoid in Isochrysis aff. galbana: Characterization of Extraction for Commercial Application. J Korean Soc Appl Bi. 2012;55(4):477-83.

50.   Pagels F, Pereira RN, Vicente AA, Guedes AC. Extraction of Pigments from Microalgae and Cyanobacteria-A Review on Current Methodologies. Appl Sci. 2021;11(11):5187.

51.   Torres PB, Chow F, Furlan CM, Mandelli F, Mercadante A, Alves Cursino dos Santos DY. Standardization of a protocol to extract and analyze chlorophyll a and carotenoids in Gracilaria tenuistipitata Var. Liui. Zhang and Xia (Rhodophyta). Braz j oceanogr. 2014;62(1):57-63.

52.   van Leeuwe MA, Villerius LA, Roggeveld J, Visser RJW, Stefels J. An optimized method for automated analysis of algal pigments by HPLC. Mar Chem. 2006;102(3):267-75.

53.   Dunn JL, Turnbull JD, Robinson SA. Comparison of solvent regimes for the extraction of photosynthetic pigments from leaves of higher plants. Funct Plant Biol. 2004;31(2):195.

54.   Soares AT, Marques Junior JG, Lopes RG, Derner RB, Antoniosi Filho NR. Improvement of the Extraction Process for High Commercial Value Pigments from Desmodesmus sp Microalgae. J Braz Chem Soc. 2016;27(6):1083-93.

55.   Saini RK, Keum Y-S. Carotenoid extraction methods: A review of recent developments. Food Chem. 2018;240:90-103.

56.   Chauveau-Duriot B, Doreau M, Nozière P, Graulet B. Simultaneous quantification of carotenoids, retinol, and tocopherols in forages, bovine plasma, and milk: validation of a novel UPLC method. Anal Bioanal Chem. 2010;397(2):777-90.

57.   Delpino-Rius A, Eras J, Marsol-Vall A, Vilaró F, Balcells M, Canela-Garayoa R. Ultra performance liquid chromatography analysis to study the changes in the carotenoid profile of commercial monovarietal fruit juices. J Chromatogr A. 2014;1331:90-9.

58.   Turcsi E, Nagy V, Deli J. Study on the elution order of carotenoids on endcapped C18 and C30 reverse silica stationary phases. A review of the database. J Food Compost Anal. 2016;47:101-12.

59.   Giuffrida D, Zoccali M, Mondello L. Recent developments in the carotenoid and carotenoid derivatives chromatography-mass spectrometry analysis in food matrices. Trends Analyt Chem. 2020;132.

60.   Khoo H-E, Prasad KN, Kong K-W, Jiang Y, Ismail A. Carotenoids and Their Isomers: Color Pigments in Fruits and Vegetables. Molecules. 2011;16(2):1710-38.

61.   van Breemen RB, Dong L, Pajkovic ND. Atmospheric pressure chemical ionization tandem mass spectrometry of carotenoids. Int J Mass spectrom. 2012;312:163-72.

62.   Pérez-Gálvez A, Sánchez-García A, Garrido-Fernández J, Ríos JJ. MS tools for a systematic approach in survey for carotenoids and their common metabolites. Arch Biochem Biophys. 2018;650:85-92.

63.   Amorim-Carrilho KT, Cepeda A, Fente C, Regal P. Review of methods for analysis of carotenoids. Trends Analyt Chem. 2014;56:49-73.

64.   Bijttebier SKA, D'Hondt E, Hermans N, Apers S, Voorspoels S. Unravelling ionization and fragmentation pathways of carotenoids using orbitrap technology: a first step towards identification of unknowns. J Mass Spectrom. 2013;48(6):740-54.

65.   Bushee JL, Argikar UA. An experimental approach to enhance precursor ion fragmentation for metabolite identification studies: application of dual collision cells in an orbital trap. Rapid Commun Mass Spectrom. 2011;25(10):1356-62.

66.   Rivera SM, Christou P, Canela-Garayoa R. Identification of carotenoids using mass spectrometry. Mass Spectrom Rev. 2014;33(5):353-72.

67.   Fu W, Magnúsdóttir M, Brynjólfson S, Palsson BØ, Paglia G. UPLC-UV-MSE analysis for quantification and identification of major carotenoid and chlorophyll species in algae. Anal Bioanal Chem. 2012;404(10):3145-54.

68.   Rivera SM, Christou P, Canela-Garayoa R. Identification of carotenoids using mass spectrometry. Mass Spec Rev. 2014;33(5):353-72.

69.   Schymanski EL, Jeon J, Gulde R, Fenner K, Ruff M, Singer HP, et al. Identifying Small Molecules via High Resolution Mass Spectrometry: Communicating Confidence. Environ Sci Technol. 2014;48(4):2097-8.

70.   Bustamam MSA, Pantami HA, Azizan A, Shaari K, Min CC, Abas F, et al. Complementary Analytical Platforms of NMR Spectroscopy and LCMS Analysis in the Metabolite Profiling of Isochrysis galbana. Mar Drugs. 2021;19(3):139.

71.   Zhang Y, Wu H, Wen H, Fang H, Hong Z, Yi R, et al. Simultaneous Determination of Fucoxanthin and Its Deacetylated Metabolite Fucoxanthinol in Rat Plasma by Liquid Chromatography-Tandem Mass Spectrometry. Mar Drugs. 2015;13(10):6521-36.

72.   Schex R, Schweiggert R, Steingass CB. Atmospheric pressure chemical ionization mass spectrometry of retro‐carotenoids. Rapid Commun Mass Spectrom. 2022;36(7):e9250-n/a.

73.   Shah MMR, Liang Y, Cheng JJ, Daroch M. Astaxanthin-Producing Green Microalga Haematococcus pluvialis: From Single Cell to High Value Commercial Products. Front Plant Sci. 2016;7:531-.

74.   Pantami HA, Ahamad Bustamam MS, Lee SY, Ismail IS, Mohd Faudzi SM, Nakakuni M, et al. Comprehensive GCMS and LC-MS/MS Metabolite Profiling of Chlorella vulgaris. Mar Drugs. 2020;18(7):367.

75.   Mulders KJM, Weesepoel YJA, Bodenes C, Lamers PP, Vincken JP, Martens DE, et al. Nitrogen-depleted Chlorella zofingiensis produces astaxanthin, ketolutein and their fatty acid esters: a carotenoid metabolism study. J Appl Phycol. 2015;27(1):125-40.
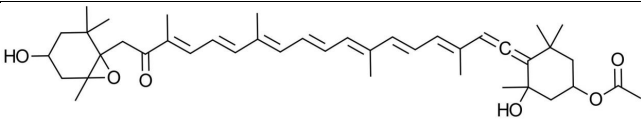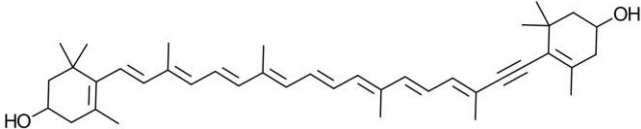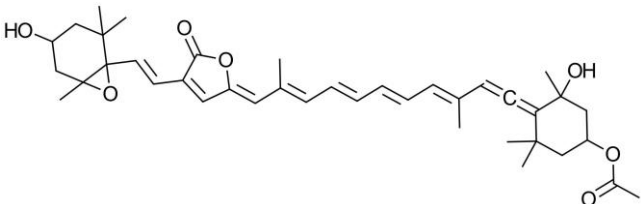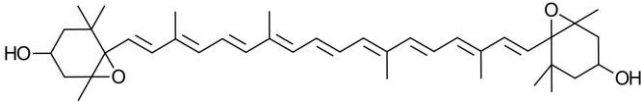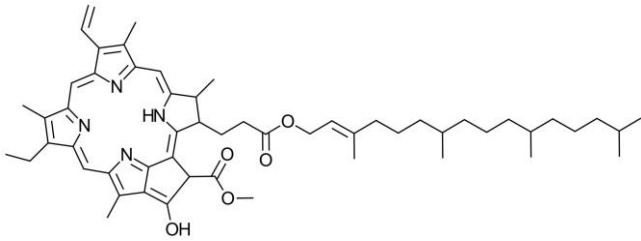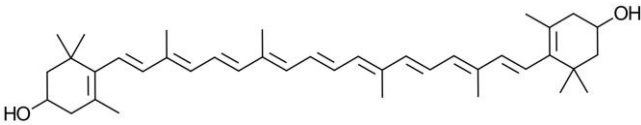
76.   Neto FC, Guaratini T, Costa-Lotufo L, Colepicolo P, Gates PJ, Lopes NP. Re-investigation of the fragmentation of protonated carotenoids by electrospray ionization and nanospray tandem mass spectrometry. Rapid Commun Mass Spectrom. 2016;30(13):1540-8.

77.   Li S, Fang K, Chen S, Xu J, Chen J, Chen H. Profiling fragments for carotenoid esters in Penaeus monodon by ultra‐high‐performance liquid chromatography/quadrupole‐Orbitrap high‐resolution mass spectrometry. Rapid Commun Mass Spectrom. 2021;35(1):e8938-n/a.

78.   Wang S-K, Stiles AR, Guo C, Liu C-Z. Microalgae cultivation in photobioreactors: An overview of light characteristics. Eng Life Sci. 2014;14(6):550-9.

79.   Rochet M, Legendre L, Demers S. Photosynthetic and pigment responses of sea-ice microalgae to changes in light intensity and quality. J Exp Mar Biol Ecol. 1986;101(3):211-26.

80.   Das P, Lei W, Aziz SS, Obbard JP. Enhanced algae growth in both phototrophic and mixotrophic culture under blue light. Bioresour Technol. 2011;102(4):3883-7.

81.   Shu C-H, Tsai C-C, Liao W-H, Chen K-Y, Huang H-C. Effects of light quality on the accumulation of oil in a mixed culture of Chlorella sp. and Saccharomyces cerevisiae. J Chem Technol Biotechnol. 2012;87(5):601-7.

82.   Marella TK, Tiwari A. Marine diatom Thalassiosira weissflogii based biorefinery for co-production of eicosapentaenoic acid and fucoxanthin. Bioresour Technol. 2020;307:123245.

83.   Lehmuskero A, Skogen Chauton M, Boström T. Light and photosynthetic microalgae: A review of cellular- and molecular-scale optical processes. Prog Oceanogr. 2018;168:43-56.

84.   Sharmila D, Suresh A, Indhumathi J, Gowtham K, Velmurugan N. Impact of various color filtered LED lights on microalgae growth, pigments and lipid production. European j biotechnol biosci. 2018;6(6):1-7.

85.   Honda M. Effects of Z-Isomerization On The Bioavailability and Functionality of Carotenoids : a Review. IntechOpen; 2018.
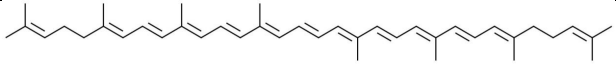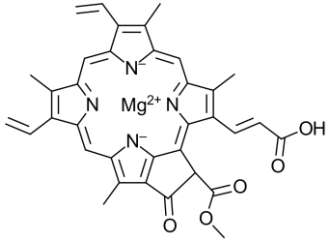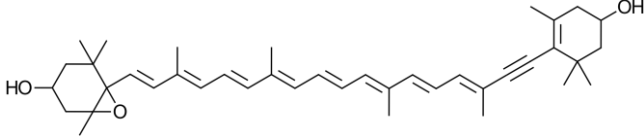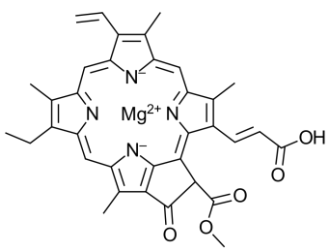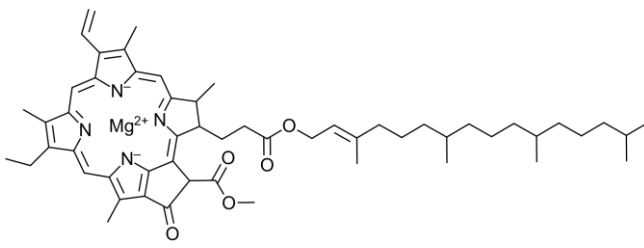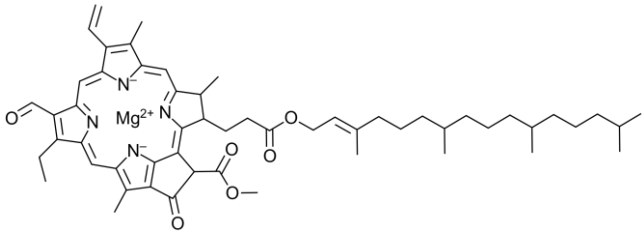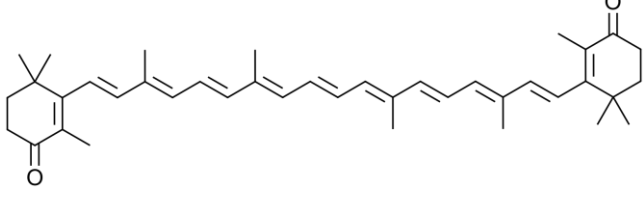
Appendix

Appendix A: DHI pigment standards
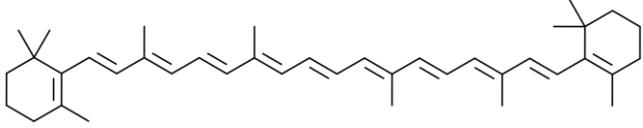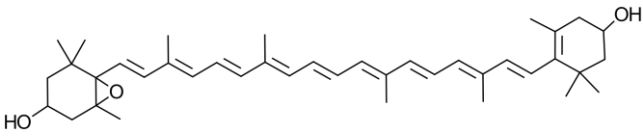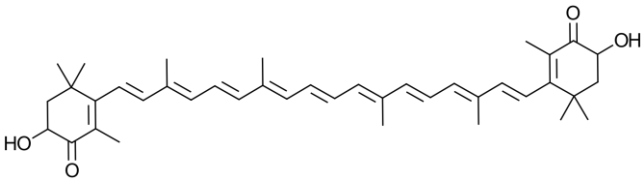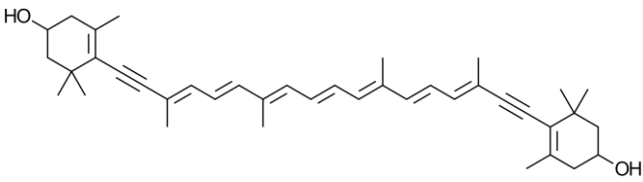
Appendix A.1 Characteristics of the DHI pigment standards

Table 15: Summary of pigment characteristic for standards purchased from DHI. Pigment, molecular formula, monoisotopic mass (Da) and molecular structure are provided.

Pigment	Molecular formula	Monoisotopic mass (Da)	Molecular structure
Fucoxanthin	$C_{42}H_{58}O_6$	658.4233	
Diatoxanthin	$C_{40}H_{54}O_2$	566.4124	
Peridinin	$C_{39}H_{50}O_7$	630.3557	
Violaxanthin	$C_{40}H_{56}O_4$	600.4179	
Pheophytin *a*	$C_{55}H_{74}N_4O_5$	870.5659	
Zeaxanthin	$C_{40}H_{56}O_2$	568.4280	

Lycopene	$C_{40}H_{56}$	536.4382	
Chlorophyll c_2	$C_{35}H_{28}MgN_4O_5$	608.1910	
Diadinoxanthin	$C_{40}H_{54}O_3$	582.4073	
Chlorophyll c_1	$C_{35}H_{30}MgN_4O_5$	610.2067	
Chlorophyll a	$C_{55}H_{72}MgN_4O_5$	892.5353	
Chlorophyll b	$C_{55}H_{70}MgN_4O_6$	906.5146	
Canthaxanthin	$C_{40}H_{52}O_2$	564.3967	

β-carotene	$C_{40}H_{56}$	536.4382	
Antheraxanthin	$C_{40}H_{56}O_3$	584.4229	
Astaxanthin	$C_{40}H_{52}O_4$	564.3866	
Alloxanthin	$C_{40}H_{52}O_2$	564.3967	

Appendix A.2 Properties of the pigment standards provided by the manufacturer

Table 16: Summary of pigment standard properties provided by DHI. Displaying pigment, batch no., concentration (mg/L) and solvent.

Pigment	Batch No.	Concentration (mg/L)	Solvent
Fucoxanthin	Fuco-124	1.490	100% Ethanol
Diatoxanthin	Dtx-145	0.641	100% Ethanol
Peridinin	Peri-122	1.154	100% Ethanol
Violaxanthin	Viol-145	1.118	100% Ethanol
Pheophytin *a*	Phta-109	3.208	90% Acetone
Zeaxanthin	Zea-147	0.782	100% Ethanol
Lycopene	Lyco-108	0.956	100% Acetone
Chlorophyll c_2	Chlc2-125	0.678	90% Acetone
Diadinoxanthin	Ddx-124	0.690	100% Ethanol
Chlorophyll c_2	Chlc1-103	0.539	90% Acetone
Chlorophyll *a*	Chla-129	1.707	90% Acetone
Chlorophyll *b*	Chlb-120	1.190	90% Acetone
Canthaxanthin	Cant-133	1.648	100% Ethanol
β-carotene	Beta-131	0.832	100% Acetone
Antheraxanthin	Ant-135	0.521	100% Ethanol
Astaxanthin	Asta-107	0.956	100% Acetone
Alloxanthin	Allo-116	0.948	100% Ethanol

Appendix B: MS acquisition

Appendix B.1 Target mass list for ddMS^2 HCD acquisition

Table 17: Target mass list of the ddMS2 HCD acquisition. The mass list includes m/z-values for both the radical- and proton adduct of each pigment standard

Compound	m/z
Fucoxanthin [M*]$^+$	658.4233
Fucoxanthin [M+H]$^+$	659.4312
Diatoxanthin [M*]$^+$	566.4124
Diatoxanthin [M+H]$^+$	567.4202
Peridinin [M*]$^+$	630.3557
Peridinin [M+H]$^+$	631.3635
Violaxanthin [M*]$^+$	600.4179
Violaxanthin [M+H]$^+$	601.4257
Pheophytin *a* [M*]$^+$	870.5659
Pheophytin *a* [M+H]$^+$	871.5739
Zeaxanthin [M*]$^+$	568.428
Zeaxanthin [M+H]$^+$	569.4359
Lycopene [M*]$^+$	536.4382
Lycopene [M+H]$^+$	537.446
Chlorophyll c_2 [M*]$^+$	608.191
Chlorophyll c_2 [M+H]$^+$	609.1988
Diadinoxanthin [M*]$^+$	582.4073
Diadinoxanthin [M+H]$^+$	583.4151
Chlorophyll c_1 [M*]$^+$	610.2067

Chlorophyll c_1 [M+H]$^+$	611.2145
Chlorophyll a [M*]$^+$	892.5353
Chlorophyll a [M+H]$^+$	893.5431
Chlorophyll b [M*]$^+$	906.5146
Chlorophyll b [M+H]$^+$	907.5224
Canthaxanthin [M*]$^+$	564.3967
Canthaxanthin [M+H]$^+$	565.4046
β-carotene [M*]$^+$	536.4382
β-carotene [M+H]$^+$	537.446
Antheraxanthin [M*]$^+$	584.4229
Antheraxanthin [M+H]$^+$	585.4308
Astaxanthin [M*]$^+$	596.3866
Astaxanthin [M+H]$^+$	597.3944
Alloxanthin [M*]$^+$	564.3967
Alloxanthin [M+H]$^+$	565.4046

Appendix B.2 Injection Sequence of the AcquireX acquisition

Table 18: Injection sequence of the acquireX acquisition. Blanks were analyzed 3 times, ID samples 5 times and 3 runs per sample parallel with Qc samples analyzed in between algae samples

Injection sequence
Blank sample (x3)
ID sample (x5)
Qc sample
Red (x3)
Qc sample
Blue 1 (x3)
Blue 2 (x3)
Blue 3 (x3)
Qc sample
White 1 (x3)
White 2 (x3)
White 3 (x3)

Appendix C: Data processing

Appendix C.1 Compound Discoverer parameters
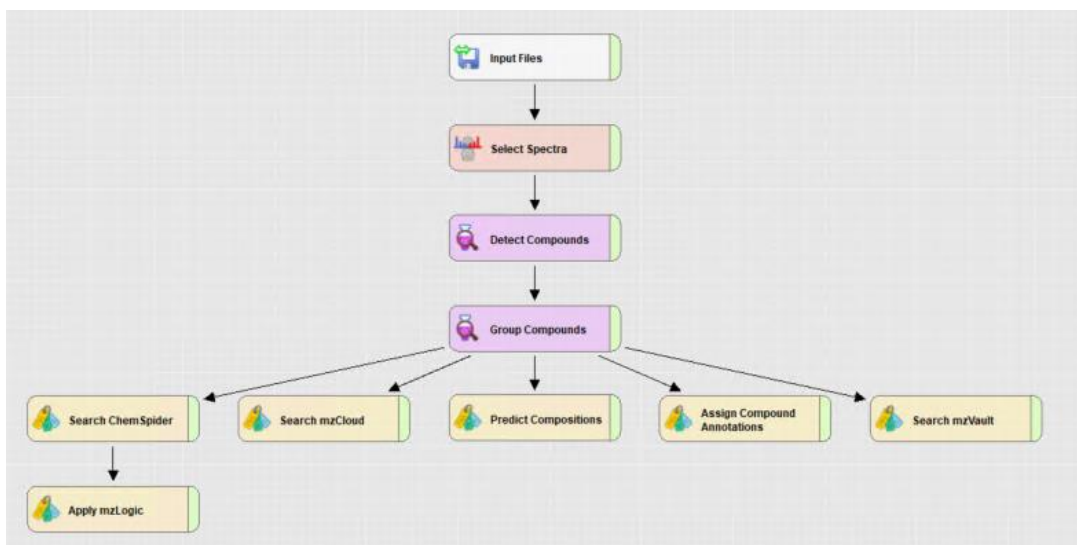
Figure 40: Data processing workflow for targeted analysis of algae samples performed by Compound Discoverer software.
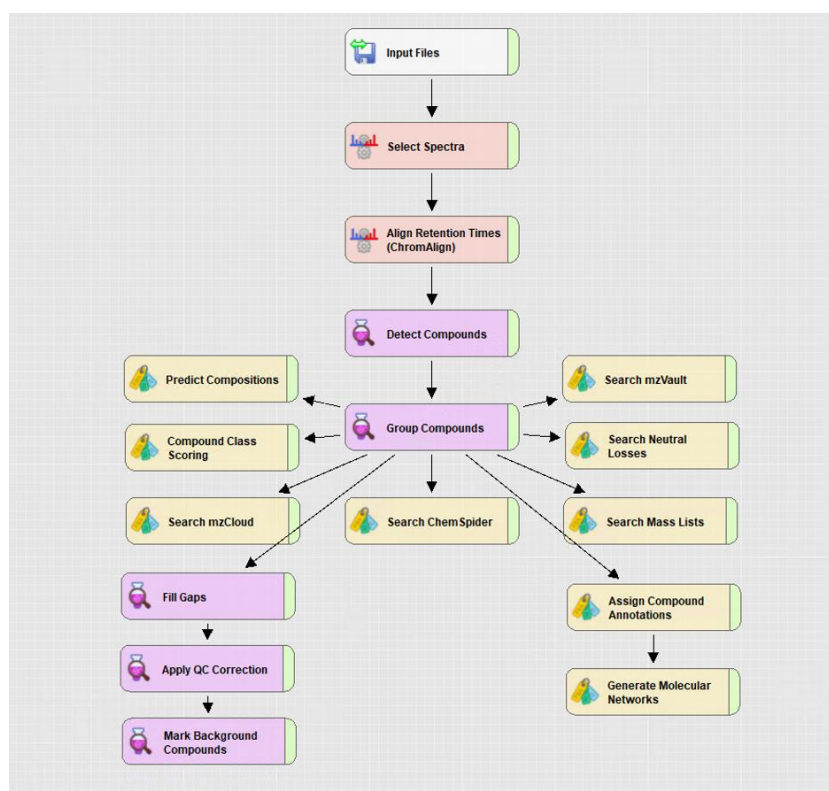
Figure 41: Data processing workflow for untargeted analysis of algae samples performed by Compound Discoverer software

Table 19:Parameter specification for algae sample data processing with Compound Discoverer

	Targeted analysis	Untargeted analysis
Select spectra		
Lower RT limit	0 (lowest available RT is used)	0
Upper RT limit	0 (highest available RT is used)	0
Polarity	Any	Any
Align Retention Times (ChromAlign)		
Reference File	-	Not specified (first QC file chosen)
Detect Compounds		
Mass tolerance	5 ppm	5 ppm
Min. Peak Intensity	250000	10000
Use Most Intense Isotope Only	True	True
Chromatographic S/N threshold	1.5	1.5
Remove Baseline	False	False
Isotope Pattern Detection	Group Isotopes	Br; Cl
Compound detection Ions	$[M+2H]^{2+}$, $[M+H]^+$	All available checked (33)
Group Compounds		
Mass tolerance	5 ppm	5 ppm
RT tolerance	0.2	0.5
Align Peaks	False	False
Preferred Ions	$[M+H-H2O]^+$, $[M+H]^+$	$[M+H]^+$, $[M+H-H2O]^+$, $[M+K]^+$, $[M+Na]^+$,
Areal Integration	Most Common Ion	Most Common Ion
Area Contribution	3	3
CV Contribution	10	10
FWHM to Base Contribution	5	5
Jaggedness Contribution	5	5
Modality Contribution	5	5
Zig-Zag Index Contribution	5	5
Peak Rating Threshold	4	4
Number of files	1	1
Search ChemSpider		
Database(s)	KEGG	BiOCyc; KEGG
Search Mode	By formula or mass	By formula or mass
Mass Tolerance	5 ppm	5 ppm
Max. # of results per compound	100	100
Max. # of Predicted Compounds to be	3	3
Apply mzLogic		
Max.# Compounds	0 (all candidates of all compounds are	
Max. #mzCloud Similarity Results to	10	
Match Factor Threshold	30	
Search mzCloud		
Compound Classes	All	All
Library	Autoprocessed; Reference	Autoprocessed; Reference
Search MSn Tree	False	False
Identity Search	HighChem High Res	Cosine
Match Activation Type	True	True

Match Activation Energy	Match with Tolerance	Match with Tolerance
Activation Energy Threshold	20	20
Apply Intensity Threshold	True	True
Similarity Search	None	None
Match Factor Threshold	60	60
Use DIA Scans for Search	False	False
Max. Isolation Width (DA)	500	500
Match Activation Type	False	False
Match Activation Energy	Any	Any
Activation Energy Tolerance	100	100
Apply Intensity threshold	False	False
Match Factor Threshold	20	20
Predict Compositions		
Mass Tolerance	10 ppm	5 ppm
Min. Element Counts	C H	C H
Max. Element Counts	C90 H190 Br3 Cl4 N10 O18 P3 S5	C90 H190 Br3 Cl4 N10 O18 P3 S5
Min. RDBE	0	0
Max. RDBE	40	40
Min. H/C	0.1	0.1
Max. H/C	3.5	4
Max. # Candidates	10	10
Intensity Tolerance (%)	30	30
Intensity Threshold (%)	0.1	0.1
S/N Threshold	3	3
Use Dynamic Recalibration	True	True
Use Fragments Matching	True	True
Mass Tolerance	5 ppm	5 ppm
S/N Threshold	3	3
Assign Compound Annotations		
Mass Tolerance	5 ppm	5 ppm
Data Source #1	MzVault Search	mzCloud Search
Data Source #2	Predicted Compositions	MzVault Search
Data Source #3	mzCloud Search	MassList Search
Data Source #4	ChemSpider Search	Predicted Compositions
Data Source #5	-	ChemSpider Search
Use mzLogic	True	True
Use Spectral Distance	True	True
SFit Threshold	20	20
SFit Range	20	20
Clear Names	False	False
Generate Molecular Networks		
Use Full MSn Tree	-	True
Match Mass Shift	-	True
Match Transformations	-	True
Variate Transformations	-	False
S/N Threshold	-	3
Mass Tolerance	-	2.3 mmu

Min. Fragment m/z	-	50
Phase I	-	All checked (15/15)
Phase II	-	All checked (19/19)
Max. #Phase II	-	1
Max. #All Steps	-	3
<u>Applied View Filters</u>	-	
Required Transformation	-	True
Required MSn	-	True
Min. MSn Score	-	50
Min. MSn Coverage	-	70
Min. Fragments	-	3
<u>Applied Thresholds</u>	-	
Require Transformation	-	False
Required MSn	-	False
Min. MSn Score	-	20
Min. MSn Coverage	-	20
Min. Fragments	-	0
Search mzVault		
mzVault Library	pigmentDB2.db	LipidBlast-V68-Neg.db and LipidBlast-
Compound Classes	All	All
Match Ion Activation Type	True	False
Match Ion Activation Energy	Match with Tolerance	Any
Ion Activation Energy Tolerance	20	20
Match Ionization Method	True	False
Apply Intensity Threshold	True	True
Precursor Mass Tolerance	10 ppm	10 ppm
Match Analyzer Type	True	False
Search Algorithm	HighChem HighRes	NIST
Match Factor Threshold	50	0
RT Tolerance (min)	2	2
Use Retention Time	False	False
Search Mass Lists		
Mass Lists	-	LipidMaps Structure Database 2021-09-
Use Retention Time	-	True
RT Tolerance [min]	-	2
Mass Tolerance	-	5 ppm
Predicted Composition		
Mass Tolerance	-	5 ppm
Min. Element Counts	-	C H
Max. Element Counts	-	C90 H190 Br3 Cl4 N10 O18 P3 S5
Min. RDBE	-	0
Max. RDBE	-	40
Min. H/C	-	0.1
Max. H/C	-	4
Max. # Candidates	-	10
<u>Pattern Matching</u>		
Intensity Tolerance (%)	-	30

Intensity Threshold (%)	-	0.1
S/N Threshold	-	3
Use Dynamic Recalibration	-	True
Fragments Matching		
Use Fragment matching	-	True
Mass Tolerance	-	5 ppm
S/N Threshold	-	3
Compound Class Scoring		
Compound Classes	-	Phosphatidylcholine Compound Class.clib
S/N Threshold	-	10
High Acc. Mass Tolerance	-	5 ppm
Low Acc. Mass Tolerance	-	0.5 Da
Use Full MS Tree	-	True
Allow DIA Scoring	-	True
Search Neutral Losses		
Natural Losses	-	Fatty Acid
High Acc. Mass Tolerance	-	5 ppm
Low Acc. Mass Tolerance	-	0.5 Da
S/N Threshold	-	3
Use DIA Scans for Search	-	False
Fill Gaps		
Mass Tolerance	-	5 ppm
S/N Threshold	-	1.5
Apply QC Correction		
Min. QC Coverage (%)	-	50
Max. QC Area RSD	-	30
Max. Corrected QC Area RSD (%)	-	25
Mark Background Compounds		
Max. Sample/Blank	-	5
Max. Blank/Sample	-	0
Hide Background	-	True

Appendix D Results

Appendix D.1 Extraction protocol development

Appendix D.1.1 Effect of extraction solvent

Table 20: Solvent extraction efficiency on pigments from P.gacialis, alternating between different extraction solvents. The values tabulated are mean peak areas, SD and RSD% of algae samples analyzed on UPLC-MS. Extractions for the different solvents were performed in triplicates. The extraction solvents utilized are listed in Table 10 with the corresponding abbreviations.

Pigment	E1				E2				E3				E4				E5			
	Area	Mean	SD	RSD %	Area	Mean	SD	RSD %	Area	Mean	SD	RSD %	Area	Mean	SD	RSD %	Area	Mean	SD	RSD %
Fucoxanthin $[M+H]^+$	9.80E+08				8.67E+08				7.21E+08				8.40E+08				9.63E+08			
	9.83E+08	9.71E+08	1.89E+07	1.95	8.65E+08	8.67E+08	1.24E+06	0.14	7.23E+08	7.11E+08	1.94E+07	2.73	8.49E+08	8.58E+08	2.37E+07	2.76	9.35E+08	9.65E+08	3.21E+07	3.33
	9.49E+08				8.68E+08				6.89E+08				8.85E+08				9.99E+08			
Diatoxanthin $[M*]^+$	3.47E+07				2.92E+07				3.35E+07				3.36E+07				3.55E+07			
	3.82E+07	3.60E+07	1.94E+06	5.39	3.22E+07	3.12E+07	1.73E+06	5.56	3.32E+07	3.33E+07	2.58E+05	0.78	3.37E+07	3.33E+07	6.79E+05	2.04	3.49E+07	3.50E+07	4.99E+05	1.43
	3.50E+07				3.21E+07				3.30E+07				3.25E+07				3.45E+07			
Violaxanthin $[M*]^+$	2.41E+06				1.70E+06				1.94E+06				2.39E+06				2.61E+06			
	2.91E+06	2.61E+06	2.67E+05	10.23	2.01E+06	1.88E+06	1.62E+05	8.65	2.02E+06	1.98E+06	5.83E+04	2.95	2.30E+06	2.31E+06	7.66E+04	3.32	2.52E+06	2.57E+06	4.76E+04	1.85
	2.50E+06				1.92E+06				1.94E+06				2.23E+06				2.58E+06			
Pheophytin *a* $[M+H]^+$	1.17E+09				1.02E+09				7.83E+08				1.20E+09				9.64E+08			
	1.42E+09	1.25E+09	1.50E+08	12.01	1.16E+09	1.10E+09	7.28E+07	6.61	7.13E+08	7.38E+08	3.90E+07	5.28	1.13E+09	1.13E+09	6.82E+07	6.02	9.98E+08	9.91E+08	2.32E+07	2.34
	1.16E+09				1.12E+09				7.18E+08				1.07E+09				1.01E+09			
Zeaxanthin $[M*]^+$	8.01E+05				8.37E+05				8.68E+05				7.13E+05				9.82E+05			
	8.50E+05	8.34E+05	2.88E+04	3.46	9.37E+05	8.92E+05	5.07E+04	5.69	8.78E+05	8.85E+05	2.06E+04	2.33	6.52E+05	6.64E+05	4.49E+04	6.76	1.01E+06	1.01E+06	2.53E+04	2.51
	8.52E+05				9.01E+05				9.08E+05				6.26E+05				1.03E+06			
Chlorophyll c_2 $[M+H]^+$	8.35E+06				6.53E+06				4.06E+06				8.45E+06				7.12E+06			
	1.13E+07	9.44E+06	1.60E+06	16.90	7.71E+06	7.27E+06	6.42E+05	8.83	4.10E+06	4.06E+06	3.57E+04	0.88	7.88E+06	7.77E+06	7.44E+05	9.58	7.38E+06	7.22E+06	1.40E+05	1.94
	8.70E+06				7.57E+06				4.03E+06				6.97E+06				7.16E+06			
	4.12E+07				3.21E+07				3.71E+07			2.13	4.13E+07				4.24E+07	4.26E+07		0.70

Compound																				
Diadinoxanthin [M+H]⁺	5.21E+07				3.69E+07				3.59E+07				4.06E+07				4.24E+07			
	4.18E+07	4.51E+07	6.11E+06	13.56	3.68E+07	3.53E+07	2.74E+06	7.78	3.57E+07	3.62E+07	7.71E+05		3.95E+07	4.05E+07	8.99E+05	2.22	4.29E+07		2.99E+05	
Chlorophyll c_1 [M+H]⁺	1.13E+07				8.60E+06				5.33E+06				1.26E+07				1.08E+07			
	1.74E+07	1.39E+07	3.17E+06	22.83	1.01E+07	9.81E+06	1.10E+06	11.2	6.07E+06	5.77E+06	3.92E+05	6.80	1.25E+07	1.23E+07	4.07E+05	3.30	9.79E+06	1.03E+07	5.06E+05	4.89
	1.30E+07				1.07E+07				5.91E+06				1.19E+07				1.05E+07			
Chlorophyll a [M+H]⁺	1.39E+09				1.22E+09				1.08E+09				1.27E+09				1.29E+09			
	1.47E+09	1.41E+09	5.15E+07	3.65	1.28E+09	1.19E+09	1.06E+08	8.88	1.23E+09	1.13E+09	8.30E+07	7.33	1.11E+09	1.18E+09	8.54E+07	7.25	1.33E+09	1.30E+09	2.19E+07	1.68
	1.37E+09				1.08E+09				1.09E+09				1.15E+09				1.29E+09			
Chlorophyll b [M+H]⁺	3.27E+06				2.54E+06				4.70E+05				3.27E+06				1.20E+06			
	4.25E+06	3.65E+06	5.24E+05	14.35	2.86E+06	2.74E+06	1.70E+05	6.19	5.86E+05	4.87E+05	9.21E+04	18.9	3.16E+06	3.16E+06	1.10E+05	3.47	1.27E+06	1.23E+06	3.77E+04	3.06
	3.44E+06				2.81E+06				4.05E+05				3.05E+06				1.22E+06			
β-carotene [M*]⁺	5.69E+07				4.92E+07				5.91E+07				5.91E+07				6.26E+07			
	6.89E+07	6.19E+07	6.26E+06	10.11	5.10E+07	5.14E+07	2.36E+06	4.59	5.50E+07	5.76E+07	2.22E+06	3.86	5.67E+07	5.76E+07	1.32E+06	2.28	6.19E+07	6.38E+07	2.68E+06	4.20
	5.98E+07				5.39E+07				5.87E+07				5.71E+07				6.69E+07			
Antheraxanthin [M*]⁺	1.08E+06				8.80E+05				9.50E+05				1.15E+06				1.32E+06			
	1.65E+06	1.38E+06	2.89E+05	20.96	1.08E+06	9.96E+05	1.05E+05	10.5	1.07E+06	1.04E+06	8.01E+04	7.70	1.29E+06	1.16E+06	1.24E+05	10.7	1.38E+06	1.36E+06	3.08E+04	2.27
	1.40E+06				1.02E+06				1.10E+06				1.05E+06				1.37E+06			
Alloxanthin [M*]⁺	2.93E+05				2.81E+05				3.21E+05				3.38E+05				3.78E+05			
	3.89E+05	3.61E+05	5.94E+04	16.44	3.02E+05	2.89E+05	1.11E+04	3.84	3.50E+05	3.47E+05	2.37E+04	6.83	3.18E+05	3.18E+05	1.99E+04	6.25	4.21E+05	4.08E+05	2.62E+04	6.41
	4.01E+05				2.84E+05				3.68E+05				2.99E+05				4.26E+05			
Astaxanthin [M+H]⁺	2.41E+05				2.25E+05				1.77E+05				2.36E+05				2.09E+05			
	3.39E+05	2.72E+05	5.83E+04	21.45	2.10E+05	2.21E+05	9.35E+03	4.23	1.44E+05	1.58E+05	1.75E+04	11.1	2.19E+05	2.29E+05	9.30E+03	4.05	1.88E+05	1.95E+05	1.25E+04	6.44
	2.36E+05				2.28E+05				1.52E+05				2.34E+05				1.87E+05			

i

Appendix D.1.2 Effect of extraction duration

Table 21: Effect of time configuration on extraction efficiency of pigments from P.gacialis. The values tabulated are mean peak areas, SD and RSD% of algae samples analyzed on UPLC-MS. Extractions for the displayed time configurations were performed in triplicates.

	5				15				30				60			
Pigment	Area	Mean	SD	RSD%	Area	Mean	SD	RSD%	Area	Mean	SD	RSD%	Area	Mean	SD	RSD%
Fucoxanthin $[M+H]^+$	9.06E+08				1.03E+09				1.00E+09				9.05E+08			
	8.95E+08	8.89E+08	1.99E+07	2.24	9.05E+08	9.47E+08	7.45E+07	7.87	9.28E+08	9.59E+08	3.70E+07	3.85	9.29E+08	9.34E+08	3.22E+07	3.44
	8.67E+08				9.03E+08				9.49E+08				9.69E+08			
Diatoxanthin $[M^*]^+$	2.42E+07				2.89E+07				2.79E+07				2.84E+07			
	2.41E+07	2.44E+07	4.02E+05	1.65	2.69E+07	2.72E+07	1.52E+06	5.57	2.70E+07	2.81E+07	1.13E+06	4.04	2.77E+07	2.91E+07	1.76E+06	6.07
	2.48E+07				2.59E+07				2.93E+07				3.11E+07			
Violaxanthin $[M^*]^+$	1.61E+06				2.02E+06				2.05E+06				2.02E+06			
	1.40E+06	1.51E+06	1.07E+05	7.10	1.89E+06	1.89E+06	1.25E+05	6.60	2.03E+06	2.04E+06	1.01E+04	0.50	2.06E+06	2.11E+06	1.21E+05	5.72
	1.52E+06				1.77E+06				2.07E+06				2.25E+06			
Pheophytin *a* $[M+H]^+$	9.38E+08				1.21E+09				1.18E+09				9.78E+08			
	8.83E+08	9.11E+08	2.78E+07	3.05	1.08E+09	1.06E+09	1.63E+08	15.4	1.05E+09	1.15E+09	8.46E+07	7.36	1.10E+09	1.10E+09	1.25E+08	11.3
	9.13E+08				8.88E+08				1.21E+09				1.23E+09			
Zeaxanthin $[M^*]^+$	7.24E+05				8.95E+05				8.35E+05				7.53E+05			
	7.75E+05	7.55E+05	2.73E+04	3.61	8.07E+05	8.41E+05	4.75E+04	5.64	7.98E+05	8.08E+05	2.31E+04	2.85	7.42E+05	7.33E+05	2.51E+04	3.43
	7.66E+05				8.22E+05				7.92E+05				7.05E+05			
Chlorophyll c_2 $[M+H]^+$	5.88E+06				8.40E+06				7.62E+06				7.22E+06			
	5.90E+06	6.22E+06	5.73E+05	9.21	6.49E+06	7.32E+06	9.81E+05	13.4	7.26E+06	7.53E+06	2.39E+05	3.18	7.49E+06	7.80E+06	7.76E+05	9.95
	6.88E+06				7.08E+06				7.71E+06				8.68E+06			
Diadinoxanthin $[M^*]^+$	3.28E+07				4.36E+07				3.70E+07				3.97E+07			
	3.46E+07	3.36E+07	8.76E+05	2.61	3.78E+07	3.85E+07	4.77E+06	12.4	3.63E+07	3.83E+07	2.79E+06	7.28	3.91E+07	4.14E+07	3.52E+06	8.51
	3.34E+07				3.41E+07				4.15E+07				4.55E+07			
Chlorophyll c_1 $[M+H]^+$	6.87E+06				1.14E+07				1.06E+07				8.30E+06			
	7.03E+06	7.02E+06	1.36E+05	1.94	8.07E+06	8.89E+06	2.26E+06	25.4	9.72E+06	1.02E+07	4.25E+05	4.18	1.03E+07	1.02E+07	1.88E+06	18.4
	7.15E+06				7.16E+06				1.02E+07				1.21E+07			

Compound																
Chlorophyll *a* [M+H]+	1.17E+09				1.23E+09				1.25E+09				1.18E+09			
	1.18E+09	1.17E+09	8.14E+06	0.69	1.15E+09	1.18E+09	4.86E+07	4.13	1.18E+09	1.21E+09	3.15E+07	2.59	1.20E+09	1.21E+09	4.05E+07	3.35
	1.17E+09				1.15E+09				1.21E+09				1.25E+09			
Chlorophyll *b* [M+H]+	2.44E+06				3.81E+06				3.57E+06				2.94E+06			
	2.40E+06	2.53E+06	1.97E+05	7.79	3.00E+06	3.22E+06	5.21E+05	16.2	3.38E+06	3.43E+06	1.20E+05	3.51	3.08E+06	3.20E+06	3.37E+05	10.5
	2.76E+06				2.84E+06				3.35E+06				3.58E+06			
β-carotene [M*]+	4.61E+07				5.35E+07				5.13E+07				4.73E+07			
	4.51E+07	4.63E+07	1.44E+06	3.10	4.77E+07	4.94E+07	3.53E+06	7.16	5.08E+07	5.21E+07	1.80E+06	3.45	5.17E+07	5.06E+07	2.90E+06	5.72
	4.79E+07				4.71E+07				5.41E+07				5.28E+07			
Antheraxanthin [M*]+	1.29E+07				1.66E+07				1.48E+07				1.46E+07			
	1.36E+07	1.32E+07	3.97E+05	3.01	1.41E+07	1.47E+07	1.66E+06	11.3	1.43E+07	1.48E+07	5.07E+05	3.41	1.53E+07	1.61E+07	2.04E+06	12.7
	1.29E+07				1.34E+07				1.54E+07				1.84E+07			
Alloxanthin [M*]+	2.35E+05				2.73E+05				2.41E+05				2.36E+05			
	2.16E+05	2.15E+05	2.12E+04	9.86	2.41E+05	2.48E+05	2.22E+04	8.94	2.17E+05	2.43E+05	2.65E+04	10.9	2.33E+05	2.60E+05	4.49E+04	17.3
	1.93E+05				2.31E+05				2.70E+05				3.12E+05			
Astaxanthin [M+H]+	2.54E+05				3.37E+05				3.06E+05				2.64E+05			
	2.39E+05	2.50E+05	9.94E+03	3.97	2.97E+05	3.09E+05	2.45E+04	7.94	2.91E+05	2.93E+05	1.12E+04	3.81	2.40E+05	2.75E+05	4.08E+04	14.9
	2.58E+05				2.93E+05				2.84E+05				3.20E+05			

Appendix D.1.3 Re-extraction requirement

Table 22: Mean peak areas obtained by the initial extraction (E1) and the second extraction (E2) form P. glacialis. Standard deviation (SD), relative standard deviation (RSD%) and the contribution of a second extraction to the total peak area (%) are displayed.

	White light						
	E1			**E2**			
	Mean	**SD**	**RSD%**	**Mean**	**SD**	**RSD%**	**%E2/total**
Fucoxanthin	1.02E+09	1.38E+08	13.6	3.32E+07	4.04E+06	12.2	3.16
Diatoxanthin	7.57E+06	3.87E+05	5.11	1.16E+06	2.05E+05	17.8	13.2
Violaxanthin	6.83E+06	4.85E+05	7.11	1.89E+05	1.73E+04	9.18	2.69
Pheophytin a	1.15E+09	2.90E+08	25.3	6.04E+07	5.28E+06	8.74	4.99
Zeaxanthin	1.28E+05	1.53E+04	11.9	1.97E+04	5.33E+03	27.0	13.4
Chlorophyll c_2	1.26E+07	2.03E+06	16.1	1.06E+06	4.60E+04	4.36	7.73
Diadinoxanthin	8.32E+07	1.80E+07	21.7	3.81E+06	7.84E+05	20.6	4.38
Chlorophyll c_1	8.47E+06	2.63E+06	31.0	6.56E+05	9.52E+04	14.5	7.19
Chlorophyll a	1.32E+09	8.28E+07	6.27	1.66E+08	1.69E+07	10.2	11.1
Chlorophyll b	3.36E+06	8.31E+05	24.7	5.21E+04	5.66E+03	10.9	1.53
β-carotene	2.51E+07	4.43E+06	17.6	4.79E+06	3.24E+05	6.76	16.0
Antheraxanthin	3.07E+06	3.46E+05	11.3	1.37E+05	1.18E+04	8.64	4.26
Alloxanthin	4.79E+06	1.13E+06	23.7	1.14E+05	2.04E+04	18.0	2.32

Table 23: Mean peak areas obtained by the initial extraction (E1) and the second extraction (E2) form P. glacialis. Standard deviation (SD), relative standard deviation (RSD%) and the contribution of a second extraction to the total peak area (%) are displayed.

	Red light						
	E1			**E2**			
	Mean	**SD**	**RSD%**	**Mean**	**SD**	**RSD%**	**%E2/total**
Fucoxanthin	6.35E+08	2.74E+07	4.31	3.79E+07	3.38E+05	0.89	5.63
Diatoxanthin	3.90E+06	7.26E+05	18.6	8.20E+05	2.19E+04	2.67	17.4
Violaxanthin	2.14E+06	5.42E+05	253	1.77E+05	8.11E+03	4.57	7,64
Pheophytin a	9.51E+08	4.92E+08	51.8	9.69E+07	2.88E+07	29.8	9.25
Zeaxanthin	9.42E+04	3.48E+03	3.69	1.01E+04	7.22E+02	7.12	9.72
Chlorophyll c_2	7.03E+06	1.59E+05	2.26	1.12E+06	9.78E+03	0.88	13.7
Diadinoxanthin	4.75E+07	3.11E+06	6.55	4.71E+06	1.93E+05	4.10	9.01
Chlorophyll c_1	6.00E+06	1.77E+05	2.94	8.28E+05	2.74E+04	3.31	12.1
Chlorophyll a	1.05E+09	6.71E+07	6.38	2.03E+08	5.29E+06	2.61	16.2
Chlorophyll b	1.90E+06	9.53E+05	50.2	6.25E+04	1.34E+04	21.4	3.18
β-carotene	3.08E+07	2.93E+06	9.54	6.89E+06	6.98E+05	10.1	18.3
Antheraxanthin	8.04E+05	1.61E+05	20.0	5.99E+04	3.34E+03	5.58	6.93
Alloxanthin	2.61E+06	1.45E+05	5.57	1.48E+05	2.18E+03	1.48	5.35

Appendix D.2 UPLC method development

Appendix D.2.1 Gradient optimization

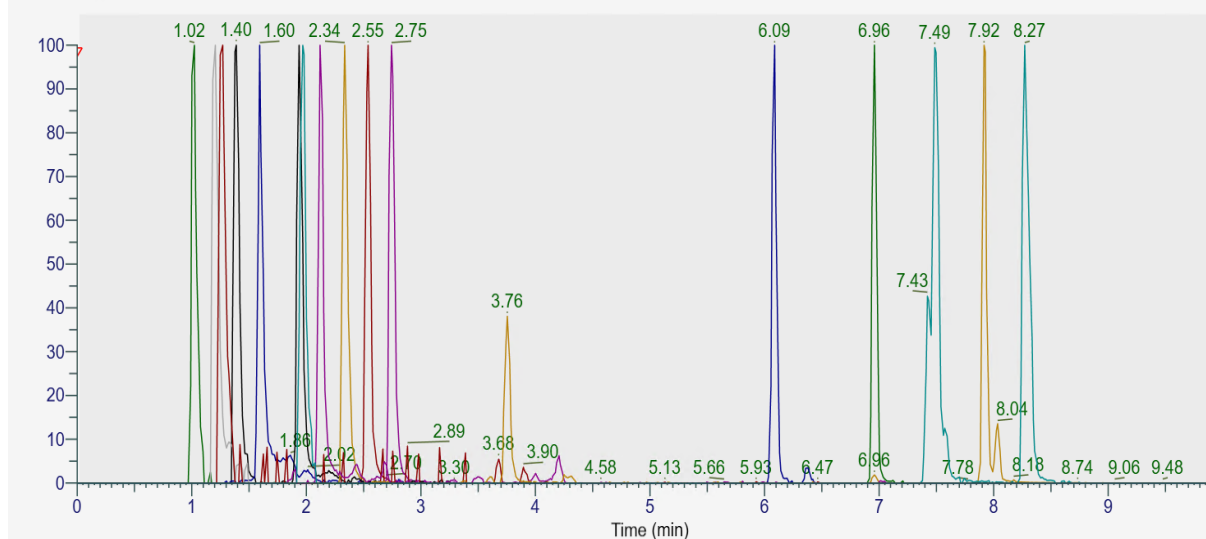*Figure 42: Gradient profile 3 composing an overlaid XIC of all pigment standards.*
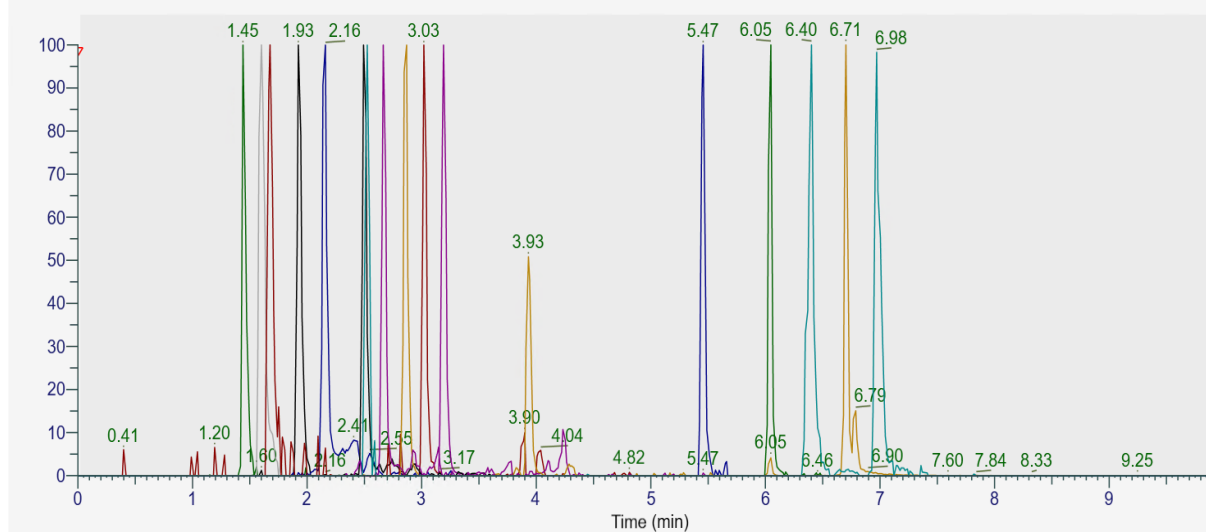

Figure 43: Gradient profile 4 composing an overlaid XIC of all pigment standards.

Table 24: Elution order of the pigment standards altering the gradient configuration

	Gradient 1	Gradient 2	Gradient 3	Gradient 4
Pigment		**Rt**		
Peridinin	1.44	1.22	1.02	1.45
Chlorophyll c_2	1.58	1.4	1.21	1.6
Chlorophyll c_1	1.66	1.47	1.27	1.68
Fucoxanthin	1.89	1.61	1.4	1.93
Violaxanthin	2.11	1.91	1.6	2.16
Diadinoxanthin	2.51	2.28	1.94	2.5
Astaxanthin	2.52	2.31	1.97	2.53
Antheraxanthin	2.75	2.48	2.13	2.67
Alloxanthin	3.07	2.7	2.34	2.87
Diatoxanthin	3.35	2.89	2.55	3.03
Zeaxanthin	3.59	3.09	2.75	3.2
Canthaxanthin	4.56	4.02	3.76	3.93
Chlorophyll *b*	6.08	5.98	6.09	5.47
Chlorophyll *a*	6.58	6.68	6.96	6.05
Lycopene	6.86	7.11	7.49	6.4
Pheophytin a	7.11	7.46	7.93	6.71
β-carotene	7.32	7.76	8.27	6.98

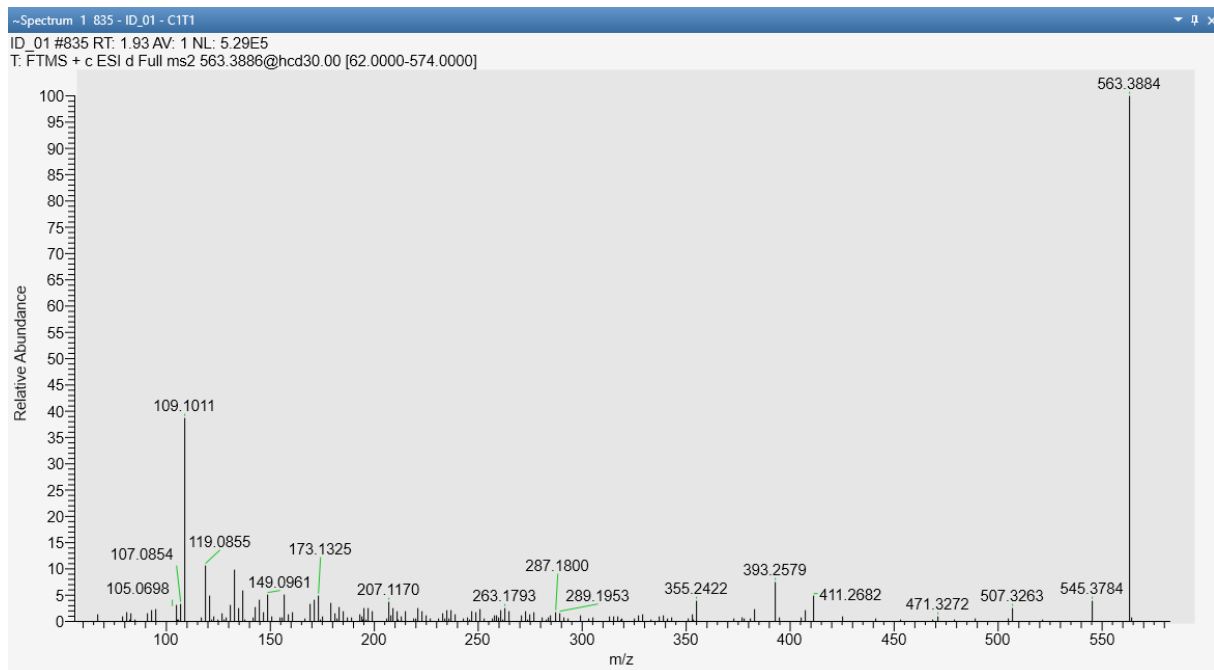# Appendix D.3   Identification of unknown substances

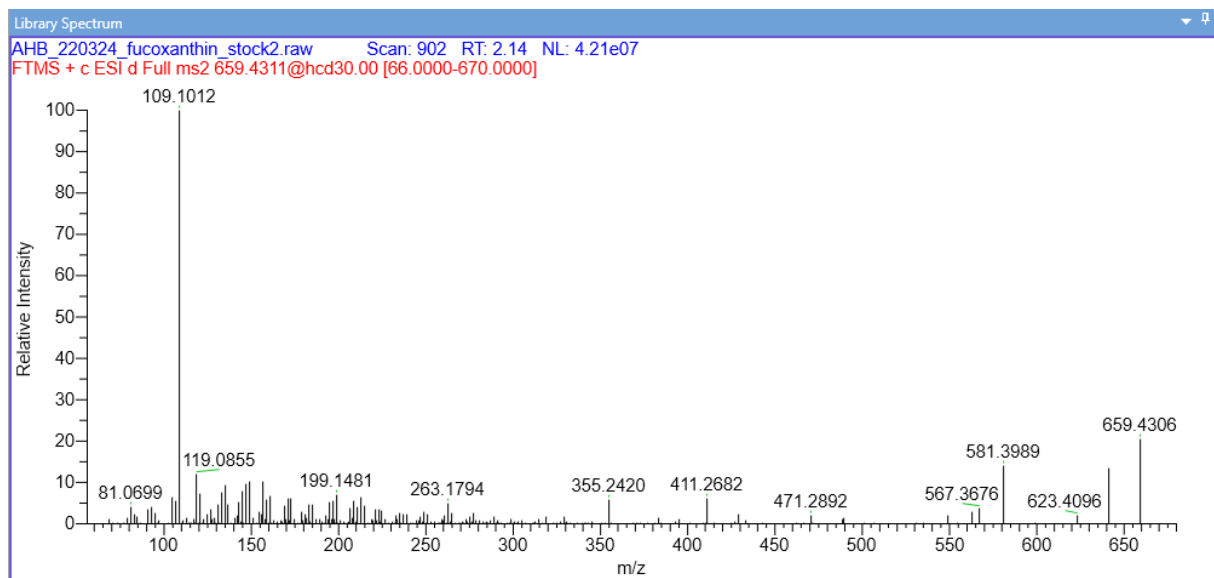*Figure 44: MS2 of the tentatively identified pigment "Rhodoxanthin" by CD*

Figure 45: The fucoxanthin MS2 spectrum of the AMRT database